Optical Performance Monitoring and Signal Optimization in Optical Networks

Petersen, Martin Nordal; Dittmann, Lars; Peucheret, Christophe; Nielsen, Mads Lønstrup

Publication date:
2006

Document Version
Publisher's PDF, also known as Version of record

Optical Performance Monitoring and Signal Optimization in Optical Networks

Martin Nordal Petersen

December 2005

Research Center COM

Technical University of Denmark

Building 345 V

2800 Kgs. Lyngby

Denmark

Abstract

This thesis studies performance monitoring for the next generation optical networks. The focus is on all-optical networks with bit-rates of 10 Gb/s or above. Next generation all-optical networks offer large challenges as the optical transmitted distance increases and the occurrence of optical-electrical-optical regeneration points decreases. This thesis evaluates the impact of signal degrading effects that are becoming of increasing concern in all-optical high-speed networks due to all-optical switching and higher bit-rates. Especially group-velocity-dispersion (GVD) and a number of nonlinear effects will require enhanced attention to avoid signal degradations.

The requirements for optical performance monitoring features are discussed, and the thesis evaluates the advantages and necessity of increasing the level of performance monitoring parameters in the physical layer. In particular, a method for optical-signal-to-noise-ratio (OSNR) monitoring is proposed, which allows for improvements in dense WDM systems in terms of OSNR evaluation accuracy as well as increased signal performance. A GVD monitoring technique is likewise described and experimentally demonstrated in 40 GB/s return-to-zero (RZ) and non-return-to-zero (NRZ) systems.

Two techniques for signal quality monitoring are proposed. One method exploits a lower frequency reference signal to monitor signal degradations in a 40 Gb/s noise limited system. In a second method, an integrated all-optical bit-parity calculator is demonstrated using 10 Gb/s RZ data. The parity-calculator was realized using an all-active integrated SOA-based Mach Zehnder interferometer.

A method for signal quality optimization is proposed and demonstrated through both laboratory and field trial experiments. Signal quality optimization and signal quality monitoring was achieved using a subcarrier tone added to the 10 Gb/s NRZ data. Through launch power tuning to several spans, the signal quality could be successfully optimized.

Finally, the thesis presents two field trial demonstrations of Ethernet-over-fiber (EoF) transmissions. The all-optical transmission of 525 km though Den-

mark as well as a large scale GRID computing experiment concluded EoF an attractive alternative to SDH/SONET for cost-effective data transmission networks.

Dansk resumé

Denne tese omhandler studier lavet inden for signalkvalitetsovervågning i den næste generation af optiske netværk. Tesen fokuser på fuld-optiske netværk med bit-hastigheder på 10 Gb/s eller derover. Den næste generation af optiske netværk byder på store udfordringer da den tilbagelagte distance i det optiske domæne øges i forbindelse med at antallet af knudepunkter med mulighed for optiske-elektriske-optiske signalregenerering mindskes.

Tesen evaluerer følgerne af optiske signalforringende effekter, som vil få forøget betydning in fuld-optiske højhastigheds netværk på grund af optisk switching og højere bit-rater. Specielt viser det sig at gruppe-hastigheds-dispersion (GVD), polarisations dispersion effekter (PMD) samt ulineære effekter vil påkræve øget opmærksomhed, hvis signalforringelser skal undgås.

Kravene til funktionaliteterne i fremtidens signalkvalitetsovervågning diskuteres, og tesen evaluerer fordelene samt nødvendigheden af at forøge antallet af parametre, der overvåges i det fysiske lag. Ydermere præsenteres en metode til at overvåge det optiske signal-støj-forhold (OSNR). Metoden giver mulighed for at forbedre nøjagtigheden af OSNR målinger i bølgelænge-multiplexede (WDM) systemer kombineret med en forbedret signalkvalitet. En metode til dispersionsovervågning er ligeledes beskrevet samt eksperimentelt demonstreret i et 40 Gb/s return-to-zero (RZ) og non-return-to-zero (NRZ) system.

Tesen introducerer også to metoder til signalkvalitetsovervågning. Den ene metode udnytter et referencesignal med en lavere bit-rate til at monitorere signalforringelser i et støjbegrænset 40 Gb/s system.

To metoder til anvendelse i signal overvågning præsenteres. Den ene metode anvender et reference signal med lavere frekvens til at monitorere signalforringelser i et 40 Gb/s støjdomineret system. I den anden metode demonstreres en optisk integreret løsning til udregning af bitparitet af et 10 Gb/s RZ datasignal. Bitpariteten udregnes via et integreret Mach-Zehnder interferometer med aktive halvlederforstærkere (SOA).

En teknik til optimering af signalkvaliteten demonstreres via eksperimenter i både laboratoriet samt feltforsøg. Både monitorering samt optimering af signalk-

valiteten opnås ved at anvende en subcarrier adderet til 10 Gb/s NRZ datasignalet. Det vises at signalkvaliteten kan optimeres ved at tilpasse den optiske indgangseffekt til ét eller flere span i systemet.

Endelig præsenterer tesen to Ethernet-over-fiber (EoF) feltforsøg. Første del omfatter 525 km transmission gennem Danmark og gennemføres uden elektrisk konvertering af signalet. I anden del demonstreres et GRID netværkseksperiment i samme netværk. I tilfælde af billige data transmissions netværk, viser begge feltforsøg, at Ethernet-over-fiber kunne være et attraktivt alternativ til SDH/SONET.

Acknowledgements

A great thanks goes to my supervisor Lars Dittmann for providing me with the opportunity to work and study here at the Research Center COM for the past years as a Ph.D. student. Not to forget all the people in the Networks Group; No doubt, it has been a great experience, both in terms of professional life and social life. Acknowledgements and thank-you goes to my co-supervisors Christophe Peucheret and Mads Lønstrup Nielsen. With patience Christophe always had time for helpful talks, and Mads for invaluable advice and endless discussions about research as well as other topics.

Experiments in the lab went smoothly thanks to the assistance and collaborations with Christophe Peucheret, Leif Oxenløwe and Torger Tokle. I would especially like to thank Torger and Christophe, who have also shown good patience with me during VPI related discussions. Special thanks to Jacob Buron, Martin Nord and Mads Lønstrup Nielsen for the long nights in the lab, and also to Martin Brock and especially Mikkel Hasse Olesen for good collaboration during the lengthy field trials.

Especially I would like to thank the people who provided valuable suggestions in relation to my work on this thesis: Lars Dittmann, Mads Lønstrup Nielsen, Christophe Peucheret, Torger Tokle, Thomas Tanggaard Alkeskjold, and Michael S. Berger. I send my thanks to Peter Vingaard Larsen for the numerous late night dinners here at COM while both trying to wrap up each our thesis!

Now finally, I would like to send my warm thoughts to my parents who have always supported me in my doings and given me spirit to complete my Ph.D.

Martin Nordal Petersen

Chapter 1

Introduction

Since erbium doped fiber amplifiers became commercially available in the mid-nineties, optical communication has over the years revolutionized the world of communication [1]. Wavelength division multiplexing (WDM) and other high-speed bit-rate developments have opened up possibilities for a wide rage of broad band services for consumers. Whereas telephony was the main part of traffic across networks until around 2000, the vast majority of all transferred bits today constitutes Internet and data traffic [2]. The rapid growth in Internet users during the late-nineties, as well as a equally rapid growth in Internet based businesses, affected the telecommunication industry and great investments were made to assure the future capacity needs.

With the collapse of the "IT bubble" in 2000, the telecommunication industry suffered substantially, and the prospected developments in optical communication were at best put on hold. Several companies encountered massive layoffs whereas several start-ups were forced to completely shut down. There is a common agreement that the general expectations to the business and its growth had been vastly exaggerated and this in turn led to the great collapse [3], [4]. After years of status quo, new signs are now indicating a rising optimism although with a pace immensely different from what was seen prior to the collapse [5].

While the telecommunication community is slowly regaining momentum, the interest in new Internet based services with high bandwidth requirements is also increasing. Real-time video streaming such as High-Definition TV (HDTV), IP based TV (IPTV) and other high quality media services will eventually require both back-bone and access network capacities that exceeds what is currently available. The overestimated demand in the early part of this century led to an overcapacity in the networks, an overcapacity that seems to be depleting.

The back-bone technology in the current telecommunication industry is strongly dominated by the use of SDH and SONET [6]. These transport technologies

have since 1992 proven themselves very effective and reliable. However, as they surfaced about 13 years ago, SDH and SONET were developed with telephony being the strong force driving the development in structure and functionalities of the technologies. It is generally agreed that SDH and SONET are less than perfect transport technologies in a world dominated by data traffic rather than telephony. So a question arises as to whether or not SDH and SONET will prevail? Some believe that SDH and SONET still has a lot to offer, although in an improved *next-generation SDH/SONET* version [7], while others give credences to emerging technologies such as Ethernet-over-Fiber (EoF) [8].

Either way, a general consensus regarding the next generation optical networks is that, along with the bit-rates, the distance between regeneration nodes in the network will increase. This is made possible due to all-optical regeneration (3R) [9] and optical switching technologies such as micro electrical mechanical systems (MEMS) that can switch wavelengths all-optically through rotation of small mirrors [10], [11]. The full vision of the future optical network is an all-optical transparent network, where an end-to-end optical transmission of virtually all bit-rates, protocols and modulations formats is made possible.

In almost any optical communication system, performance monitoring plays an important and often vital role. System operators need to verify that the data arrives to its destination in a quality that meets prior arranged quality level agreements. SDH and SONET networks are generally considered very reliable, largely due to the comprehensive management and performance monitoring abilities built into the SDH/SONET structure. Thanks to bit-parity checking performed in the SDH/SONET regenerators, the bit-error performance can be effectively monitored [12]. Considering the prospective introduction of all-optical transparent networks, this model of performance monitoring becomes obsolete as the distance between optical-electrical-optical (O-E-O) regenerators substantially increases and all-optical 3R regeneration gains momentum. Keeping the signal in the optical domain for longer transmission distances introduces further implications that are magnified with an increase in bit-rates. Optical signal parameters such as group velocity dispersion (GVD), polarization mode dispersion (PMD), optical-signal-to-noise-ratio (OSNR) and nonlinearities will generally require much more attention to avoid signal impairments [1]. To overcome the potential problems in a future high-speed optical network, the traditional transport layer performance monitoring functionalities should be supported by monitoring of relevant performance parameters found in the physical layer [13], [14], [15].

This thesis will focus on performance monitoring done in the physical layer of all-optical transmission systems. This includes monitoring of specific parameters such as for example GVD and OSNR, but also signal quality monitoring based on bit-error-rate (BER) estimation and all-optical bit-parity calculation. The thesis

will treat performance monitoring in separate groups: a) Monitoring of signal parameters such as GVD, PMD and OSNR and b) Monitoring of signal quality using methods such as BER-estimation and bit-parity checking. The distinction is necessary, as each of the two types of monitoring will provide information from which only separate conclusions can be made. Group a) can provide information relating to the source of a signal degradation but not necessarily provide information about the signal quality itself. Likewise can the b) type monitoring provide more direct information about the signal quality but not the source of the problem.

Apart from proposing various performance monitoring technologies, the thesis will also discuss their need and requirements. Depending on the network specification, some types of performance monitoring can potentially be more appropriate than others.

Closely related subjects such as fault localization, forward-error-correction and network protection and resilience are not the focus of this work, and will thus not be discussed in detail. Furthermore, performance monitoring of optical packet switched networks is beyond the scope of this thesis, and will not be studied here.

1.1 Thesis structure

Chapter 2 will review the most relevant signal degrading effects that need to be considered for all-optical high-speed networks. The chapter includes experimental investigations of a number of the effects.

Chapter 3 will introduce performance monitoring in general terms, and identify the need for including more advanced types of performance monitoring in the physical layer. The specific requirements to what performance parameters should be considered, will be discussed.

Two optical signal quality monitoring techniques are proposed in Chapter 4. Experimental results will be presented for signal quality monitoring of noise limited systems and all-optical bit-parity calculations.

Chapter 5 deals with monitoring of optical signal parameters. A method for dispersion monitoring in non-return-to-zero (NRZ) and return-to-zero (RZ) systems using side-band filtering is proposed. By carefully selecting the optical filter de-tuning, the filtered signal was related both to residual dispersion as well as signal quality. Chapter 5 also presents an OSNR monitoring technique based on polarization interleaving channels in a WDM system. The method is useful for dense WDM systems where OSNR measurements can otherwise be impossible.

The launch power to the optical fiber has a major influence on the signal quality due to nonlinearities excited at high input powers. Chapter 6 proposes

a method for optimizing the signal quality in multi-span optical systems by optimizing the launch power. The optimization is achieved by successfully relating the power of an in-band subcarrier tone to the signal quality. Due to nonlinearities in the system. the dispersion map proves to have significant influence on the results. Cases of pre-, post-compensation and residual dispersion are investigated.

Chapter 7 discusses a potential development in next generation optical networks. Ethernet-over-fiber has been suggested as transmission layer technology, being very data-efficient. Ethernet, however, does not provide any native means of performance monitoring as well as protection and guarantees, in contrast to SDH/SONET. The chapter also describes two Ethernet-over-fiber field trials in the Danish Research Network.

Chapter 8 closes the thesis with a conclusion.

Chapter 2

Signal degrading effects in optical communication systems

Optical communication is a technology that requires a broad knowledge about the physical effects governing the transmission of signals in single mode fibers (SMF). In short range or low bit-rate optical communication systems, the range of problems that can arise are smaller when compared to long range and high bit-rate systems. A number of optical effects can be identified as the main contributors to limiting the bit-rate and transmission distance. These effects will seriously degrade the signal if certain precautions are not taken.

This chapter will give an introduction to various signal degrading effects playing a significant role in long-haul or high bit-rate systems. Where relevant, recent and current work within the field regarding monitoring of a specific parameter or effect, will be shortly discussed.

2.1 Noise

The accumulation of noise is one of the major concerns in optical transmission systems. Spontaneous emission is an inevitable physical effect that takes place in all optical amplifiers [16], [17]. The photons emitted by spontaneous emission are in turn amplified in the amplifier leading to amplified spontaneous emission (ASE). The amount of ASE added to a signal in each amplifier is strongly dependant on the power of the signal entering the amplifier, such that a weak signal will give rise to more ASE generated than a relatively stronger signal will.

Although many precautions and improvements can be made to reduce the impact of noise in an optical system, ASE will inevitably add to the signal and in turn limit the transmission distance. The potential impairments of noise can be reduced by optical filtering underway to avoid gain saturation caused by ASE

power. Optical filtering prior to detection in the photodiode is also practised to reduce signal-to-noise (SNR) degradations in the receiver. If this is not done, beating between the noise and the signal will lead to a power penalty in the system.

2.1.1 Quantifying the noise in the system

The optical-signal-to-noise-ratio (OSNR) is an often used parameter to quantify the amount of noise in an optical communication system. OSNR is defined as the ratio between the power in the optical signal and the in-band noise and is usually measured in dB's as illustrated in Figure 2.1a). The OSNR has a major influence on the BER, and if the system performance is dominated by noise and thus OSNR degradation, the BER and the OSNR will be correlated. Figure 2.1b) shows the development in BER as the OSNR changes. The figure has been generated through a VPI simulation[1] on a 40 Gb/s NRZ system using a pre-amplified receiver. For this particular system, an OSNR of at least 22 dB is needed to assure a BER performance of $1{\cdot}10^{-9}$. It is not unusual to see OSNR values of 45-55 dB right after the transmitter, and this will drop throughout transmission as noise is added to the system in each amplifier stage.

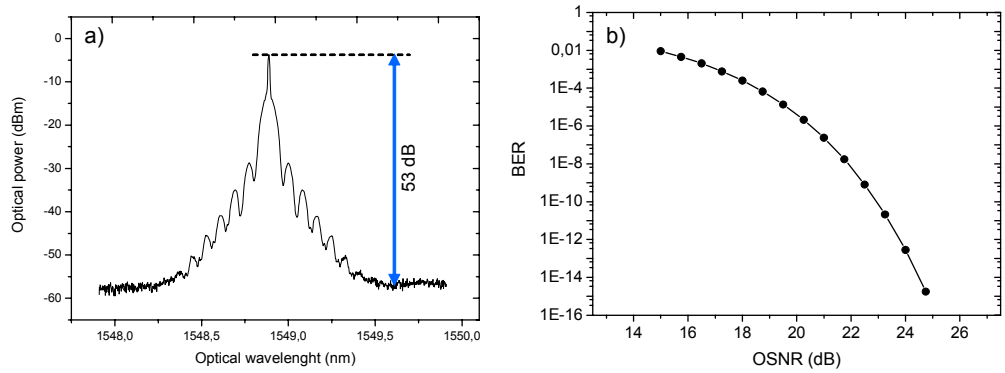

Figure 2.1: a) Illustration of the conventional method used for OSNR measurements. The spectrum is from a 40 Gb/s NRZ experiment. b) BER versus OSNR for a VPI simulated 40 Gb/s NRZ system. The OSNR is varied by varying the signal input power to an EDFA.

When quantifying OSNR, it is important to specify the spectral resolution bandwidth used in the measurement as this will have an effect on the OSNR value. 0.1, 0.5 nm and 1.0 nm are common values, and in Figure 2.1a) a resolution bandwidth of 0.1 nm was used whereas 0.5 nm was used in Figure 2.1b). Strictly, a 40G signal cannot be measured in a 0.1 nm (12.5 GHz) resolution bandwidth, and

[1] VPI Transmission maker version 6.5 was used for the simulations. More details on the model can be found in Appendix B.

the resulting OSNR will be underestimated. However, a resolution bandwidth of 0.1 nm will still provide valuable information about the system, and it is chosen here to comply with results later in the thesis.

2.1.2 Problems when measuring OSNR

Several problems can arise when trying to measure the OSNR in a WDM system. Normally the OSNR evaluation is done by assuming that it is possible to interpolate the background noise level within a channel to the noise level next to the channel as illustrated in Figure 2.1a). Measuring the channel power and the power beside the channel thus provides the OSNR. This method, however, becomes problematic in WDM systems as well as single channel systems in some cases:

1. In single channel systems, optical filtering will suppress the noise level, which leads to a wrong estimation of the accumulated in-band noise.

2. In a WDM system, when a channel is demultiplexed, the suppression of the noise beside the demultiplexed channel leads to an artificially lower noise level and, similar to case 1, to a wrong evaluation of the in-band OSNR.

3. In dense WDM systems a very high spectral resolution is needed to resolve the noise levels between two neighboring channels. If the channels are placed close, the side bands of two neighboring channels will overlap, making it impossible to estimate the noise level even with very high spectral resolution. This issue will be further discussed in Chapter 5.

The first two points are illustrated via Figure 2.2a). The spectrum shows a case where one channel has been demultiplexed using a 0.6 nm triple stage optical band pass filter. In the experiment, three channels with a 100 GHz spacing were transmitted over three dispersion compensated spans of 80 km each. Due to loss in the dispersion compensating fiber (DCF) modules as well as transmission fiber loss, the signal passes through as much as 7 erbium doped fiber amplifiers (EDFA) underway, which all add noise. Referring again to Figure 2.2a), the demultiplexing clearly rejects the neighboring channels as well as the noise. Using the method illustrated in Figure 2.1a) would not yield a good OSNR evaluation. This is equivalent to a single channel system where an optical filter is used to remove out-of-band ASE from the spectrum. The situation would resemble that shown in Figure 2.2a) where a shaping of the noise has occurred. Although a broader filter, such as 1.5 nm, would be used in a single channel system the filter still shapes the spectrum to a degree making the OSNR evaluation inaccurate.

Figure 2.2b) illustrates the amount of in-band noise collected during the transmission over three 80 km spans. The center channel has simply been turned off but the de-multiplexing filter is still used, hence the spectral shaping. This illus-

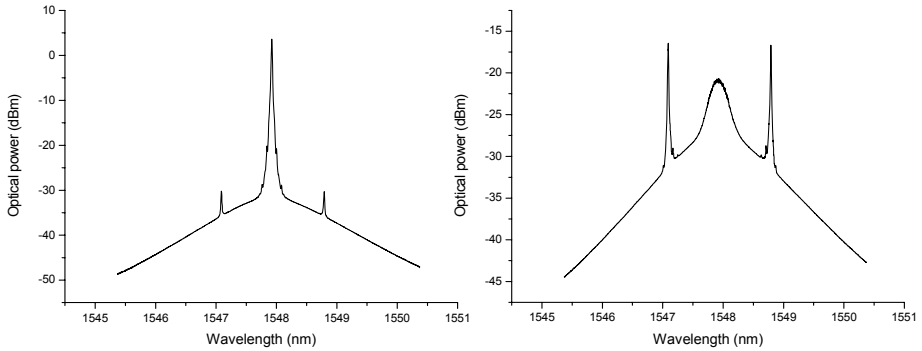

Figure 2.2: The figures show the optical spectra of a 3 channel system transmitted 3 × 80 km. Left: System with all three channels turned on. Right: Center channel is turned off, showing the collection of noise during transmission.

trates the problem of using the interpolation method as the amount of collected in-band ASE is very different from the noise level found next to the channel.

Noise is definitely an important issue in optical communication systems, and with the growing wish for keeping the signals longer in the optical domain this seriously suggest the use of OSNR monitoring.

Several alternatives to the rather simple interpolation method have been developed, but most attention has been given to a method using polarization extinction. While the data signal remains almost 100% polarized, ASE is randomly polarized. Using this fact, M. Rasztovits et al. [18] have developed a method that can reveal the OSNR more accurately in such problematic cases as just described. When passing the signal through a rotating polarizer, the minimum power reading will represent a spectrum without the signal which also corresponds to half of the total ASE power. The maximum reading will mainly hold the signal power, and together these maximum and minimum readings will provide the OSNR. Several other OSNR monitoring techniques have spawned from this, for example OSNR monitoring using Stokes parameters or the degree of polarization (DOP) [19]. In fact has Teralink Communications Inc. developed an optical spectrum analyzer that is capable of measuring the "true OSNR" through the use of polarization filtering. Another method uses polarization nulling [15]. Both are based on the principle described in [18]. The principle of polarization extinction has inspired another OSNR monitoring technique which will be presented in Chapter 5.

2.2 Group velocity dispersion

Almost all optical fibers used today, exhibit group velocity dispersion (GVD). Group velocity dispersion, which will be denoted *dispersion* from here on, means that the various frequency components in the signal will travel at different speeds, and thus disperse. Said in another way, the phase changes experienced by a certain frequency component will vary depending on the frequency. As a data signal contains a spectrum of frequency components this means that they will arrive at different times or with different phase changes at the destination. The direct outcome of this is a change in pulse shape; a dispersed pulse as illustrated in Figure 2.3.

The pulse broadening can lead to pulse overlap within the bit-slots and this in turn leads to bit errors. In many cases dispersion can be successfully compensated using DCF, which have a dispersive effect opposite to that of standard SMF and thus return the pulse to its original form.

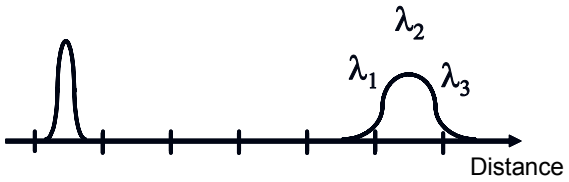

Figure 2.3: Due to dispersion in the fiber, some parts of the pulse will travel faster than others and therefore the pulse will disperse.

First order dispersion can be described through the following formula [1]:

$$D = -\frac{2\pi c^2}{\lambda^2}\beta_2 = -\frac{2\pi c^2}{\lambda^2}\frac{d^2\beta}{d\omega^2} \tag{2.1}$$

where c is the speed of light, λ and ω are the wavelength and the angular frequency, respectively, of a spectral component, $\beta_2 = \frac{d^2\beta}{d\omega^2}$ is called the GVD parameter and β is the propagation constant. D is usually in the range of 15-17 ps/nm/km for standard SMF and for DCF, typical value are around -90 to -100 ps/nm/km [20].

Dispersion is not a big issue in low bit-rate optical systems as these signals can be transmitted very long distances before dispersion begins to severely influence the signal quality. At 2.5 Gb/s for example, the 1 dB penalty dispersion limit is around 1000 km [21], so dispersion compensation is rarely needed for these bit-rates. Today, when systems are transmitting at bit-rates exceeding 10 Gb/s, dispersion becomes of much bigger concern. A NRZ coded 40 Gb/s signal, for example, can only sustain about 70 ps/nm of accumulated dispersion in order

to stay below a 1 dB penalty limit. This indicates that it is very important to manage the accumulating dispersion in high-speed transmissions properly.

There exist various examples of cases that can lead to imperfect compensation of dispersion in optical communication systems:

- Dispersion variations caused by temperature changes are often brought forward as a serious issue in future high-speed all-optical networks [22], [23]. For SMF, the thermal coefficient is about -0.0025 ps/km/nm/^{o}C [24]. Although this value might seem small, it can lead to significant dispersion variations in high-speed long-haul transmissions [21].

- In optically re-configurable networks the signal can be optically switched through various paths with various dispersion characteristics. If each part of the network is not 100% link compensated, this could lead to residual dispersion depending on the switched path.

- Imperfect slope compensation. The dispersion slope for a fiber refers to the wavelength dependant dispersion parameter. Due to the dispersion slope in a fiber, different WDM channels will accumulate different amounts of dispersion. In high-speed WDM systems it is crucial to use DCF with a dispersion slope that matches that of the transmission fiber in order to make sure that all channels are compensated appropriately. Additionally, the dispersion slope can change over time due to for example fiber replacements where the newly installed fiber does not have the same dispersion slope properties. In conclusion, WDM systems spanning over large spectral ranges constitute a complicated challenge in fully avoiding residual dispersion.

All these examples can lead to considerable penalties in high speed optical communication systems if not handled in the right manner. A way to overcome the issue of residual dispersion is by applying tunable dispersion compensation, which can be done e.g. via tunable fiber Bragg-gratings [25] or etalon all-pass filters [26]. However, in order to track the dispersion variations and compensate them accordingly, a suitable method for dispersion monitoring is necessary.

Numerous methods for dispersion monitoring have been developed and only a few will be mentioned here. Dispersion monitoring is often based on a method that enables detection of phase changes between two spectral components. This can for example be realized by monitoring the relative phase shift between two WDM signals [27] or by adding a subcarrier tone and subsequently detecting the phase changes of the subcarrier side bands that have a well-defined frequency separation. This phase change can be detected either via filtering out the subcarriers

and detecting them [28] or via RF fading of the subcarrier tone due to dispersion [29], [30]. The last mentioned method using RF fading to monitor residual dispersion is also sensitive to polarization mode dispersion and nonlinearities, which can be a problem in high power or PMD influenced optical systems. The sensitivity of this method towards nonlinearities has been used in Chapter 6 to develop a method for launch power optimization. Another promising dispersion monitoring technique applies phase-modulation-to-amplitude-modulation (PM-AM) conversion where a weak phase modulation is induced to the optical carrier [31]. Via the effectiveness of PM-AM conversion, which is controlled by the accumulated dispersion in the system, the residual dispersion can be quantified. This method is less sensitive to PMD and nonlinearities [21], and is thus an interesting alternative to the above mentioned subcarrier based methods. The mentioned technologies all rely on adding an external signal, a subcarrier modulation or phase modulation, which in turn functions as a dispersion sensor. Adding external signals is not without complications, and can bring about considerable cost as well as cause signal impairments. A method has also been developed that uses no external signal modulation, and thus no transmitter modification is needed. It is based on clock regeneration and clock fading in NRZ and RZ coded systems [32], [33]. Pulse distortion due to dispersion causes the clock component to be either regenerated or faded in NRZ and RZ systems respectively. The clock component can be detected and a correlation to the residual dispersion can be made. Although this method is also sensitive to PMD, it is still attractive as no transmitter alterations are necessary, thus allowing a relatively easy implementation.

Although dispersion constitutes a problem in high-speed optical communication systems, it can help to reduce other signal impairing effects. The walk-off effect that dispersion brings about, helps to significantly reduce cross phase modulation (XPM) in WDM systems [1]. Furthermore, the pulse broadening effect of dispersion decreases the effect of self phase modulation (SPM), which is strongly dependant on the pulse peak power [1].

2.3 Polarization mode dispersion

Polarization mode dispersion (PMD) is another effect that can lead to signal distortions in high-speed optical communications systems. PMD is caused by birefringence in optical fibers that has its origin in small departures from the perfect cylindrical symmetry in the core. The fiber birefringence leads to two orthogonal polarization modes being supported in the fiber, each with slightly different group velocities. When an optical signal is launched into the fiber and both modes are excited, the pulse will disperse as illustrated in Figure 2.4.

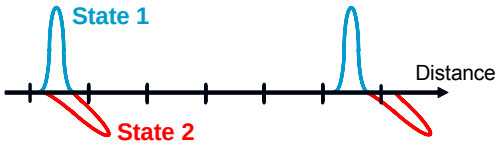

Figure 2.4: PMD in a birefringent fiber causes pulse dispersion due to different group velocities associated with each polarization mode.

The delay induced between each orthogonal polarization state of the signal can be quantified through the differential group delay (DGD). Figure 2.5 shows the induced effect of 20 ps and 40 ps DGD on a 10 Gb/s NRZ signal. Note how the signal almost separates into two different components when the DGD becomes large. At DGD values as large as 40 ps the 10 Gb/s signal will be severely impaired and most probably impossible to recover.

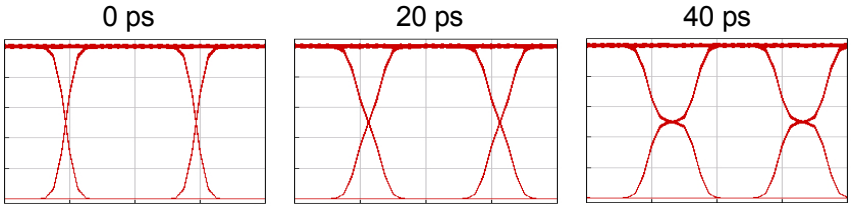

Figure 2.5: The figure illustrates the effect of DGD on a 10 Gb/s NRZ data signal eye diagrams. The results are from a VPI Transmission Maker 6.5 simulation. The horizontal time frame duration is 250 ps in each image.

Unlike group velocity dispersion, PMD is of statistical nature and is therefore non-trivial to characterize. The statical nature of PMD arises from random coupling between the two modes induced by various perturbations throughout the fiber. Non-uniform fiber geometry, fiber splices, bending of the fiber and temperature variations will all change the PMD in the system, so only an average value can be given for the PMD. D_p is the PMD parameter and $D_p \approx \sigma_T/\sqrt{L}$, where σ_T is the root-mean-square (RMS) value of the DGD value over a fiber of length L. D_p can be used to characterize a fiber, and usually has values under 0.1 $ps/\sqrt{km}$ for modern fibers. Old fiber types, however, can have PMD values exceeding 1 $ps/\sqrt{km}$ in which case high-speed systems can face a PMD problem. Notice though that the PMD parameter is only an average value, and DGD values much higher can be observed occasionally.

PMD has been a popular subject the last years, and a lot has been written in terms of PMD being a serious obstacle in real-life systems or not. In today's communications systems, which are mostly running at 10 Gb/s and below, PMD is not considered a problem, but increasing the distance between 3R regeneration points as well as increasing the bit-rate can possibly make PMD an issue that

needs to be dealt with. Some still argue that modern fiber types with PMD parameters below 0.1 $ps/\sqrt{km}$ virtually remove the issue from most practical systems [34], [35]. However, as mentioned, old fiber types can have much higher D_p values and, in the case of system upgrades to higher bit-rates on existing fibers, PMD could become an issue.

PMD monitoring techniques have been developed, although PMD impaired signals can be difficult to rectify in terms of compensation. In the case of first-order PMD, which is described above, the principle state of polarization (PSP) and the DGD are assumed constant within the signal bandwidth. This simplifies the problem considerably in terms of PMD compensation [36]. In the higher-order PMD description, the PSP and DGD cannot be assumed constant, and an analytical description is non-trivial [37], [35]. Methods exist both for monitoring first-order PMD [14] as well as higher-order PMD [38], although first-order PMD monitoring techniques are more represented. Extensive research has already been conducted within this field and, as mentioned in the introduction, PMD monitoring has not been the focus of this thesis and a further detailed description of the subject will not be given here.

2.4 Fiber nonlinearities

Fiber nonlinearities are an important matter in optical communications that find use in, for example, pulse compression [39], Raman amplifiers [40] as well as wavelength conversion [41] but can also severely damage an optical signal. Fiber nonlinearities includes several effects: Self phase modulation (SPM), cross phase modulation (XPM), four wave mixing (FWM), stimulated Raman scattering (SRS) and stimulated Brillouin scattering (SBS) are considered the most important ones considering signal impairments. The next sections will briefly describe the influence of these nonlinear effects in today's optical communication systems.

2.5 Self phase modulation

The frequency dependence of the refractive index leads to dispersion in optical fibers as described above. Due to the non-zero third-order susceptibility, $\chi^{(3)}$, in silica fibers, the refractive index is also dependant on the optical power giving rise to phase changes, hence spectral broadening of the signal. As the signal itself causes these phase changes the effect is called self-phase-modulation (SPM), which can be described through [42]:

$$\phi_{NL} = \gamma P_{in} L_{eff} \tag{2.2}$$

where ϕ_{NL} is the phase change caused by a signal with input power P_{in}. γ is the nonlinear coefficient of the fiber and $L_{eff} = [1 - \exp(-\alpha L)]/\alpha$ is the effective length of the fiber with length L and loss coefficient α. ϕ_{NL} remains constant if the power in the fiber remains constant, but this is not the case in intensity modulated systems so in practise ϕ_{NL} varies with time, effectively frequency chirping the pulses in the data signal. Note that the intensity changes giving rise to ϕ_{NL} are related to the pulse shape and pattern of the signal making it difficult to predict the resulting phase changes of the signal. In itself, SPM does not cause any signal degradation, but through dispersion, the phase changes lead to a change in the pulse shape, which can result in severe signal impairments. As SPM depends on the pulse peak power, dispersion and SPM will interact with each other so a parameter N can be defined that describes which is the dominating effect:

$$N^2 = \frac{L_D}{L_{NL}} = \frac{\gamma P_{in} T_0^2}{|\beta_2|}$$

where L_D and L_{NL} are the dispersion length and nonlinear length, T_0 is the pulse width[2] and β_2 is the dispersion parameter defined in Equation 2.1. In regimes where dispersion is the dominating effect $N << 1$ and if SPM dominates $N >> 1$.

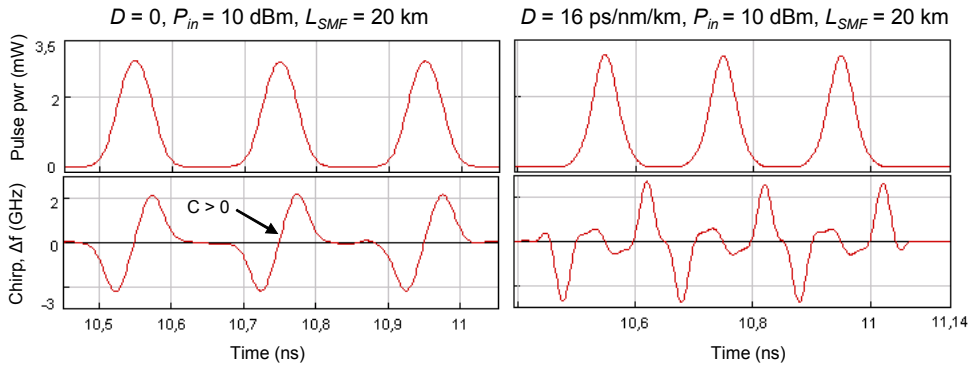

Figure 2.6: 10 Gb/s RZ pulses after 20 km transmission without dispersion (*left*) and with dispersion (*right*). The input power to the fiber is 10 dBm and the nonlinear index of the fiber is $2.6 \cdot 10^{-20}$ m^2/W.

Normally in communication systems $N << 1$ such that dispersion dominates. However, if the launch power increases or the pulse width decreases to make $N \simeq 1$ this means that SPM and dispersion will both influence the pulse shape. In the normal regime ($\beta_2 > 0$) SPM will cause a more rapid broadening of

[2]Note that T_0 is of mostly theoretical interest as it accounts for single pulse studies.

the pulses compared to the case where only GVD broadens the pulse. In the anomalous regime ($\beta_2 < 0$) SPM induces a positive chirp ($C > 0$) to the pulse whereas the GVD induced chirp is negative and this in conclusion can lead to a initial pulse compression; the same effect is exploited in soliton systems[3]. Figure 2.6 illustrates this effect. Pulse shape and chirp is shown for a 10 Gb/s RZ pulses transmitted over 20 km with a fiber input power of 10 dBm. The left figure shows the a case where without dispersion, $D = 0$, and the positive chirp is pointed out. In the right figure, $D = 16$ ps/nm/km and the chirp is clearly affected. Notice how the pulse shape is sustained due to interactions between dispersion and SPM induced chirp.

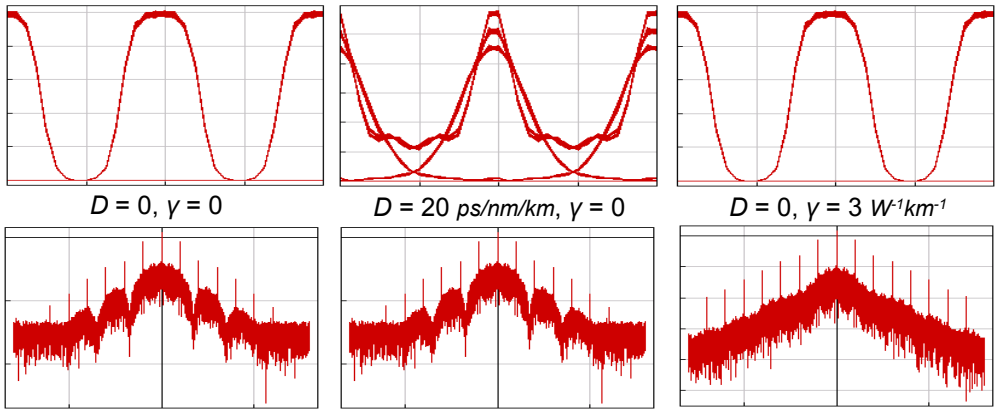

Figure 2.7: Simulations of a 10 Gb/s RZ system where SPM and dispersion have been turned on and off to illustrate their effect on the eye diatram and optical spectrum. The input power to the 20 km fiber span is 12 dBm in all cases.

Figure 2.7 shows various combinations of dispersion and SPM in terms of pulse shape and optical spectrum. The figure illustrates what influence dispersion alone and SPM alone, has on the eye diagram and the optical spectrum. Notice how dispersion alone will cause pulse shape changes while leaving the optical spectrum unchanged whereas SPM alone only broadens the spectrum and leaves the pulse shape intact.

Figure 2.8 illustrates the SPM-dispersion interaction dependence on the magnitude of the dispersion parameter. If D is high, the pulses will quickly broaden and thus lead to less SPM phase changes as a direct consequence of Equation 2.2. On the other hand, a low D value will lead to more spectral broadening as the peak power of the pulses will only slowly decrease throughout transmission. At low input powers, dispersion will dominate and optimal signal quality will be found at zero residual dispersion. At high input powers, where SPM effects

[3]By *SPM induced positive chirp* is meant that the main part of the pulse is exposed to a positive chirp as can be seen in Figure 2.6. This holds true only for RZ pulses.

become significant, the optimal amount of residual dispersion will vary with the input power due to this SPM-dispersion interaction [43].

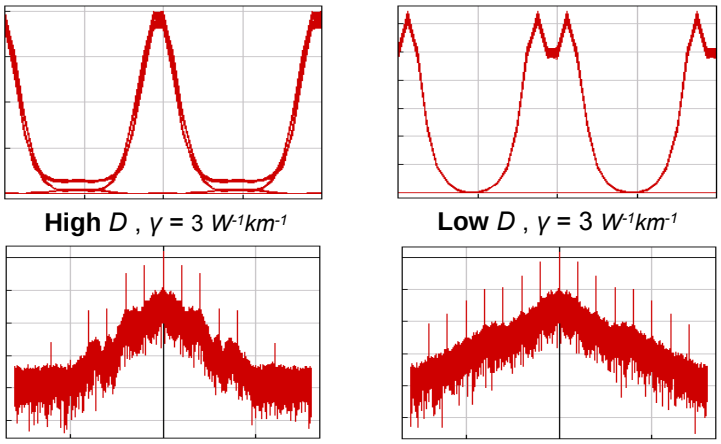

Figure 2.8: VPI simulations of a 10 Gb/s RZ system illustrating how the SPM-dispersion interaction is dependant on the dispersion parameter. The input power to the 20 km fiber span is 12 dBm in all cases.

SPM-dispersion interactions can also be exploited to achieve a higher launch power and thus higher transmission distance if the signal is initially launched to a DCF fiber, a so-called pre-compensation dispersion map. Chapter 6 will show examples of this effect where the signal quality is optimized through the launch power and thus exploiting the normal dispersion regime in the DCF fiber. Initially transmitting the high powered signal through the DCF fiber leads to broadening of the spectrum as well as the pulse. Combined with the further transmission through SMF (anomalous dispersion regime) the pulse in turn re-shapes to the initial form. The extra pulse broadening caused by SPM in the DCF requires a relatively longer SMF span afterwards to compensate for it and thus an increased transmission distance is achieved. Note however that the phase changes caused by SPM cannot be assumed to be linear with respect to frequency like the phase changes caused by dispersion, and can therefore not be completely compensated by dispersion in the SMF, which in turn limits the launch power.

A way of monitoring SPM in an optical network is to monitor the nonlinear phase shift ϕ_{NL}, which depends on factors such as coding type, pulse shape, modulator chirp and data pattern. Due to all these factors, the phase changes will vary along transmission, which makes ϕ_{NL} insufficient for use as a measure for SPM. As SPM leads to spectral broadening, the optical spectrum could possibly provide some information regarding the degree of SPM influence. Although SPM can be measured somehow, the information might not be of much use as the effect of SPM on the signal quality will depend on factors like dispersion map, residual

dispersion, power variation throughout the fiber, and again the mentioned pulse shape characteristics. Monitoring of SPM induced changes should instead be done by Q-factor monitoring or by inspecting the pulse shape or eye diagram of a signal [44], [45].

2.6 Cross phase modulation

Cross-phase-modulation (XPM) is always accompanied by SPM and the physical origin of the two is indeed the same. Where SPM arises from the intensity dependant refractive index being modulated by the signal itself, XPM denotes the refractive index variations caused by other channels being transmitted simultaneously at other wavelengths. This means that the nonlinear phase shift in a channel is not only dependant on the intensity in the channel itself, but also depends on the co-transmitted channels. The total nonlinear phase shift induced in a specific channel is thus a combination of SPM and XPM:

$$\phi_{NL} = \phi_{SPM} + \phi_{XPM} = \gamma L_{eff} \left(P_0 + 2 \sum P_m \right)$$

where P_0 is the power of the channel itself and P_m is the power of the m^{th} co-propagating channel. Notice that XPM is independent of wavelength i.e. channel separation and also that XPM is twice as effective as SPM for the same optical input power. Although XPM is wavelength independent, it is influenced by the walk-off time between the signals which is governed by the group-velocity mismatch. Although fiber dispersion can be effective in reducing XPM in WDM systems, XPM is often the factor limiting the launch power when many channels are co-transmitted [46]. The relatively new non-zero-dispersion-shifted-fiber (NZDSF), which have low D values, can give rise to XPM if the channels are transmitted together in for example a 100 GHz spacing grid [47]. XPM in turn leads to spectral broadening like SPM, which can result in pulse shape distortions and thus signal impairments.

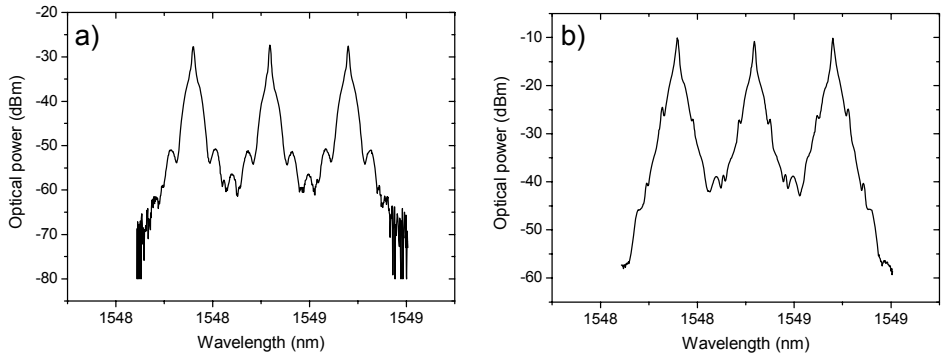

Figure 2.9: Optical spectra of a 3 channel system with 50 GHz spacing after 3×80 km dispersion compensated spans. a) 5 dBm launch power, b) 14.5 dBm launch power to the SMF. Notice the spectral broadening due to SPM and XPM.

Figure 2.9 shows the optical spectra from an experiment with a 10 Gb/s NRZ signal that has been transmitted through three spans of 80 km SMF. The total input power is a) 5 dBm and b) 14.5 dBm and no de-correlation fiber was used to emulate the worst possible situation for exciting XPM[4]. The spectral broadening is caused by a combination of SPM and XPM.

2.7 Stimulated Raman scattering

Stimulated Raman scattering (SRS) is another nonlinear effect that can lead to signal degradation in WDM systems. The effect is related to scattering of a photon by a molecule to a lower frequency photon. The consequence of SRS is that one channel in a WDM system can effectively transfer optical power to another channel when both simultaneously carries a one-bit. Not only does this lead to a power loss of the pumping channel, but it also leads to cross-talk distortions of the channel being pumped [48], [49]. SRS is of most concern in WDM systems, as the Raman threshold is very high for single channel systems [42].

Because Raman scattering is a broad band effect, it also has applications for optical amplification in long-haul high bit-rate systems [40], [50]. In Raman amplified systems, a lower wavelength pump laser is used, and via SRS, power is transferred from the pump signal to the data signal.

The detrimental effects of SRS are controlled to a large extent by factors such as bit-rate, SPM as well as group-velocity mismatch between the channels

[4]De-correlation fiber is often used in laboratory experiments as the same modulator is used to modulate all channels. If the channels are not de-correlated, the resulting XPM impairments would only represent the worst possible case.

in question and can thus offer certain challenges in terms of predicting the impact of SRS.

SRS is not a typical effect that is attractive to monitor as most systems are pre-designed to avoid SRS implications and, for most systems, XPM is usually of greater concern. One of the effects of SRS is to cause a power tilt in WDM systems due to lower wavelength channels loosing power to higher channels. This can though be rectified through channel power equalization in the amplifier stages. On the other hand is the crosstalk effect of SRS an effect that is preferably avoided as it cannot be compensated.

2.8 Four wave mixing

Like SPM, four wave mixing (FWM) is a parametric effect that has its origin in the non-zero third-order susceptibility, $\chi^{(3)}$, for silica fibers. If a number of signals are co-propagating in a fiber, FWM can give rise to new signals at new wavelengths. FWM can be a serious problem in WDM systems where the channels are spaced with equal frequency spacing, as the FWM-generated signals can have wavelengths coinciding with co-propagating channels. Apart from channel spacing, other factors also have to be met in order for FWM to be significant. A phase matching condition has to be satisfied between the channels in order for the FWM products to successfully form. Dispersion successfully limits FWM so nearly dispersion free fibers can constitute problems if used for WDM transmissions [51], [52]. Figure 2.10 shows the result from a 10 Gb/s NRZ transmission of three channels with 50 GHz spacing. The channels were transmitted over three spans of 80 km SMF with corresponding dispersion compensation.

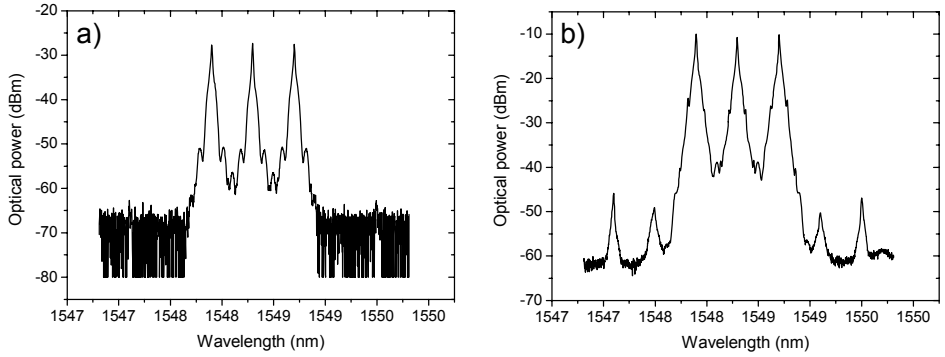

Figure 2.10: Optical spectra of a 3 channel 3×80 km span system with 50 GHz spacing. a) The input power is 2 dBm, b) The input power is 20 dBm.

In Figure 2.10 a) is shown the spectrum for a launch power of 2 dBm to each span, and Figure 2.10 b) the same spectrum for a launch power of 20 dBm.

It is clearly seen how FWM products are formed at the high input power at frequencies ± 100 GHz and ± 200 GHz relatively to the center channel. These FWM products would have caused cross-talk and severe signal impairments if other channels had been present at these wavelengths.

Similarly to SRS, FWM will not be discussed further in depth as FWM effects have not been the focus of investigations in this thesis.

2.9 Stimulated Brillouin scattering

Stimulated Brillouin scattering (SBS) has been studied relative extensively due to its importance in a method for signal quality optimization described in Chapter 6. SBS is a nonlinear scattering effect similar to SRS in many aspects. While optical phonons participate in the process of SRS, acoustic phonons are involved in the case of SBS. In SBS, the pumping wave generates an acoustic wave through electrostriction [53]. The travelling acoustic wave modulates the refractive index, which leads to a backward scattered wave similar to the case of a diffraction grating. SBS is, unlike SRS, a very narrowband effect that is only effective on signals less than 100 MHz wide, and the downshift in frequency associated with SBS is in the order of 11 GHz for silica fibers at 1550 nm. Figure 2.11 illustrates the SBS process showing the backward travelling Stokes wave in the fiber together with a spectral representation.

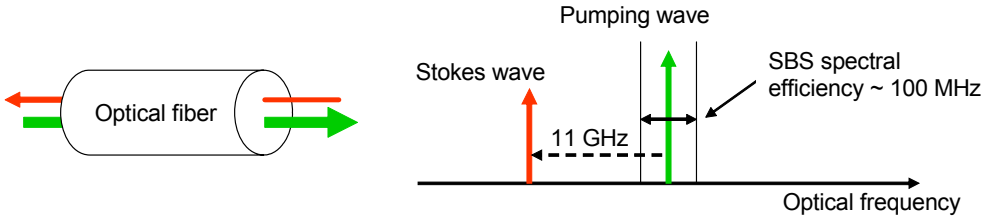

Figure 2.11: Illustration of the SBS process resulting in a backward travelling Stokes wave. The SBS spectral efficiency is the bandwidth in which SBS is effective. In Brillouin amplifiers this is also referred to as the SBS gain bandwidth.

SBS is usually not considered a big issue in high-bit rate systems as the SBS threshold can be increased by increasing the signal line width, but as will be seen in Chapter 6, it can contribute strongly in limiting the performance of 10 Gb/s systems. The degradation caused by SBS is mainly related to power loss of the signal, rather than crosstalk, as the Stokes wave involved in SBS is backward scattered. However, in more extreme cases, the backward travelling Stokes wave can itself be SBS scattered and thus turn up travelling forward within the data-band of the original signal. It is also reported in [54], how SBS can cause intensity noise in optical transmission systems.

2.9.1 Experimental investigations of SBS scattering

The setup shown in Figure 2.12 was used to experimentally investigate the impact and effects of SBS in a 80 km SMF post-compensated link for a 10 Gb/s NRZ modulated system, as well as for a system using subcarrier amplitude modulation of the optical carrier. Subcarrier modulated systems have previously been reported to be vulnerable towards SBS due to the often low subcarrier bandwidths as well the non-modulated narrow optical carrier [55], [56], [57].

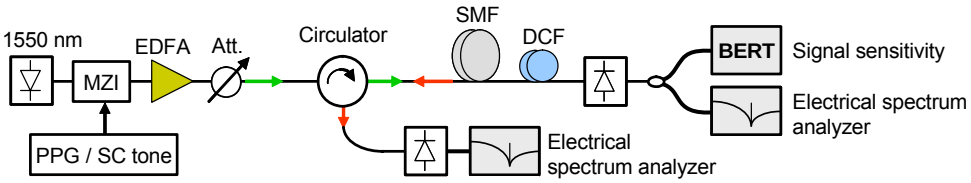

Figure 2.12: Experimental setup used for SBS investigations.

The key component in the setup is the circulator, which enables the separation of the forward and the backward travelling signals. The signal, either a 10 Gb/s NRZ data signal or a 3 GHz subcarrier tone modulated signal, is amplified and transmitted through 80 km SMF followed by a DCF module whose dispersion is closely matched to that of the 80 km SMF span. The forward travelling signal continues to a photodiode, which is followed by a bit-error-rate-test-set (BERT) and an electrical spectrum analyzer (ESA). The backward travelling signal is separated using the circulator, and also sent to an ESA.

Figure 2.13 shows the electrical spectrum for two different cases of a transmission experiment. The left spectrum shows the electrical spectrum of the backward travelling signal in the case of a 10 Gb/s NRZ signal with 0 dBm input power to the SMF. The little insert in the spectrum shows a part of the original forward travelling data spectrum with a 10 GHz clock component, denoted "C", clearly visible. Due to reflections from connectors and fiber splices, this clock component is also visible up in the reflected spectrum; the peak at "D". More interesting are the two points "A" and "B". "A" is the reflected carrier. The carrier is backward scattered via SBS and "B" is the backward travelling Stokes. The Brillouin shift, ν_B, can be observed to be approximately 10.84 GHz. The Stokes wave is downshifted in optical frequency, but ends up at +10.84 GHz, seen relative to the carrier, in the electrical spectrum due to beating in the photo diode. It is interesting that SBS is already observed at 0 dBm input to the fiber, much earlier than any SPM effects can be observed. However, although SBS is observed, it has no influence at the signal quality at 0 dBm input power.

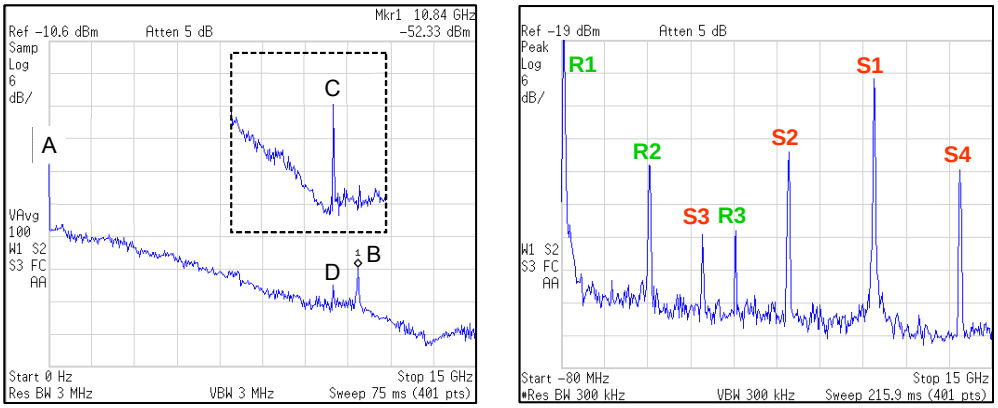

Figure 2.13: Electrical spectra from an experiment where optical signals were transmitted over 80 km SMF. The figure illustrates the effect of SBS. *Left:* The backward travelling signal when a 10 GB/s NRZ signal is launched at 0 dBm. *Right:* A 1550 optical carrier is subcarrier modulated with a 3 GHz tone and launched at 9 dBm.

The right spectrum in Figure 2.13 shows the electrical spectrum from a transmission experiment using only a 3 GHz subcarrier modulation of the carrier. Again the spectrum shows the backward travelling components of the signal. The input power to the 80 km SMF fiber span was 9 dBm.

Several frequency components can be observed in the spectrum. R1, R2, and R3 all denotes originally forward travelling components, which have been reflected, so they now appear in the backward travelling signal as well. S1, S2, S3 and S4 are all related to SBS scattering. The forward travelling carrier, R1, has been SBS scattered and S1 is the peak generated in this process. R2 is the 3 GHz subcarrier component, and R3 at 6 GHz is the second order harmonic associated with R2. R2 and R3 are both SBS scattered leading to peak S2 and S3 respectively. Their frequencies relative to the carrier can be calculated as $f_{S2} = f_{R2} - \nu_B = 3$ GHz-10.84 GHz $= -7.84$ GHz, which shows up in the electrical spectrum at $+7.84$ GHz. Equally, f_{S3} is calculated to be 4.84 GHz. The peak at S4 (13.84 GHz) is generated from the left side-band component of the 3 GHz subcarrier modulation. This way $f_{S4} = -3$ GHz -10.84 GHz $= -13.84$ GHz.

SBS can be a problem for subcarrier modulated systems, and effort has been put into decreasing or working around the effect of SBS, especially for cable television (CATV) applications [55], [56]. SBS scattering of subcarriers will find a very useful application in terms of signal optimization, as will be seen in Chapter 6.

The setup shown in Figure 2.12 was also used for other experiments where the SBS impact was investigated for different bit-rates as well as different fiber types. Specifically, 2.5 Gb/s and 10 GB/s NRZ systems were transmitted in a 80 km

span of either SMF or NZDSF followed by a matching dispersion compensation. NZDSF distinct itself from SMF by a lower dispersion parameter and, more interestingly for this context, a lower effective area, A_{eff}, so a NZDSF fiber would be expected to display SBS effects at lower input powers than SMF. Finally, a pre-compensation dispersion map was also investigated. The table in Figure 2.14 shows some typical values for dispersion parameters and nonlinear coefficients for SMF, NZDSF and DCF.

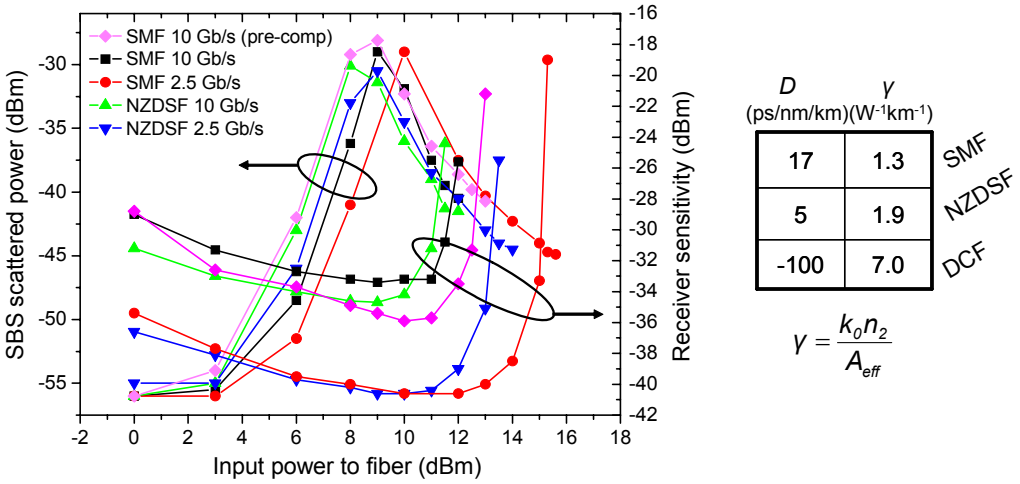

Figure 2.14: Comparison of the SBS scattered signal and receiver sensitivity versus optical input power for various fiber and bit-rate configurations.

Figure 2.14 shows some of the results of the investigations where the SBS scattered power and receiver sensitivity have been plotted versus optical input power to the fiber. The SBS scattered power is found by measuring the backscattered carrier component found at 10.84 GHz, 10.77 GHz and 9.82 GHz for the case of SMF, NZDSF and DCF respectively. The curves reveal that SBS can be observed quite early, and also that the development in the Stokes power is not very different in the considered cases. However, as expected in the cases of DCF (pre-compensation) and NZDSF, the SBS effects kicks in sooner than for the SMF case. The drop in Stokes power that occurs when the input power passes 9-10 dBm is not an indication that SBS decreases, but merely an indication that the Stokes power itself has passed the Brillouin threshold and thus is scattered.

Although the SBS effect is observed early in the course of events, it does not have significant impact on the signal quality. The degradation of the data that initiates at higher input powers will be a combination of both SBS and SPM. Which effect is dominating depends on the bit-rate, but also on the pulse shape as SPM can improve the signal quality in certain cases, so a generalization cannot be made in terms of SBS or SPM being the dominating effect.

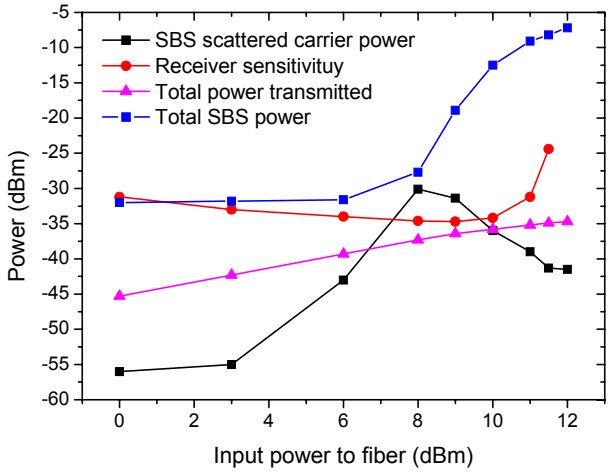

Figure 2.15: A power analysis from the transmission of 10 Gb/s NRZ through 80 km NZDSF with 100% post-compensation. The analysis was done using the setup shown in Figure 2.12.

Figure 2.15 shows an example of a power analysis from the transmission of 10 Gb/s NRZ through 80 km NZDSF with 100% post-compensation. Notice how the linear increase of the total power transmitted through the fiber ends at around 8 dBm input power to the fiber, due to scattering. The *total SBS power* is the total backward travelling power which is related to SBS only[5]. Notice how the total scattered SBS power continues to rise even after the scattered carrier starts to decrease. This phenomenon is most probably due to additional scattering of other spectral components that has passed the SBS threshold and thus keeping the total SBS power high.

Very little attention has been put into monitoring SBS in the literature. There can be a number of reasons for this, including difficulty and complexity in the process of monitoring the scattering effect. As SBS is a backward scattering effect, a circulator or equivalent device is needed to separate out the SBS signal. The anti-Stokes component can be difficult to see in a high-speed data-spectrum as the Brillouin shift is in the order of 10 GHz, effectively making the Stokes component hidden in the in-band data spectrum at bit-rates of 10 Gb/s or higher. Additionally, as the SBS spectral efficiency is rather low, the problem of SBS is expected to be insignificant in 40 Gb/s systems where other nonlinear effects such as SPM and XPM will dominate. Even though SBS can limit 10 Gb/s systems, SPM becomes effective at about the same time as SBS, leaving lower bit-rate and subcarrier systems the main interest in terms of SBS.

[5] A part of the backward travelling power is related to connector reflections of the data signal. In the *total SBS power,* this reflected power has thus been removed so it denotes only SBS related scattering.

2.10 Chapter summary

This chapter has introduced what is considered to be the main sources for signal degradation in today's and the next-generation optical communication networks. Several of the potential signal degrading effects have caught a lot of attention in terms of monitoring. Especially noise, dispersion, and nonlinear effects need increased attention when moving towards higher bit-rates. In particular can SPM and XPM severely limit the system performance. SBS was identified as a significant effect in 10 Gb/s and lower bit-rate systems but will not be a limiting factor in 40 Gb/s systems and above. SRS also deserves attention as it can cause performance degradations in WDM systems. This will take place as a channel power tilt and crosstalk between the channels.

PMD can also constitute a problem, however it is expected that due to new fiber types which have sufficiently low PMD values, the problem will be eliminated in most cases. Old fiber types, though, can still exhibit high PMD values and thus present a problem when upgrading such systems to for example 40 Gb/s.

Chapter 5 will continue to present a number of technologies being able to monitor some of the optical signal parameters presented here.

Chapter 3

Performance monitoring

Performance monitoring is a vital part of digital communication systems. It is necessary to detect and prevent errors in order to maintain carrier uptime and quality of service (QoS) agreements. Often the required availability is specified as 99.999%, which means that only 5 minutes of down-time within one year is acceptable. In order to verify and assure that the guaranteed limits are kept, accurate performance monitoring as well as network protection is necessary. Current SDH/SONET[1] restoration times are specified within a 50 ms limit to ensure an undisrupted service.

This chapter will discuss the term performance monitoring, and take a deeper look at how performance monitoring could develop in a future all-optical network. It will also identify the potential need for performance monitoring and discuss when and to what extent performance monitoring is necessary.

First, some of the terms used in performance monitoring of all-optical networks should be properly defined. *Performance monitoring* is here defined as the general performance of the signal, which can be either electrical or optical in nature, whereas *optical performance monitoring* is restricted to performance monitoring of optical signals. Optical performance monitoring can be used to monitor the optical signal in terms of wavelength, dispersion and OSNR and also bit-error monitoring. Optical performance monitoring can be divided into categories of *optical signal parameter monitoring* such as wavelength, PMD, dispersion and OSNR monitoring, and *optical signal quality monitoring,* which covers bit-error monitoring and Q-value monitoring primarily, i.e. methods for direct signal quality estimation. The *all-optical network* is defined as an optical system where the signal remains in the optical domain. This implies no optical-electrical-optical

[1] SDH and SONET being very similar, evolved simultaneously. SDH is the European standard whereas SONET is primarily used in North America. The main difference between SDH and SONET is found in the bit-rates in higher order layers VC-4 and VC-3 respectively, [6] page 55.

(O-E-O) regeneration. *Optical performance monitoring* refers specifically to non-intrusive performance monitoring of optical signals in all-optical networks. It can include electrical conversion of a tapped-off monitoring signal, but the main data carrying signal must remain in the optical domain.

Regarding the use of signal sensitivity throughout the thesis
Generally, the signal quality is eventually the main concern when discussing performance monitoring in optical systems. Several parameters have been proposed as a measure of the signal quality including bit-error-rate (BER), Q-factor, eye-opening penalty and receiver sensitivity or power penalty. In general though, the number of bit-errors is the most accurate measure for the quality of a signal at a given time.

In order to establish a useful reference throughout this work, this thesis will use the receiver sensitivity of the signal as a measure of signal quality. The sensitivity of a signal is defined as the input power to the receiver that achieves a BER of $1 \cdot 10^{-9}$.

3.1 Layered performance monitoring

Performance monitoring in communication networks can and should be done in several of the network layers. Going from the physical layer to the transmission layer and further up, each layer carries a part of the responsibility to assure the data integrity.

Monitoring in the physical layer, which can be the optical channel in a fiber, includes monitoring of wavelength, wavelength drift, channel power and total WDM power to mention the most significant parameters considering today's optical communications networks. These parameters are of physical nature, and will give no indication of the signal quality except from loss of signal (LOS) indications. Performance monitoring in the physical layer is in fact normally dominated by optical signal parameter monitoring as defined above.

Performance monitoring in the transport layer is today typically managed by SDH or SONET and is the current lowest layer where signal quality monitoring is done, and in this case, via a bit-error evaluation. The next section will discuss the means of performance monitoring in SDH/SONET networks.

The higher layers such as the switching and the routing layers can also include capabilities for performance monitoring. For example asynchronous transfer mode (ATM), which is able to make classes of service (CoS) and quality of service (QoS) differentiation based on requirements to the packet loss ratio and delay performance. This thesis however, will mainly focus on optical performance monitoring in the physical layer. This includes both optical signal parameter monitoring as well as optical signal quality monitoring.

3.2 Legacy performance monitoring

This section will not provide a detailed discussion or investigation on the existing means of performance monitoring in the transport layer, but merely review the functionalities and requirements for performance monitoring in the current SDH and SONET networks.

SDH and SONET have been around for several years, and are currently the most preferred transmission layer technology. The technologies were implemented around 1992 as a successor to the plesiochronous digital hierarchy (PDH) technology. A wish for better interoperability, more effective capacity utilization and several other reasons prompted the development of a new technology. SDH/SONET possesses several advantages, some of which are listed below:

- SDH and SONET are international standard allowing equipment from different vendors to communicate with each other and thus replacing equipment only having a purpose of interfacing.
- Synchronous networks mean no bit-stuffing, which makes multiplexing and demultiplexing more efficient and simple and thus reduces equipment cost.
- SONET/SDH include robust network management functionalities and in addition means for signal performance monitoring as well as fast and effective protection switching. PDH did not allow for structural inclusion of performance monitoring capabilities.

Although SDH/SONET possess many advantageous features it also receives criticism for being costly in terms of equipment. It requires a considerable overhead to support all the functionalities and as overhead consumes bandwidth, less bandwidth is available for payload. Furthermore, SDH/SONET is a technology developed for telephony, and is therefore not optimized for the increasing percentage of data traffic seen today. The future continued or discontinued use of SDH/SONET as transport layer technology will be further discussed in Chapter 7.

As already mentioned, performance monitoring plays a vital role in communications systems. Operators have to meet the guarantees given to their customers and therefore it is necessary to monitor the performance of the network. This includes monitoring if the link path has actually been established, if the signal is getting though to its destination and if the signal quality is acceptable. The SDH frame structure has been designed to provide information about various properties such as management and signal quality. Below are listed some of the functions the SDH frame header carries information on.

- Alarm indication signals (AIS).
- Error performance monitoring using bit interleaved parity bit checking (BIP-n) or cyclic redundancy check (CRC).
- Path status.
- Path and section trace.
- Remote defect, error, and failure indications.
- Automatic protection switching (APS) control.

Features such as the AIS, error performance monitoring using BIP-n, remote defect, error, and failure indications etc. are used to ensure the signal integrity. Note, that these mentioned signal parameters can only be recovered through optical-to-electrical (O-E) conversion followed by a SDH multiplexing unit.

In this context, the BIP-n functionality that monitors bit-errors is of most interest as it is directly related to performance monitoring. The BIP-n method is a bit-interleaved-parity check where groups of bit's are constantly analyzed for errors.

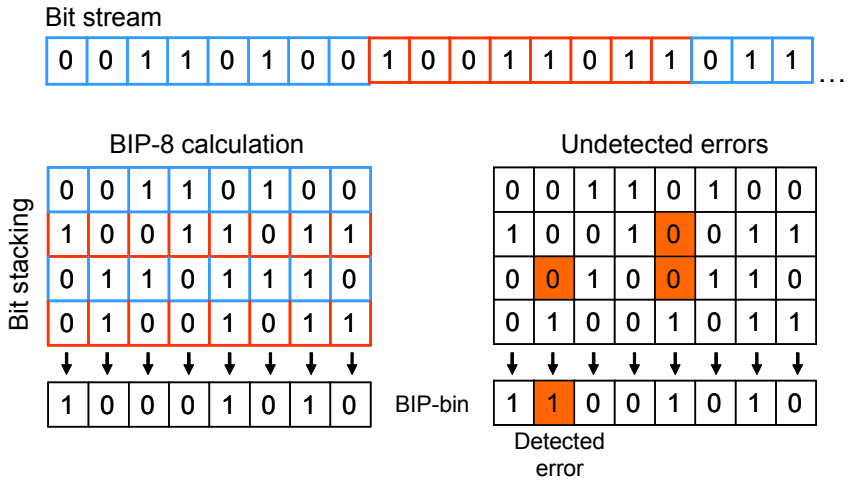

Figure 3.1: *Left:* Illustration of a BIP-8 calculation. *Right:* The first payload error is detected by the BIP-8 check, but in the other case, the parity-bit is still "1" due to the double-error.

Figure 3.1 illustrates the principle of a BIP-8 check. The bit stream is broken up into 8 bit segments, which are then stacked and a parity-bit is found and added to the header. Later the operation can be repeated and any discrepancies will be interpreted as bit-errors. However, as can be seen in the right part of Figure 3.1, situations can occur when bit-errors are not detected. Likewise can

corrupted bit's in the BIP-bin itself lead to the wrong conclusion that the payload has erroneous bits. Note that the ITU G. 826 standard recommends that for in-service monitoring purposes, the probability to detect an error event is higher than 90%. This can either be done using the BIP-n or CRC method.

Although the BIP-8 is quite effective for performance monitoring, it does not provide an exact BER. It will provide an indication of errors based upon the BIP-8 parity check, which in many cases will be sufficient. Extracting the exact BER is in practise impossible due to the fact that real data consists of unknown bit's and therefore the necessary bit-comparison and in turn a precise bit-error count can never be realized. In this context, the relatively new ITU recommendations for optical transport networks (OTN) should be mentioned. OTN has support for a range of services like SDH/SONET, Ethernet, ATM and IP based services while adding the possibility for extra performance enhancements. The ITU G.709 standard, for example, describes the digital wrapper in OTN, which includes forward error correction (FEC) [58]. Through a coding algorithm [59], the signal is encoded upon transmission and decoded after transmission such that a certain number of errors can be corrected depending on the coding algorithm. Using a so-called RS(255, 239) coding algorithm[2], an input BER of $1.4{\cdot}10^{-4}$ can be corrected up to $1{\cdot}10^{-13}$ [58]. At the cost of an increased bit-rate, FEC significantly reduces the BER requirements for data transport and furthermore it enables performance monitoring in the form of a BER estimation retrieved through the FEC decoding [60], [61].

The OTN is a transport layer technology and it thus suffers from the same drawback as SDH and SONET in terms of performance monitoring. There is no immediate posibility of determining the source of arising bit-errors in the system.

The built-in performance monitoring capabilities of SDH/SONET or OTN networks can beneficially be combined with optical performance monitoring such as wavelength monitoring, power monitoring and in some instances OSNR monitoring to increase the level of performance information. The need for more advanced types of optical performance monitoring is usually not necessary in SDH/SONET systems carrying bit-rates up to 10 Gb/s. The obstacles this type of network can encounter will most likely not require e.g. dispersion monitoring or PMD monitoring. Extreme cases of very long distance between regeneration points as well as higher bit-rate SDH/SONET systems could benefit from dispersion monitoring or PMD monitoring. Notice however, that any signal alterations such as the addition of subcarriers, phase or frequency modulations

[2] RS(255, 239) means that the total number of symbols is 255, and 239 is the number of information symbols. A symbol consists of 8 bits. This particular Reed-Solomon algorithm can correct up to 8 symbols [58].

used for performance monitoring will be lost in the O-E-O regeneration process and will have to be re-inserted again after regeneration. This can also be the case for all-optical regeneration [9], where the reshaping process can remove any sub-modulation added earlier at the transmitter.

3.3 Optical performance monitoring

In SDH/SONET, all switching, adding and dropping, multiplexing etc. are performed in the electrical domain. As mentioned in the introduction in Chapter 1, steps and initiatives are being taken towards all-optical networks, which include the use of optical switching, optical add-drop multiplexers, all-optical 3R regenerators and of course optical amplification. All are factors that increase the distance in which the signal will remain in the optical domain. The fact that the signal transverses longer in the optical domain, held together with increasing bit-rates, can enable a build up of the signal degrading effects described in Chapter 2. Furthermore, if a future all-optical network is expected to support a variety of bit-rates and modulation formats, it could very well be feasible and to some extent necessary to assign a number of the performance monitoring tasks to the physical layer. This is a natural consequence of the decreased access to the individual signals being transmitted in the same fiber.

This section will discuss what capabilities and features could be expected if performance monitoring is done in the physical layer. It will also review the current advances in optical performance monitoring, which should also serve as an entry for the next chapters.

3.3.1 What should be monitored?

A fully flexible all-optical network would imply almost infinitely many combinations of signals types in the optical fiber. For example, one second four 10 Gb/s NRZ signals could be transmitted, and the next, two 40 GB/s differential quadrature phase shift keying (DQPSK) signals could be added to the WDM system. It is clearly a very comprehensive task to perform optical signal quality monitoring on every thinkable signal that might be switched into a particular transmission path at any given time. However, with certain basic assumptions, the problem can be simplified somewhat. Some examples are listed below:

- Fully dispersion compensated spans. This simplifies dispersion monitoring considerably as the monitoring can be done on the span rather than on individual channels.

- Consider the case where a monitor signal is associated with each channel. If each channel carries a relevant monitor signal of some kind, the signals can be monitored individually within the network.
- There exist some limitations as to which signals are allowed in the network. For example bit-rate and modulation format restrictions. This would effectively reduce the performance monitoring complexity.

The last point obviously removes partly the idea about the transparent all-optical network, but a performance monitoring technique capable of monitoring all kinds of signals at every imaginable bit-rate has yet to be developed. Probably some compromises must be made. Fully compensated spans could be realized, and if not, the performance monitoring of the channel is required to be done on a traveled path basis. This is possible by applying for example subcarrier tone modulation, which can be used for channel identification [62], dispersion monitoring [30] or PMD monitoring [14].

Returning to the matter of what capabilities an optical performance monitor technology should possess, a number of parameters can be assumed as basic requirements. They have been listed below:

- Individual channel power and composite channel power (total power of all WDM channels).
- Wavelength and wavelength drift.
- OSNR.
- Laser power and/or laser bias current.

Possible causes for bit-errors can be amplifier degradations, which add noise, a physical fiber cut, laser drifts and other equipment failures and degradations. These problems can be detected by monitoring a few and simple parameters such as the ones listed above. With the prospective introduction of optically switched networks, the number of significant optical signal parameters grows. Therefore, apart from these basic required parameters, additional optical signal parameters can be identified as possible candidates for monitoring:

- Dispersion.
- PMD.
- Optical channel crosstalk.
- Spectral bandwidth.

- Nonlinear scattering effects such as SBS and SRS.
- Nonlinear effects such as SPM, XPM and FWM.
- Q-factor.
- BER.

The last two, Q-factor and BER estimations are different from the rest as they evaluate the overall quality of the signal rather than a specific optical parameter.

Ideally, monitoring the BER of a signal would be preferred as the number of bit-errors is the only true and digital measure of the quality of the signal. However, as mentioned above, the bits in a signal are random in nature and therefore it is practically impossible to monitor the exact BER. Only approximate evaluations are possible.

As an alternative to making approximate BER evaluation, which can be rather complicated [63], a number of the above listed parameters can instead be monitored and used to evaluate the quality of the signal. This also brings along other advantages. Q-factor and BER evaluations do not provide sufficient information about the source of the signal degradation, whereas dispersion monitoring combined with OSNR monitoring can either confirm noise or dispersion changes as the source, or at least exclude those as possible reasons. The same holds for the BIP-8 bit-parity check done in SDH/SONET. An increase in bit-errors does not explain the cause of the errors, so the OSNR and other physical parameters should be consulted.

It is difficult to state exactly which of the above listed items will be necessary to monitor and which will not. This will depend largely on the specific network in question. However, dispersion, Q-factor, and PMD qualify as very likely candidates considering the identified signal degradations listed in Chapter 2. Monitoring various types of nonlinearities could also prove to be interesting as new functionalities such as optical switching can alter the power levels in an optical fiber considerably and thus excite various effects like SPM, XPM, FWM and SBS. Under normal circumstances though, these effects should be avoided by system design and power budget considerations. In those cases, monitoring of the nonlinear effects would not be strictly necessary if the power margins are large enough to assure no sudden variation or influence from these effects.

Dispersion and PMD variations are effects than can be difficult to avoid as discussed in Chapter 2, especially as the O-E-O regeneration distances and the bit-rates increase. Combining dispersion monitoring and PMD monitoring with OSNR and Q-factor/BER evaluation could prove a likely candidate for optical performance monitoring in the physical layer, in the future all-optical networks.

However, it depends on the specific network in question and other variations will unquestionably be possible.

3.3.2 Current advances in optical performance monitoring

This section will briefly review the most recent advances and current trends seen in optical performance monitoring research. Specific work done on the various optical parameter monitoring techniques have already been discussed in Chapter 2.

In the matter of optical signal quality monitoring, there has been developed techniques that successfully indicate the quality of an optical data signal. Q-factor monitoring is a very promising field of study that has been subject for a lot of attention due to a usually very good agreement with the BER [45], [44], [64]. The Q-factor evaluation is made possible via analysis of the amplitude histogram. The amplitude histogram can be achieved from the eye-diagram but also via asynchronous sampling of the optical signal [45], [65]. Methods using asynchronous sampling has the advantage of being independent on the bit-rate. The principle of a amplitude histogram can be seen in Figure 3.2. The amplitude histogram can be generated either through asynchronous sampling (left) or synchronous sampling (right).

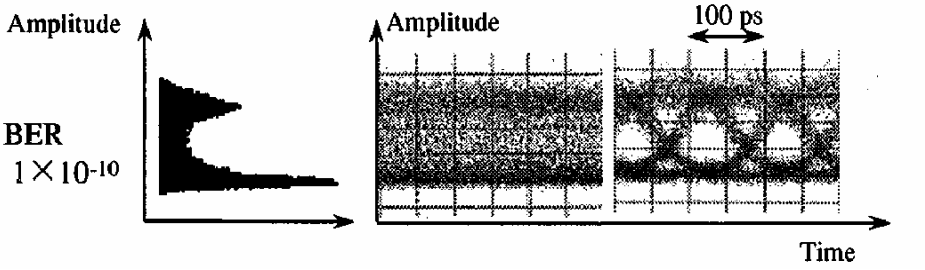

Figure 3.2: Figure taken from [66], where Shake et al. demonstrates signal quality monitoring of dispersion degraded signals. The figure illustrates how the amplitude histogram is generated.

Analysis of the histogram is a promising technique because the same method can be applied for several modulation formats and bit-rates. Furthermore, histogram analysis can to some extent reveal the source of degradation, so in addition to the Q-factor monitoring, information regarding OSNR and residual dispersion can also be achieved in some cases [66], [67], [68].

Monitoring technologies using histogram analyzing are relative mature technologies that have a possibility of being implemented in commercial systems within a reasonable future. The same accounts for a technology often termed analog symbol monitoring (ASM) [69], [70]. Using ASM the histogram can be generated without sampling by using a variable threshold circuit and counting

"1" events. The generated histogram can then be used to estimate a Q-factor and BER estimations for the system, and to some extent also identify the source of a signal quality degradation, for example in the case of dispersion related degradations [69].

All-optical parity checking, a less mature technology, has been demonstrated for bit-rates of 2.5 Gb/s and 10 Gb/s [71], [72]. In [72] the parity calculation was realized using optical XOR gates. All-optical parity checking could be an interesting application for bit-error checking in optical networks as it in principle can be performed very fast and thus eliminate bit foot-print and high power consuming electronics. Similar to most other optical signal quality monitoring techniques, all-optical parity checking suffers from not being able to recognize the origin and magnitude of the problem causing the detected bit-errors. The all-optical parity calculation reported in [72] will be discussed further in Chapter 4.

3.4 Chapter summary

The need for performance monitoring in modern communication systems has been established. The basic principles of legacy performance monitoring done in the transport layer was discussed, and it was concluded that current means of performance monitoring in the physical layer are not sufficient for the next-generation all-optical network. Requirements to optical performance monitoring will change with a significant reduction of optical-electrical-optical (O-E-O) conversions and will thus make optical performance monitoring a necessity in cases where the signal quality cannot be assured by traditional means.

In order to take optical networks to the next level of higher efficiency, capacity and flexibility, many obstacles have to be overcome, and optical performance monitoring is one of the key issues.

Chapter 4

Optical signal quality monitoring

Depending on factors like network size and complexity of the optical network, monitoring one or more of the signal parameters, described in Chapter 2, can be enough to sustain the required information about the signal quality. However in other cases, it can be beneficial to obtain an overall information about the signal quality, where several signal parameters are taken into account. In this case Q-factor monitoring or BER monitoring can be appropriate methods. The previous chapter also discussed how optical signal quality monitoring and optical signal parameter monitoring could be combined effectively to provide information about the signal quality as well as the origin of the observed signal degradations.

This chapter will present two methods for optical signal quality monitoring. The first method co-transmits a known reference signal along with the unknown data signal and thus investigates correlations between these two signals that can be exploited for signal quality monitoring. The second method presents an all-optical parity calculator using an integrated SOA based XOR gate with feedback.

4.1 Signal quality monitoring using polarization multiplexing

The main problem by directly monitoring the quality or BER of a signal is the fact that the signal consists of unknown data, making it impossible to determine the BER in a data commercial network. In SDH/SONET the BIP-8 parity check is used to electrically generate a series of parity bit's that later in the network can be recognized and compared to an expected value.
Section 4.2 describes an optical parity calculator but parity checking has not fully

matured yet to be used in optical networks.

Knowing the actual content of the transmitted signal is the most accurate way to determine the signal quality, so a straight forward solution would be to transmit a reference or monitoring signal along with the data channel. Another possibility would be to transmit a full PRBS coded signal at a different wavelength adjacent the data channel, which could be BER evaluated at selected points. There are several problems with this approach, the first being that the monitoring signal takes up valuable spectral space. Furthermore, the monitor signal only informs about the signal quality at that specific wavelength. Optical filtering and uneven amplification of the channels can make the signal quality vary significantly within the channels in a WDM grid. Furthermore, the bit rate of the monitoring signal should be equal to the data channel in order to reflect the signal degradations realistically. In a 40 Gb/s system this would be very costly to employ such a channel.

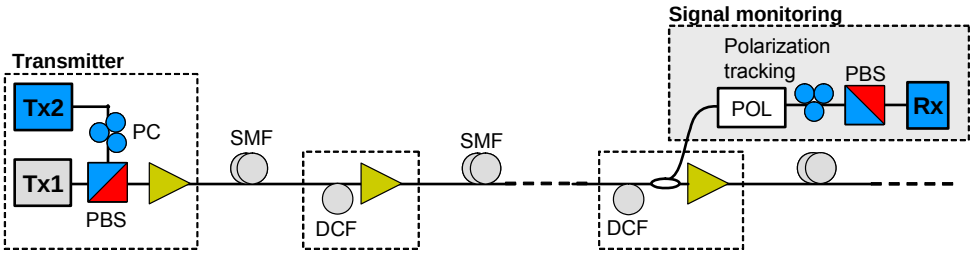

Figure 4.1: A signal from Tx2 is polarization multiplexed onto the same wavelength as the high-speed data signal. Later this monitor signal from Tx2 can be extracted and used for evaluating the high-speed data signal.

This section investigates the possibility of developing a useful monitoring channel in an optical network. More specifically, the idea here is to transmit a lower bit rate reference signal, which has been polarization multiplexed onto the same wavelength as the high bit rate data signal. Figure 4.1 illustrates the principle. The main data to be transmitted is generated in Tx1 and the known reference data used for monitoring is generated in Tx2. The two signals transmitted at the same wavelength are combined using the polarization combiner/splitter (PBS), and the combined signal is transmitted through the network. At some point of interest, a part of the combined signal can be tapped off and utilizing a second PBS the reference signal can be separated from the data signal and thus BER evaluated. This model obviously implies that there exist some correlations of the signal degradations between the data and the reference signal. As will be seen in the following it is possible to develop a useful relation between the reference signal and the data signal in noise limited systems. In noise limited systems, OSNR monitoring can often be successfully used, as changes in the OSNR will have a

well defined effect on the BER. In dense WDM systems, however, monitoring the OSNR of individual channels might not be possible as seen in Chapter 2. Correlating the data channel with a polarization multiplexed reference channel carrying a known data pattern can help overcome this problem. Furthermore, this monitoring approach has the advantage that the reference signal will follow the data signal throughout transmission and thus undergo the same OSNR degradations in an optically switched network.

4.1.1 40 Gb/s signal monitoring using a reference signal

As illustrated above, a reference signal can be used to monitor a data signal provided that there exist some correlations between the reference signal and the data signal itself. To investigate these potential correlations and the use of a polarization multiplexed reference signal as a signal monitor, a number of 40 Gb/s experiments were carried out using a 2.5 Gb/s reference signal. The setup used in the experiment is shown in Figure 4.2.

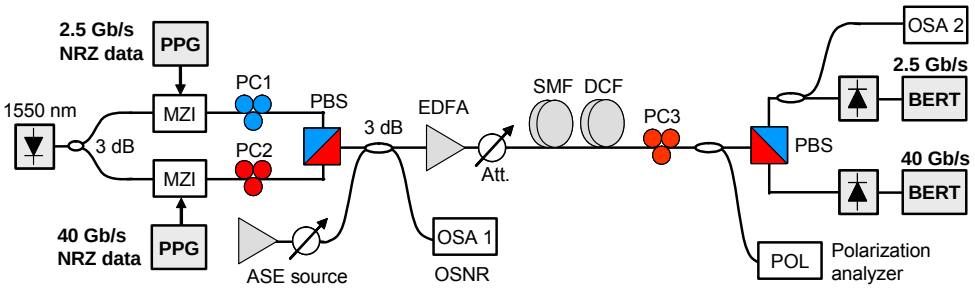

Figure 4.2: Setup used in the 40Gb/s signal monitoring investigations. The method uses a reference signal at 2.5 Gb/s to monitor the 40 Gb/s signal.

A laser source emitting CW light at 1550 nm is split up using a 3 dB coupler into two equal parts. One part is directed to a Mach-Zehnder (MZ) modulator being driven by a 40 Gb/s PRBS 2^{31}-1 (data) signal and the other part is directed to another MZ modulator being driven by a 2.5 Gb/s PRBS 2^{7}-1 (reference) signal. Before the signals are combined using a PBS, the polarization of each signal are optimized using polarization controllers PC1 and PC2. This is done as the PBS will only accept light having a correct aligned linear polarization. The polarization optimization process, as well as the relative power of the signals can be monitored using the optical spectrum analyzer OSA1. After combining the signals the composite signal is amplified and transmitted through 44 km SMF and 100% dispersion compensated using DCF. For OSNR measurements, additional ASE noise can be added using a EDFA with no input signal, followed by an optical attenuator.

The polarization control denoted PC3 is a critical component in the setup. This polarization control aligns the signal to the PBS separating the two signals before they continue to each their receiver. If the polarization control PC3 is incorrectly aligned this will result in crosstalk between the data and reference channel, which in turn will cause degradation to both signals. This will become evident later in Figure 4.7 (right). The polarization analyzer shown in the setup was used to track any changes in polarization, again to ensure a correct polarization state of the signal incident to the receiver PBS.

4.1.2 Preliminary simulations

This section will focus on a system impaired by noise, i.e. signal quality drop due to a drop in the OSNR, to investigate useful data-reference BER correlation proving the method effective for BER monitoring in a noise limited system.

Before moving on to the experimental results, it is interesting to consider the theoretical expected behavior of the system depicted in Figure 4.2. Therefore, the principle setup shown in Figure 4.2 was used in a number of simulations[1] where the OSNR was changed using the ASE noise source. While changing the OSNR in the system, both the reference (2.5 Gb/s) and the data signal (40 Gb/s) are BER evaluated in order to identify correlations between the signals. The simulation parameters, such as rise time, extinction ratio, optical and electrical filter bandwidths are kept in agreement with laboratory figures.

Figure 4.3 shows the result of a simulation where the data/reference signal power ratio was varied. The receiver sensitivity (measured at BER $1{\cdot}10^{-9}$) versus OSNR is plotted for the 40 Gb/s data signal being kept at constant power of -6.1 dBm to the SMF, while the 2.5 Gb/s reference signal is launched at two different powers: -8.5 dBm and -18.5 dBm; a difference of 2.4 dB and 12.4 dB respectively. Notice the horizontal axis, "40 Gb/s OSNR", denotes that the OSNR value for the 40 Gb/s signal is used as a reference. Only the 40 Gb/s OSNR will be used as reference as this is the original signal of interest. The 2.5 Gb/s OSNR will have a similar shape but a different evolution that depends on the respective power difference between the two signals.

[1] VPI Transmission maker version 6.5 was used in these simulations. Please refer to Appendix B for details on parameters and setup.

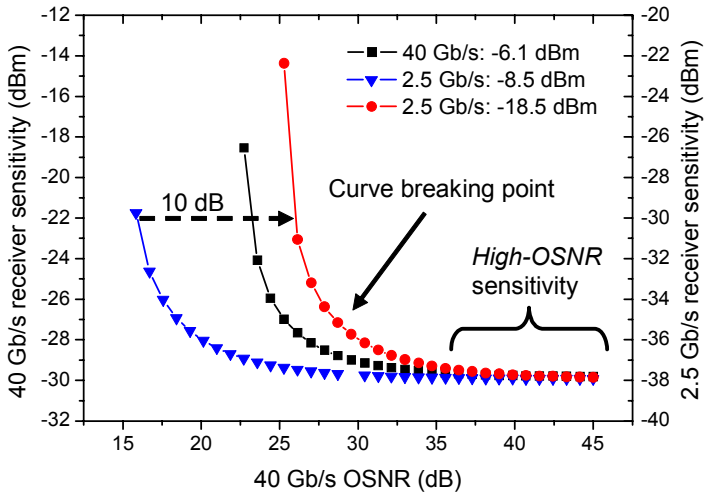

Figure 4.3: A simulation result where the data/reference signal power ratio was varied. The 40 Gb/s data signal is kept at constant power of -6.1 dBm to the SMF, while the 2.5 Gb/s reference signal is simulated using -8.5 dBm and -18.5 dBm.

Observing again Figure 4.3, there clearly is no straight forward correlation between the signals in this particular case but the curve behaviors can be well explained. Although both the signals are expected to individually display a curvature behavior as in Figure 4.3 they are not necessarily expected to be synchronous/overlapping. In order to explain this, two factors needs to be considered. First, for a 40 Gb/s signal at high OSNR values, the receiver sensitivity (at BER $1{\cdot}10^{-9}$) is expected to be 12 dB higher (worse) than a 2.5 Gb/s signal at the same OSNR if both the optical filter in the pre-amplifier and the electrical low-pass filter bandwidths are scaled accordingly. This is usually not the case though, as optical filters do not become that narrow without suffering from very high losses. Therefore, in this case an 0.8 nm optical pre-amplifier filter was used both for the 40 Gb/s and the 2.5 Gb/s signals. This has no practical meaning for the concept of the method, but is mentioned because the actual difference in sensitivity can be useful as will be seen below.

Figure 4.3 also shows how a relative change in the 2.5 Gb/s signal power will shift the sensitivity curve horizontally while keeping the *high-OSNR sensitivity* constant at -38.0 dBm. This is expected as the optimal sensitivity at high OSNR values is dependant on the electrical bandwidth in the receiver, whereas *the break of the curve* is determined by the launch power of the 2.5 Gb/s seen relative to the 40 Gb/s signal power. Figure 4.3 demonstrates this as the power of the 2.5 Gb/s signal is changed 10 dB from -8.5 dBm to -18.5 dBm. Notice how the 10 dB relative power change corresponds to a 10 dB horizontal parallel shift of the 2.5 Gb/s sensitivity curve.

Adjusting the sensitivity curve for the 2.5 Gb/s (known) reference signal to the sensitivity curve for the 40 Gb/s (unknown) data signal could provide a useful correlation between the two signals as the data signal quality in this case can be monitored using the known reference signal. In order to establish a useful correlation between the 40 Gb/s data signal and the 2.5 Gb/s reference signal the 2.5 Gb/s sensitivity curve needs to be adjusted to overlap with the 40 Gb/s curve. Referring back to Figure 4.3, the figure indicates that a useful correlation, i.e. curve overlap of the two signals can be developed by ensuring a relative power difference of approximately 8 dB between the 40 Gb/s data and the 2.5 Gb/s reference signal. An 8 dB power difference would lead to an exact overlap and, in theory, a perfect correlation of the two signal qualities. In this particular simulation the sensitivity difference is 8 dB using standard bandwidths for the electrical band-pass filters. The 8 dB difference is dictated by several factors such as the optical filter in the pre-amplified receiver, the electrical low-pass filter as well as other transmitter related factors as will become evident in the investigation below.

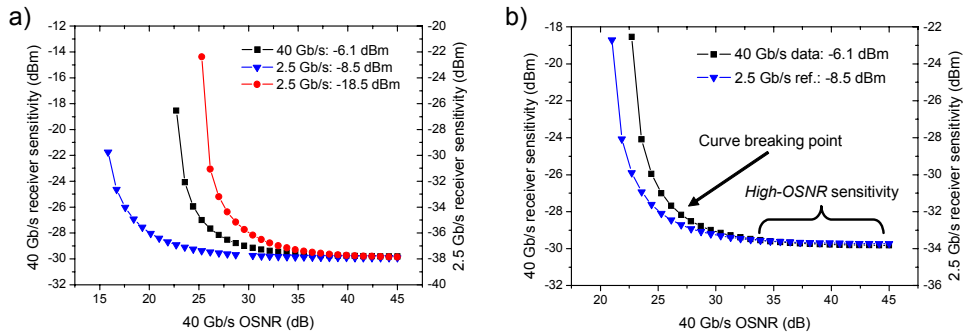

Figure 4.4: Simulation showing the effect of changing the low pass bandwidth from 1.75 GHz to 8.75 GHz. a) The 2.5 Gb/s signal receiver low-pass bandwidth is 1.75 GHz. b) The low-pass bandwidth has been changed to 8.75 GHz.

The relative power difference of the two signals is not the only thing that will shift the curves. Figure 4.3 assumed an optimal electrical 3 dB bandwidth of 70% [73] of the bit rate, corresponding to 1.75 GHz and 28 GHz for the 2.5 Gb/s and the 40 Gb/s signals respectively. In the simulations this was realized by Bessel-shaped low-pass filters. Figure 4.4 illustrates a case where the low-pass bandwidth in the 2.5 Gb/s receiver has been changed from 1.75 GHz to 8.75 GHz, while keeping the relative power difference of 2.4 dB. Figure 4.4a), which identical to Figure 4.3, is shown for comparison. Figure 4.4b) shows how the 2.5 Gb/s signal curve makes a shift due to the change in the low-pass filter bandwidth. A change from 1.75 GHz to 8.75 GHz allows more noise into the system as explained in Appendix A, so a reduction in sensitivity is expected.

Numerous simulations has been performed to clarify the correlation between the shift of the curves and the change in relative signal power as well as low-pass filter bandwidth. The details of these simulations are not relevant in this context, but the following fact was confirmed:

A change in either relative power difference or electrical receiver bandwidth that leads to a X dB decrease in the sensitivity also leads to a X dB change in the breaking point of the curve. Furthermore, the equalization of high-OSNR sensitivities for both the signals would achieve equalization of the curve breaking points and thus a perfect correlation. The terms *curve breaking point* and *high-OSNR sensitivity* was explained in Figure 4.3 and Figure 4.4b). This can be formulated in a simple equation for the power difference required to achieve curve overlap of the sensitivity curves:

$$\Delta P_{dB} = S_{Data} - S_{Ref} \tag{4.1}$$

where S_{Data} and S_{Ref} are the receiver sensitivities of the data and the reference signal respectively.

Considering these preliminary investigations, it is clearly important to perform a characterization of the receiver sensitivity performances in the system such that the specific behavior can be clarified. Once that is done, it is possible to very accurately predict the behavior of the 2.5 Gb/s reference signal in respect to the 40 Gb/s data signal. Even though the synchronization between the data and the reference signal can be achieved through adjusting either the relative power difference or the electrical receiver bandwidth, it will most often be more easy and more cost-effective to correlate the signals using the relative power difference. It is even so convenient that the difference in sensitivity between the two signals will reveal the relative power difference required to correlate the two signals.

4.1.3 Experimental results

Using the setup in Figure 4.2, a number of experiments were carried out to verify the concept. Due to practical reasons, it was necessary to use a series of electrical amplifiers with bandwidths exceeding what is normally expected for a 2.5 Gb/s system. Electrical amplifiers tailored to 2.5 Gb/s systems were simply not available. As already discussed, this will have an effect on the 2.5 Gb/s receiver sensitivity evolution as more noise will be allowed into the receiver. In these experiments, electrical amplifiers having a 3 dB bandwidth of 10 GHz were used, which means that 4 times more noise will be allowed into the receiver compared to a 2.5 GHz amplifier. Referring to the discussion in Appendix A this experimental system setup is expected to be limited by spontaneous-spontaneous beat noise,

which means that the deterioration in receiver sensitivity will scale with $\sqrt{B_e}$ where B_e is the electrical low-pass filter bandwidth. A 4 times increase is thus expected to give a $\log(\sqrt{4}) = 3$ dB receiver sensitivity deterioration compared to the ideal case.

The normal expected pre-amplified receiver sensitivity for an ideal 2.5 Gb/s system is around -41 dBm; about 12 dB lower than the sensitivity for a 40 Gb/s NRZ system[2]. In these experiments, the best receiver sensitivity for the 2.5 Gb/s system was found to be approximately -39 dBm - 1 dB better than expected considering the higher electrical bandwidth. This difference can be explained by the cascading of several electrical amplifiers with different bandwidth characteristics, which can reduce the effective bandwidth such that a noise filtering effect is obtained.

The 40 Gb/s sensitivity was not as expected either, although close. The experimentally achieved sensitivity was -27.5 dBm, which is 1.5 dB from the optimal expected -29 dBm. In this case the performance is worse than the expected sensitivity for an ideal system. It is difficult though to reach this optimal performance for the 40 Gb/s system as the requirements on electronic transmitter and receiver components are very high, and therefore -27.5 dBm is considered acceptable. The discussed values for 2.5 Gb/s and 40 Gb/s can be found in the table below[3]:

Bit-Rate	**Expected**	**Experiment**	**Deviation**
2.5GB/s	-38 dBm*	-39.0 dBm	1.0 dB
40Gb/s	-29 dBm	-27.5 dBm	-1.5 dB

*-38.0 dBm (-41.0 dBm + 3 dB) due the 3 dB increase of the electrical receiver bandwidth.

Table 4.1: Expected and experimental receiver sensitivity values

The sensitivities in Table 4.1 was measured using equal powers in the 2.5 Gb/s and 40 Gb/s channels.

Keeping the above numbers in mind, it is possible to estimate the approximate launch power configuration for the two signals that is needed to achieve an overlap of the two sensitivity curves; i.e. a synchronous BER behavior. If both systems scale in general performance, a difference of 12 dB is required to attain a synchronous BER behavior. The difference can be achieved via either changing

[2]The ideal expected values were found through VPI simulations using ideal parameters for the transmitter and receiver configuration.

[3]The PPG used for the 2.5 Gb/s reference signal was capable of delivering up 12.5 Gb/s PRBS signals as well as the MZI modulator that was designed for 12.5 Gb/s signals. In effect this leads to a rise-time performance that is not normally expected for a 2.5 Gb/s system. This can give a relative difference when comparing to the 40 Gb/s PPG and MZI designed for 44 Gb/s signals.

the power ratio or electrical bandwidth in the 2.5 Gb/s electrical receiver. This can be expressed via the following equation:

$$12 \text{ dB} = \log(\sqrt{\Delta B_e}) + \Delta P_{\text{dB}} - \delta_{\text{tot}} \tag{4.2}$$

Where ΔB_e is the deviation in dB from the standard 2.5 Gb/s electrical receiver bandwidth, ΔP_{dB} is the power difference of the two signals in dB and δ_{tot} is the total deviation from the expected receiver sensitivity values from Table 4.1. Basically the equation expresses that the total change in the 2.5 Gb/s electrical receiver bandwidth plus relative difference in power should equal 12 dB to achieve equal BER performances at low OSNR values, i.e. when the signals are subjected to excessive noise. The factor δ_{tot} regards the artifacts and deviations that can arise from various factors such as the extra filtering effect described above. δ_{tot} is found via characterization of the receivers.

Inserting the known values in Equation (4.2) this gives

$$12 \text{ dB} = 3 \text{ dB} + \Delta P_{\text{dB}} - (1.0 \text{ dB} - (-1.5 \text{ dB})) \Leftrightarrow \tag{4.3}$$

$$\Delta P_{\text{dB}} = 11.5 \text{ dB} \tag{4.4}$$

This means that for these given experimental parameters, a relative power difference of 11.5 dB is needed to experience equal BER performance for the 40 Gb/s and the 2.5 Gb/s signals. This agrees with Equation (4.1): $\Delta P_{dB} = S_{Data} - S_{Ref} = -39 \text{ dB} - (-27.5 \text{ dB}) = 11.5 \text{ dB}$.

One factor has not been taking into consideration yet. Up until now, including the simulations, the PBS have been considered to be ideal, such that there is no crosstalk between the channels. This is in practise not the case and some crosstalk will take place. Furthermore, if a power difference of 11.5 dB is considered, the crosstalk contribution from the higher powered 40 Gb/s channel in the 2.5 Gb/s channel will have a stronger impairment to the 2.5 Gb/s channel than visa versa. Equation 4.2 does not take this into consideration. The effect of increasing ΔP_{dB} will thus be associated with an extra crosstalk contribution that leads to further increase of the 2.5 Gb/s receiver sensitivity. If the effect of PBS crosstalk is included in Equation 4.2 the formula now becomes:

$$12 \text{ dB} = \log(\sqrt{\Delta B_e}) + \Delta P_{\text{dB}} - \delta_{\text{tot}} - F(\Delta P_{\text{dB}}, C_{PBS}) \tag{4.5}$$

where C_{PBS} is related to the crosstalk between the two principal states of polarization. Notice how the crosstalk function F also depends on the relative power difference between the data and reference signal. This crosstalk term can be difficult to predict as it is regulated both by the quality of the PBS as well as the ability to adjust the polarization control PC3 in Figure 4.2. Obviously, the preferred is to eliminate this term by assuring good PBS rejection capabilities as

well as accurate polarization control. It was in these experiments not possible to eliminate these factors, so instead a number of experiments were carried out to obtain the required ΔP_{dB} to correlate the two signals.

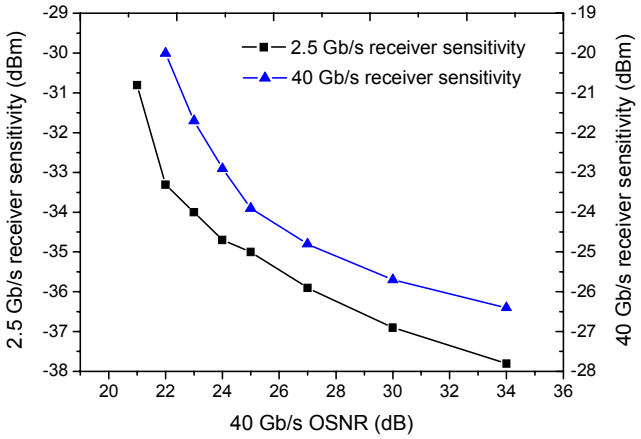

Figure 4.5: 2.5 Gb/s reference and 40 Gb/s data receiver sensitivity versus OSNR. The power of the reference signal is 2.5 dB less than the data signal.

Figure 4.5 shows the receiver sensitivity curves for the case of $\Delta P_{\mathrm{dB}} = 4.0$ dB. As desired, the curves are synchronous such that a 1 dB penalty in the 40 Gb/s system will correspond to a 1 dB penalty in the 2.5 Gb/s system. This way, the known 2.5 Gb/s reference data can be used as a probe to reveal the BER performance of the unknown 40 Gb/s data signal. From this can also be concluded that, in these experiments, the crosstalk term has had a significant influence in retrieving ΔP_{dB}. The difference of 11.5 dB - 4.0 dB = 7.5 dB is thus attributed the crosstalk term described through Equation 4.5.

In cases where a synchronous BER behavior is replaced by a desire for using the reference signal as a pre-warning signal, the relative power difference can be further adjusted. Figure 4.6 shows another case where $\Delta P_{\mathrm{dB}} = 12.5$ dB. In this case the sum on the right side of Equation 4.5 exceeds 12 dB and the break of the 2.5 Gb/s sensitivity curve occurs prior to the 40 Gb/s signal. This way, the 2.5 Gb/s reference now reveals any possible BER degradations before they will influence the 40 Gb/s data signal significantly. Degrading amplifiers can display slow degradations rather than sudden breakdowns and in these cases this kind of pre-warning system could be useful [74], [75].

Figure 4.6 shows that the sensitivity of the 2.5 Gb/s signal has dropped after the relative change in power. Ideally, this is not expected, as only a change in the receiver bandwidth is supposed to change the sensitivity level at high OSNR values. In this particular case though it is in fact expected as the crosstalk from

the 40 Gb/s channel will further impair the 2.5Gb/s as ΔP_{dB} has increased to 12.5 dB. The result of the imperfect rejection of the 40 Gb/s signal in the 2.5 Gb/s channel causes a 3 dB receiver sensitivity penalty.

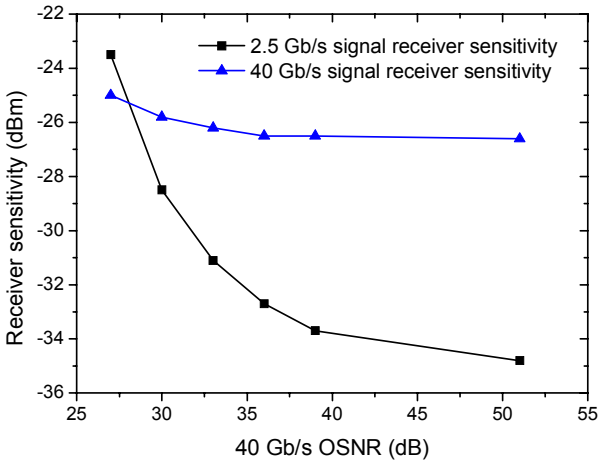

Figure 4.6: 2.5 Gb/s reference and 40 Gb/s data receiver sensitivity versus OSNR. The power of the reference signal is 12.5 dB less than the data signal.

To summarize, the effects of changing the relative power ratio and the electrical receiver bandwidth are as follows:

- **Power ratio:** Changing the power ratio will control the point where the curve breaks. It can, however, also influence the receiver sensitivity if the crosstalk between the channels is not minimized sufficiently. Minimizing the polarization crosstalk substantially simplifies the operation of the monitoring technique.
- **Electrical receiver low-pass filtering:** Changing the bandwidth in the electrical receiver (for example using a 10 GHz receiver for a 2.5 Gb/s reference signal) will control the point where the curve breaks and also the receiver sensitivity at high OSNR values.

There is no real advantage in aligning the receiver sensitivity values for the two signals at high OSNR's as this is only a matter of scaling. The breaking point of the curve at sufficient low OSNR is more interesting as this is what needs to be correlated in order to predict the 40 Gb/s signal BER and use the concept for signal quality monitoring in OSNR limited systems. Furthermore, it will be very costly to use a 40 Gb/s receiver for the 2.5 Gb/s signal while it would be simple to adjust the power of the 2.5 Gb/s channel and in this way assure overlapping curves for the reference and the data signal.

The problems related to inaccurate OSNR measurements in dense WDM systems was earlier described in section 2.1 and will be discussed further in section 5.2 also. The concept described here is applicable for these cases where the OSNR can be difficult or even impossible to evaluate with traditional means.

Possible polarization multiplexing issues

It was discussed above how the 40 Gb/s signal impaired the 2.5 Gb/s signal due to crosstalk. Adding a 2.5 Gb/s reference signal by polarization multiplexing it with a 40 Gb/s data signal could easily arise some concern as to weather the 40 Gb/s data signal also would experience any detrimental effects due to crosstalk from the 2.5 Gb/s signal.

Figure 4.7 shows BER curves for the 40 Gb/s data signal. *Left:* Two cases are shown to investigate the possibility of crosstalk - with and without the 2.5 Gb/s reference signal. $\Delta P_{\mathrm{dB}} = P_{40Gb/s} - P_{2.5Gb/s} = -6.1$ dBm $-$ 8.5 dBm $= 2.4$ dB. *Right:* 40 Gb/s eye diagrams illustrating the effect of bad polarization aligning (PC3 in Figure 4.2).

The BER curves shows that with a correct adjusted polarization to the demultiplexing PBS, virtually no crosstalk from the 2.5 Gb/s channel is observed. Note that the 40 Gb/s power is greater than the 2.5 Gb/s, which is also relevant in achieving the small crosstalk penalty. Fortunately, due to the nature of the concept, the lower bit-rate reference signal will always have a lower power than the high bit-rate data signal.

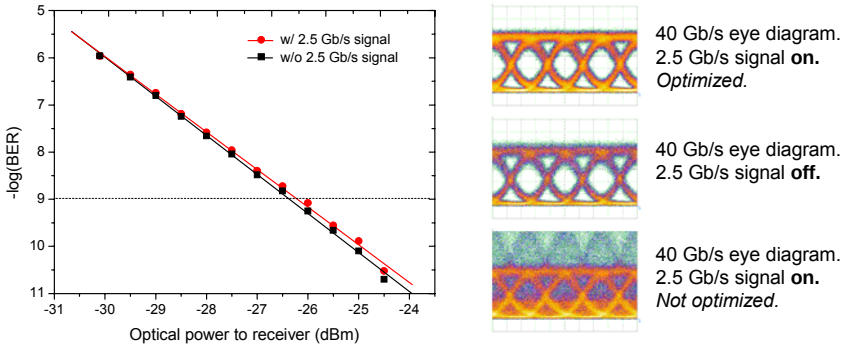

Figure 4.7: Experimental BER curves for the 40 Gb/s data signal. Two cases are shown: with and without the 2.5 Gb/s reference signal.

Initially the data signal and the reference signal is launched orthogonally to each other and they vastly stay orthogonal throughout transmission. Although the two channels will remain orthogonal the combined state will change during transmission due to fiber imperfections, fiber bends and temperature fluctuations

so the polarization control PC3 in 4.2 needs to be adjusted and optimized frequently. Preferably, a polarization tracker should be used in a real system as the changes there will happen more rapid compared to a lab environment. During these experiments the polarization remained stable for about 20 minutes if the setup was left untouched. This was verified through long-term BER measurements on the 40 Gb/s signal.

Figure 4.7 (right) shows the eye diagrams of the 40 Gb/s signal in different situations. In the top eye diagram the data and reference signal is transmitted together and the two signals are separated by correctly adjusting the polarization controller PC3 seen in Figure 4.2. The middle eye diagram shows the 40 Gb/s signal when the reference channel is turned off. Comparing to the top eye diagram it can be seen that if PC3 is properly adjusted, the 2.5 Gb/s signal will not impose any degradations on the 40 Gb/s eye. However, if PC3 is not optimized and thus misaligned, this becomes clearly visible in the 40 Gb/s eye displayed last in Figure 4.7.

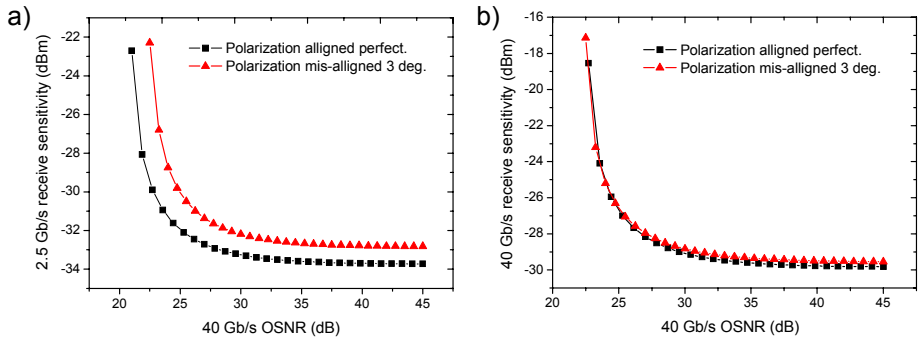

Figure 4.8: Simulated receiver sensitvity curves are shown in a reference to the 40 Gb/s OSNR for perfect and imperfect polarization allignment for: *Left: The* 2.5 Gb/s reference signal and *Right:* 40 Gb/s data signal. $\Delta P_{\mathrm{dB}} = P_{40Gb/s} - P_{2.5Gb/s} =$ 3 dB.

A misalignment of PC3 can a have deep impact on the qualities of both signals. Figure 4.8a) and b) show a VPI simulation of a case where the polarization control PC3 have been misaligned by 3 degrees prior to polarization multiplexing. The effect on the 2.5 Gb/s signal is clearly visible in Figure 4.8a). Whereas the 3 degrees misalignment causes a 1 dB penalty to the 2.5 Gb/s signal the effect on the 40 Gb/s signal is negligible - Figure 4.8b). Again, this can be assigned the relative difference in channel power, which in this case is 3 dB in favour of the 40 Gb/s channel. Although the effect on the 40 Gb/s data channels is negligible in this case, PC3 should still be aligned correctly in order to reduce the crosstalk factor in Equation (4.5).

4.1.4 Detecting other signal degradations

To further analyze the method, this section will investigate if method is useful towards systems being degraded by other effects such as for example dispersion, PMD and nonlinearities. A relative low bit-rate signal like the 2.5 Gb/s used here will not be useful for monitoring dispersion or PMD induced BER changes in a 40 Gb/s system as the sensitivity towards these effects is strongly dependant on the bit-rate [4]. Possibly, the dispersion sensitivity of the reference signal can be enhanced sufficiently by pre-chirping the 2.5 Gb/s signal but this has not been considered further here.

Instead it was tested if the method can be used to detect BER degradations caused by nonlinear effects. It is well known that a signal can suffer from various effects such as SPM, XPM, FWM as well as SBS. A problem arises, though, regarding the required correlation between the data and the reference signal as different bit-rate signals suffer from different nonlinear effects. For example will a low bit-rate signal be degraded by SBS at a lower input power seen relative to a higher bit-rate signal. This is due to the narrow gain bandwidth of the SBS effect, which is around 100 MHz in SMF. Although no correlations were expected between the BER performance for the 2.5 Gb/s signal and the 40 Gb/s signal, an experiment was performed to assure that this was the case. The result is seen in Figure 4.9.

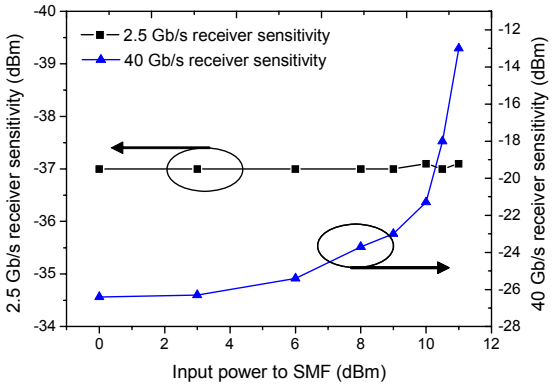

Figure 4.9: The receiver sensitivity for the 2.5 Gb/s and the 40 Gb/s signals are plotted together versus optical input power. As expected, no correlation is seen between the signals.

As expected, the sensitivity decreases much earlier for the 40 Gb/s signal compared to the 2.5 Gb/s signal. This is because the 40 Gb/s signal is strongly affected by SPM at high input powers whereas the 2.5 Gb/s signal is not.

[4] For example is a 40 Gb/s signal 16 times more sensitive to chromatic dispersion than a 10 Gb/s signal.

As discussed in Chapter 3, it is vital to identify the important and necessary factors to monitor in a system. Whereas dispersion, PMD and nonlinearities can be both useful and, at times necessary to monitor, noise created BER degradations will remain one of the more important parameters to monitor. This work is a presentation of a possible solution for providing a more accurate BER evolution in networks where this is normally not noticeable. The use of a 2.5 Gb/s signal for monitoring, was merely chosen for practical reasons, but in a practical implementation, a lower bit-rate can be used as the concepts described here holds true in general.

4.2 Optical parity calculator

At present, all signal processing in commercial networks is done in the electronic domain. Issues such as power consumption, footprint requirements, and cost of high-speed electronics will make optical solutions more attractive as the bit rate increases, and thus simpler signal processing tasks may move into the optical domain.

Parity checking is widely used today in the electrical domain, and is a simple method of error checking. As an example of a bit parity check, section 3.2 briefly touched the BIP-8 method used in SONET/SDH. As also mentioned in regards to BIP-8 bit parity checking it is not a complete error check as two errors within the same data block can pass undetected. However, the method provides a simple solution for indicating errors, a solution that is sufficient in many cases.

This section describes a simple method of all-optical bit parity calculation using a Mach Zehnder interferometer (MZI) with integrated SOA's. All-optical bit parity calculations can be used in various schemes, which also will be discussed.

4.2.1 Parity bit calculating and checking

The principle of bit parity calculating and checking builds on the logic XOR function illustrated in Figure 4.10. Following the XOR logic table, the parity bit is calculated from the bit stream and subsequently transmitted with the data bits in a header, for example. At destination the parity bit is again calculated and compared to the check bit. If there are any discrepancies it is assumed that there exist corrupted bits in the data stream. However, this method is inaccurate in various cases. If the parity check bit itself is corrupted the healthy bit-stream will be discarded or if two errors occur in the data stream, the result could be that an error is not discovered. The longer the string of bits per check bit, the higher the risk of inaccuracy.

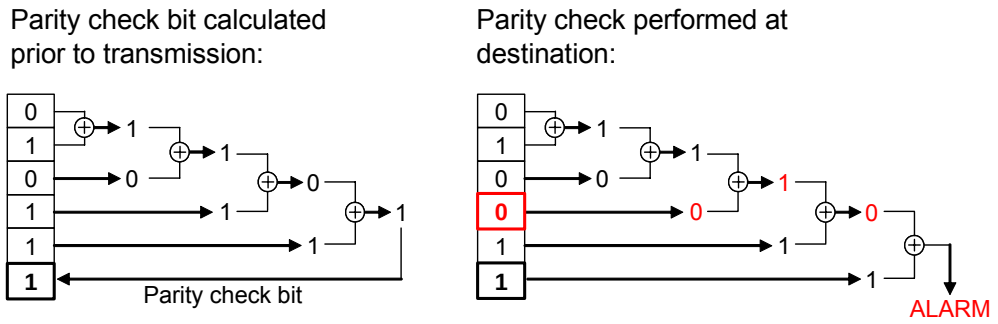

Figure 4.10: Parity bit calculating and checking on a 5-bit stream. The parity bit is inserted as the 6th bit and transmitted along with the data.

Developing parity calculating and checking in an all-optical environment is not an easy task due to integration difficulties and the lack of optical random access memory (RAM). The lack of RAM means that the task would have to be performed real-time, so the latency in the optical circuit must necessarily be equal to one bit time-slot. In a 10 Gb/s system this corresponds to 100 ps - less than 5 cm of optical fiber.

Instead of performing a full parity calculation on every single bit in the packet or bit stream, a compromise can me made by performing the parity check on a selected bit sequence, also called a bit-word. This was done in [71], where a double tera-Hertz optical asymmetric demultiplexer (TOAD) construction was used in an optical loop to create an all-optical bit-word parity checker. The bit-word circulated in the loop a number of times corresponding to the length of the word, in this case 144. In another case, a circulating shift register was created using a nonlinear interferometer [76]. Both cases however being fiber and EDFA based technologies suffered from high round-time latency making real-time parity checking impossible. In order to reduce the round time latency, or time-of-flight, sufficiently an integrated solution is needed. The next section describes how an integrated Mach-Zehnder interferometer (MZI) was used as an XOR gate with feed-back to perform real-time parity calculations.

4.2.2 MZI with integrated SOAs as an optical XOR gate

In the experiments, the optical XOR gate is accomplished using a MZI with integrated SOA's as illustrated in Figure 4.11. This type of MZI has previously been used successfully to realize logic functions such as OR and XOR [77], [78]. A data sequence **A** is input in the upper arm no. 1 and sequence **B** in the bottom arm no. 2, both at 10 Gb/s RZ. A 10 Gb/s clock is injected counter-propagating into the MZI in arm no. 4, and the resulting signal, **A** XOR **B** (**A** $\oplus$ **B**) is received at the center left arm no. 3.

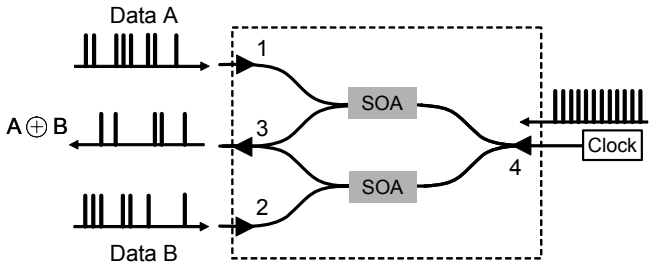

Figure 4.11: The all-optical XOR function is realized in a Mach-Zehnder interferometer with integrated SOA's. Illustration shows the interferometer in counter propagating operation.

This illustration shows the interferometer in a counter propagating operation, which is necessary for the parity calculation as will be seen. More information about co- and counter propagation operation as well as other applications of the MZI can be found in [79] and [80]. The integrated MZI chip illustrated in the dashed box has a length of a few millimeters.

The MZI in Figure 4.11 can be transformed into a parity calculator by simply connecting arm no. 2 and arm no. 3 and thereby making a feed-back loop as illustrated in Figure 4.12. Notice though, that in order to perform a sequential real-time parity calculation utilizing every bit in the bit-stream, the time-of-flight in this feed-back loop should match the bit time-slot exactly. Although not impossible, this requires exact integration of the entire MZI plus feed-back circuit, which was not an option in our experiments.

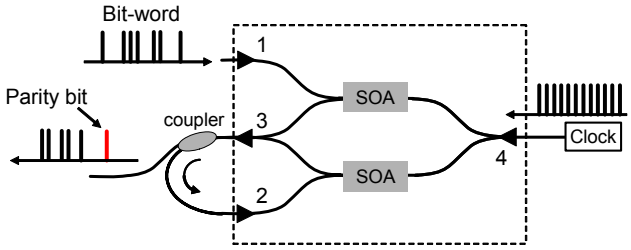

Figure 4.12: Real-time sequential parity calculation on a bit-word using a feed-back. This requires a time-of-flight in the feed-back circuit of exactly one bit timeslot. In a 10 Gb/s system this is 100 ps.

Instead of performing a sequential parity calculation the focus was on performing real-time parity calculations on selected bit's in a bit-word or packet. Similar to the case of BIP-8 this will not provide a complete BER evaluation of the signal, but rather give an indication of the BER. The principle is illustrated in Figure 4.13 where a bit-word, or in this case a data packet, is entering the parity calculator. If the total feed-back delay equals the length of a packet, the same bit-slot in a packet, for example a header bit, will be selected for parity

calculation. This can be useful for e.g. header error monitoring. If alternatively the total feed-back delay is different from the packet length, the bit-slot for parity calculation will wander through the packet. This is easier to manage, as the delay does not have to be adjusted to a specific packet length that additionally also might be variable. The resulting parity bit can thus originate from a combination of both payload bits and header bits. The gated clock is used to select the bit positions in the incoming data stream. In practise these gating pulses correspond to an AND function between the gating pulses and the incoming data bits.

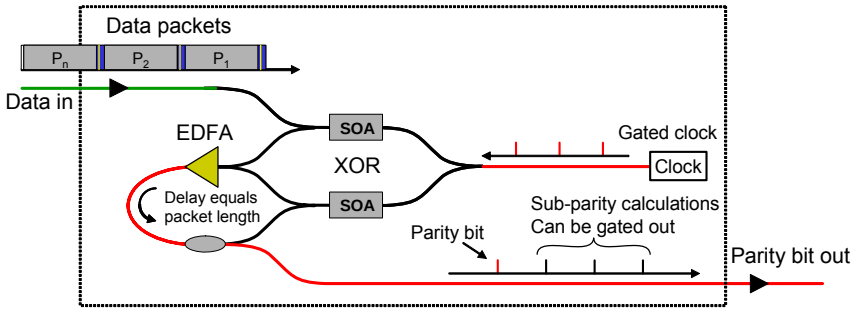

Figure 4.13: Illustration of header error monitoring using the parity calculator. The feed back delay is adjusted such that a specific header bit is used for parity calculation.

In the figure, a number of sub-parity calculation bits can also be seen. These bits originate from working calculations that will exit the system at a rate equal to the gated clock signal. If the parity calculation is done using 10 payload bits, the 10th bit exiting the system will be the parity bit of interest. The bit's arriving prior to the parity bit can be discarded.

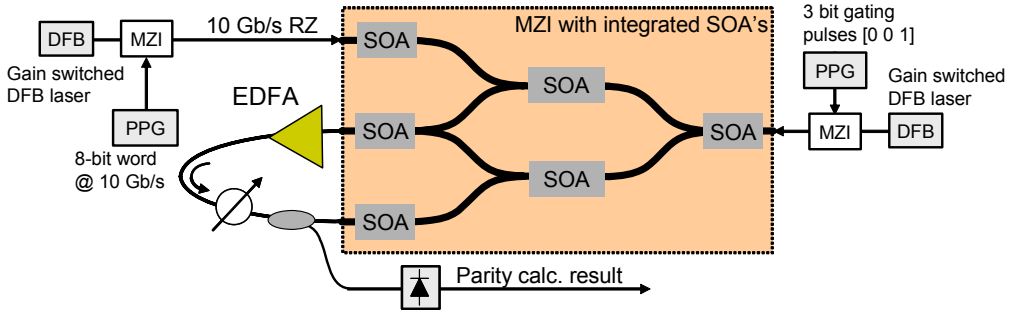

Figure 4.14: Illustration of the setup used for parity calculations of an 8-bit word at 10 Gb/s.

In the practical experiment the total time-of-flight was increased to approximately 500 bit's (at 10 Gb/s) corresponding to about 20 meters of fiber. The parity calculations were verified using an injected data word consisting of 8 bits [0 1 0 0 1 0 1 1], and a gating sequence of 3 bits [0 0 1]. This rather short

data-word was necessary in order to be able to gate the result and visualize it on an oscilloscope. The experiment served as a demonstration and proof of concept, and should not be considered to be a realistic parity calculation example. The experimental setup is shown in a reduced version in Figure 4.14.

The experimental work on the parity checker was performed in collaboration with M.L. Nielsen, and a more detailed description on the physical mechanisms in the MZI as well as other experimental results, less relevant for this thesis, can be found in [81].

4.2.3 Performance monitoring of payloads in packet based networks

This section will discuss a couple of parity check schemes for performance monitoring of packets in optical networks. Figure 4.15 shows a diagram of how the parity checker could be used in a practical situation.

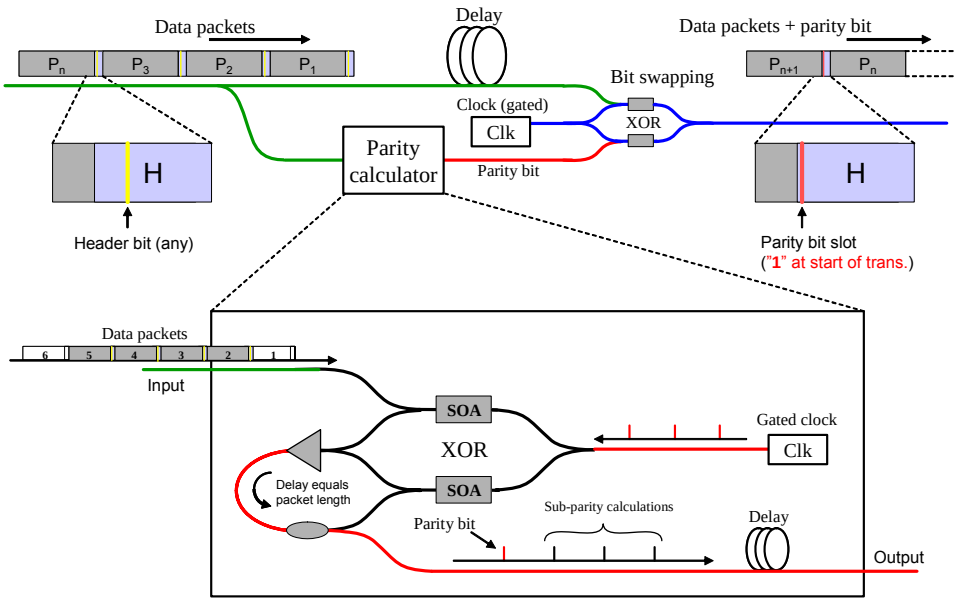

Figure 4.15: Parity determination of selected header bits. Writing of parity to allocated parity bit-slot in packet.

The figure shows the all-optical calculation and insertion of a header parity bit into an optical packet prior to transmission. The model here is intended for detection of error bursts in optical transmission systems [82], [83]. The system described here is packet based, and one bit-slot in the packet is reserved for parity checking.

Before transmission, the packets are sent to the parity calculator and the parity bit, for a pre-selected number of packet header bits, is found. By sending the data signal through a delay fiber, the parity bit can be included into the header. The parity bit is written to the header parity bit-slot by using the XOR function of another XOR gate, which is possible as the pre-determined value of this slot is a "1"-bit. I.e. if the parity bit calculated is "1", the resulting parity bit inserted into the header is "0" and visa versa. Although the parity bit is inversed, the bit will uniquely describe the parity of the foregoing header-bits.

Also in this case, the parity bit-slot itself is vulnerable to errors as the bit-slot is assumed to be ”1” when the bit is written to the header using the XOR gate. If the parity bit is ”0” due to an error in the parity bit slot, the whole array of packets will be labeled with ”error” at reception even though there is none. Equally, potential errors in the parity bit-slot during transmission will also result in an error and the whole packet will be marked as errornous although it is not.

Another possible implementation and utilization of the optical parity calculation is illustrated in Figure 4.16 and 4.17.

In the scenario shown in Figure 4.16, the signal integrity is frequently checked by passing the parity calculator and error detector.

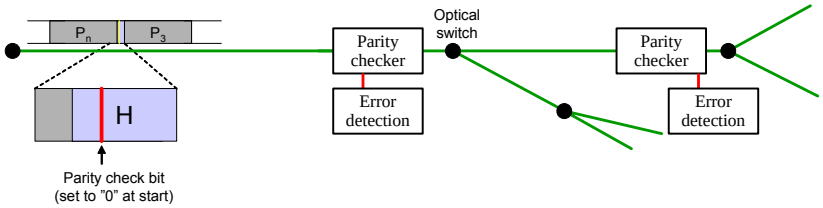

Figure 4.16: A possible scenario for use of the parity checker in an optical packet switched network.

Similar to the previous example described in Figure 4.15, a specific header bit is pre-coded, this time as a "0" bit. During transmission, the signal can be exposed to an effect causing an error in a header bit, for example an error burst. Figure 4.17 explains what happens when an error occurs in the parity bit's. As the parity bit slots in the packets are pre-coded with "0", an error in one of these bit's would generate a "1" bit. Following the XOR gate logic table the output from the parity checker would thus remain "1"s until another error occurred. By detecting the output of the parity checker, it is thereby possible to track any errors occurring in the header parity bits. Further more, if one assumes the frequency of errors to be slow, a slow low-cost receiver would be able to detect these changes in the "1" and "0" parity streams as the length of each stream of one's and zero's would be relatively long before a change would take place.

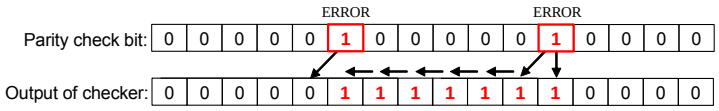

Figure 4.17: The output from the parity checker in case an error occurs in the header parity bit.

4.3 Chapter summary

Two methods for optical signal quality monitoring have been discussed. By polarization multiplexing a lower bit-rate signal with a unknown high bit-rate signal it was possible to establish a correlation between the reference signal quality and the data signal quality in the case of a noise limited system. It was also verified that the concept was not readily applicable in the case of systems dominated by dispersion or nonlinear effects.

Secondly a method for all-optical parity calculation at 10 Gb/s was presented. An integrated MZI and active SOA's made basis for the XOR gate. By applying a feedback it was possible to perform parity calculations on selective bits in the 10 Gb/s bit-stream. A full parity calculation involving all adjacent bit's implied the length of the feedback fiber to be controlled very strictly, which was not realizable in this case.

Chapter 5

Optical signal parameter monitoring

The overall quality of a signal will often be an attractive way to ensure up-time in an optical network. However, due to the nature of the techniques, it can be difficult or even impossible to determine the nature of the fault. This chapter picks up from Chapter 2, where various optical effects were introduced. These potential detrimental effects can be monitored to gather information about the quality of an optical signal. In addition, optical signal parameter monitoring can provide valuable information to determine the cause of a potential signal degradation.

The following sections will focus on dispersion monitoring and OSNR monitoring.

5.1 Chromatic dispersion monitoring

Group velocity dispersion monitoring, or dispersion monitoring as it is referred to here, is considered one of the optical signal parameters that is important to monitor [30], [84]. As stated in Section 2.2, various methods have already been developed to monitor the dispersion in an optical network. In this section the focus will be on a dispersion monitoring method that was developed through inspiration from [13] and [84]. The method, which is described through experimental work, has applications both as dispersion monitoring as well as for signal quality monitoring in systems impaired by residual dispersion.

In [84], a technique to monitor chromatic dispersion of a 40 Gb/s return-to-zero (RZ) signal using pulse compression followed by optical side-band filtering in a highly nonlinear fiber (HNLF), is reported. The dispersed RZ signal is pulse

compressed in order to amplify the spectral broadening effect that takes place in the HNLF. The broadened spectrum is then filtered at +2.5 nm relative to the carrier wavelength, and that signal in turn provides information about the dispersion in the system.

The technique proposed here and experimentally demonstrated is similar to that of [84] as sideband filtering is also used to gather information about the accumulated or residual dispersion. However, in this approach we omit pulse compression, which in addition to simplifying the setup makes the scheme applicable to the RZ as well as the NRZ data format. By tapping off a portion of the light, exploiting the spectral broadening effect associated with SPM, and applying optical side-band filtering, it is possible to obtain a monitoring signal that can be correlated to the dispersion and/or the BER of the data signal. The experimental demonstration is done for 40 Gb/s NRZ and RZ data.

5.1.1 Principle of Operation and Experimental Setup

This dispersion monitoring technique exploits the effects of SPM induced spectral broadening in a nonlinear medium due to high signal peak power. As dispersion has a direct influence on the shape and peak power of a pulse, the instantaneous effect of SPM on the pulse will translate into a spectral broadening that can be quantified through optically side-band filtering the signal as documented in [84] for RZ pulses. As the dispersion increases, the peak power drops, thereby reducing the nonlinear phase shift, which in turn means that the power in the side-bands will drop accordingly. Positioning an optical filter in one of the side-bands provides a dispersion monitoring signal.

For the NRZ data format, however, it is non-trivial to predict the spectral changes arising from SPM in the nonlinear medium. The one-level will in general drop for increasing dispersion as for RZ, but for consecutive one's an overshoot will rise up at the leading and trailing edges and thus give rise to an increase in SPM. The result is two effects working to decrease and increase SPM respectively. As will be seen in the following, it is possible to find various behaviors of the spectral filtered signal depending on the de-tuning of the filter. It is shown that by carefully choosing the position of the optical filter a useful monitor signal can still be extracted.

The experimental setup used for the demonstration is shown in Figure 5.1. A 40 Gb/s optical signal is generated and sent through SMF to simulate residual dispersion. After subsequently splitting the signal, one part continues to the receiver and the bit-error-test-set (BERT) and the other part is used for monitoring. The tapped off signal is sent through an EDFA to boost the signal to a level exciting SPM in the HNLF. The optical spectrum analyzer (OSA) is used instead of an optical filter as it allows us to vary the spectral width of the filter

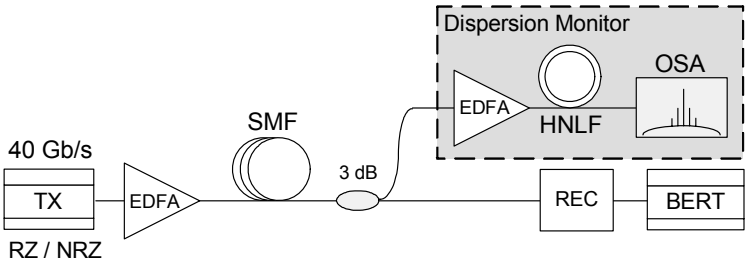

Figure 5.1: Experimental setup used to demonstrate the 40 Gb/s RZ or NRZ signal monitoring.

as well as tuning the central wavelength. In a practical use, the OSA would be substituted with either a wavelength tunable or fixed wavelength optical filter.

The HNLF fiber used had a nonlinear coefficient $\gamma = 10.6$ $W^{-1}km^{-1}$ and a length of 1.5 km. The power launched into the HNLF was kept at a constant level of 21 dBm. The two values were used to investigate the effect of the differences in power level.

5.1.2 Experimental results

Experiments have been performed for both the RZ and NRZ data format using the setup shown in Figure 5.1.

RZ data format

A 40 Gb/s optical RZ signal is transmitted through various amounts of SMF and a portion is tapped off for monitoring. The result of the experiment is shown in Figure 5.2. The figure shows the pre-amplified receiver power penalty variations versus the optically filtered power, and how this signal in turn provides an indication of the signal quality. The filter is placed at + 0.96 nm relative to the carrier with a bandwidth of 0.5 nm (OSA resolution bandwidth).

As seen in Figure 5.2, the minimum of the filtered signal coincides with the 1-dB dispersion penalty of the data signal. In this way the monitor signal minimum can be used as an indicator that the 1 dB penalty limit has been exceeded when the minimum is passed. Furthermore, as the curve is symmetric about 0 ps/nm, the filtered monitoring signal can be used in a feedback loop that controls a tunable dispersion compensation device to sustain zero residual dispersion. It should be noted however that chirp in the transmitter can cause this curve to be asymmetrical. The results in Figure 5.2 also demonstrate that a useful monitoring signal can be extracted using side-band filtering without applying pulse compression.

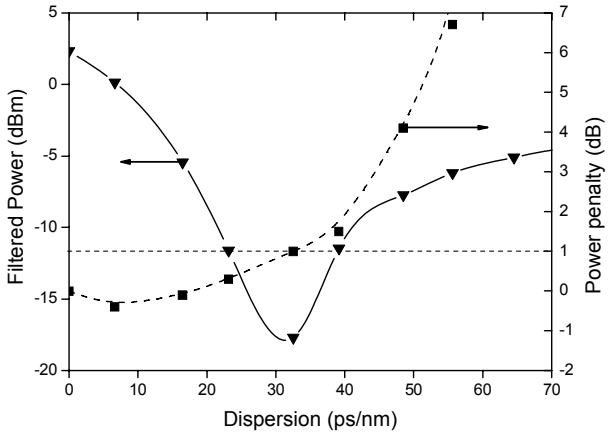

Figure 5.2: The figure shows the filtered monitor signal and receiver penalty for a 40 Gb/s RZ signal vs. dispersion. The optical filtering is done at +0.96 nm relative to the carrier.

NRZ data format

The same experiment as described above has been carried out for a 40 Gb/s NRZ signal. However, in this case, as explained above it is non-trivial to predict the behavior of the monitoring signal.

Figure 5.3 shows how the optical spectrum of the monitoring signal changes with the dispersion. The left part shows the eye diagrams of the data incident to the monitor for increasing residual dispersion and the right part shows the corresponding spectrum of the optical signal after transmission through the HNLF – the box indicating a filter position at +0.23 nm. Depending on the filter detuning, one will see various behaviors of the monitoring curve as illustrated in Figure 5.4. In a) the signal is filtered at a wavelength +0.23 nm and b) at +0.43 nm relative to the carrier - both with a resolution bandwidth of 0.1 nm. Figure 5.4 shows that by applying the appropriate optical filtering to the broadened signal, one can achieve a useful monitor signal; i.e. depending on the intended application and use of the monitor, the response can be changed accordingly by tuning the filter. For example is the monitor curve maximum in b) coinciding with the 1 dB dispersion penalty limit.

In general it is expected that this method can monitor any kind of pulse broadening effect, as the peak power has a direct influence on the spectral broadening in the HNLF. More specifically, differential group delay (DGD) changes caused by polarization mode dispersion (PMD) is expected to induce the same effects as seen here.

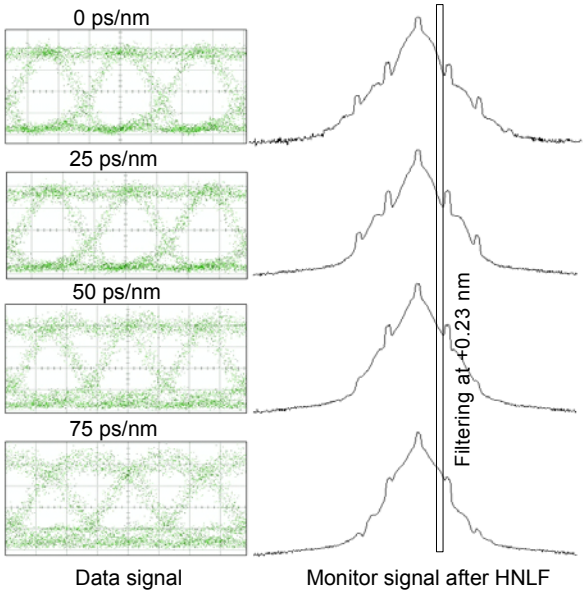

Figure 5.3: The development in the 40 Gb/s NRZ eye diagram and the corresponding change in the monitor signal spectrum after passing through the HNLF with 21 dBm input power.

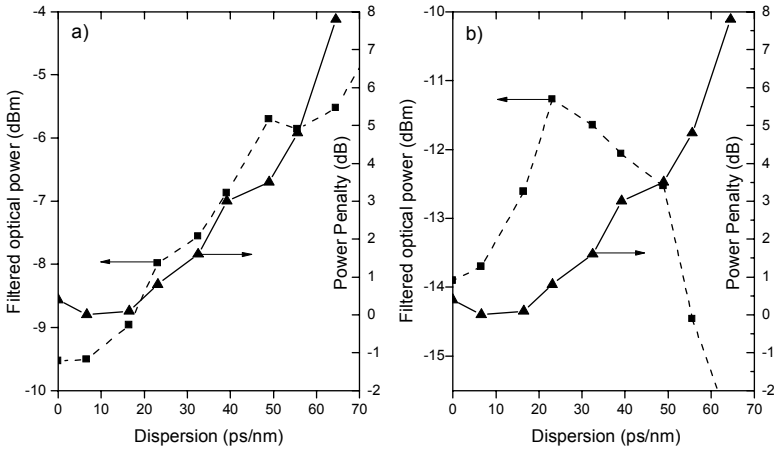

Figure 5.4: The figure shows how the filtered optical power of a 40 Gb/s NRZ signal varies with the dispersion and with the receiver penalty. The optical filter is placed at a) +0.23 nm and b) +0.43 nm relative to the carrier.

5.1.3 Simulation results

Although the pulse shape influence on the spectral broadening can be well explained through the theory of SPM induced spectral broadening, it is non-trivial to explain the exact behavior of the various spectral components. It was for example seen in Figure 5.4 how a different filtering position would create a very different result.

In order to gain better understanding of the effects and further evaluate the credibility of the results a number of simulations were varied out using VPI Transmission Maker[1]. As it is very difficult to simulate a situation identical to the one in a laboratory, a simulation tool will rarely produce results that can be compared directly to the experimental results, but they will usually help gain better understanding.

A 40 Gb/s RZ system was simulated and the results are seen in Figure 5.5a). For comparison, the experimental results are shown in Figure 5.5b). Note that the dispersion and penalty axis are the same scale to ease the comparison.

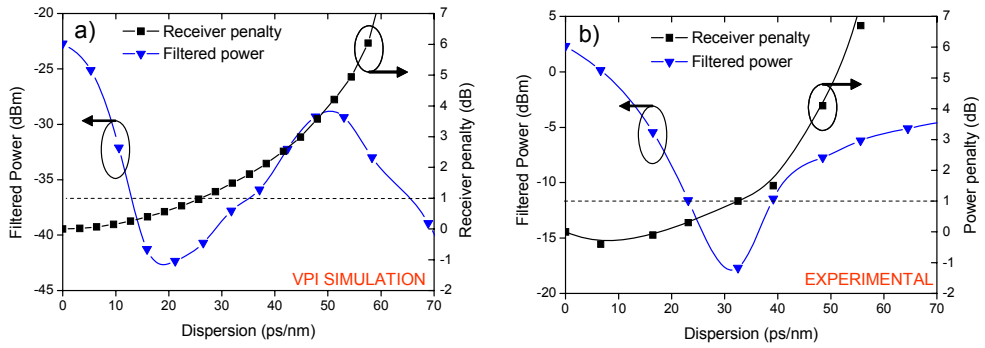

Figure 5.5: The figure shows the simulated a) and experimental case of 40 Gb/s RZ signal monitoring. The filter bandwidth is 0.5 nm in both cases, whereas the filter position is 2.1 nm and 0.96 nm for a) and b) respectively.

The figures are clearly not identical, but share a number of similarities. The simulated power penalty curve has a maximum at zero dispersion, which indicates a more ideal transmitter without chirp. This also means that the 1 dB penalty limit is shifted slightly in the two cases. Moving on to the filtered power curves it should first be noted that the filtering position is different in the two cases. For the VPI simulation +2.1 nm is used whereas +0.96 nm was used for the experimental results. The resolution bandwidth is 0.5 nm in both cases. The shape of the curve changes very little as the filter position changes, so the posi-

[1] VPI Transmission Maker version 5.1 was used for the simulations. Please refer to Appendix A for more details concerning simulation parameters.

tion with the largest dynamic range was chosen and for the VPI simulation this position was +2.1 nm. Notice how the filtered power minimum is located very close to the 1 dB penalty limit in both cases, as well as the general curvatures agrees well we each other.

Figure 5.6a) and b) shows the spectral evolution for the VPI simulation and experiment. The curves are shown for 0 ps/nm, 16 ps/nm, 48 ps/nm and 72 ps/nm residual dispersion. Although the spectra look somewhat different, they are similar in how the curves behave respective to each other within each case. This is what causes the similarities in Figure 5.6a) and b). The spectral differences can be attributed to differences in phase, pulse shape and logical pattern of the signals. These factors along with others dictates the exact appearance of the optical spectrum and with both pulse shapes and logical pattern being different in the two cases, the two spectra cannot be expected to be identical.

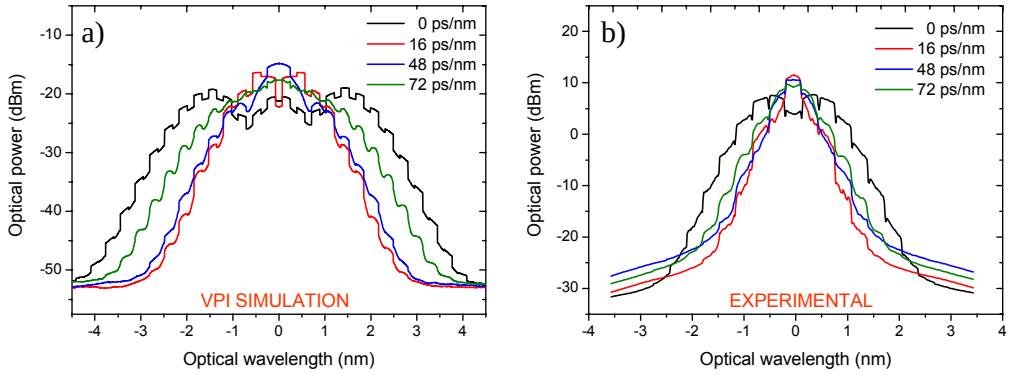

Figure 5.6: The figures illustrates the spectral developement for various residual dispersion values. a) VPI simulation. b) Experimental result.

5.2 OSNR monitoring

Optical-signal-to-noise (OSNR) monitoring is used already in today's optical networks as a mean of monitoring signal integrity. Noise is one of the most important sources to bit-errors in optical systems. Degrading optical amplifiers and lasers, lossy connectors, and general accumulation of ASE in multi-span systems are typical sources of OSNR degradations. Provided that accumulation of noise is the dominant source to signal degradation, the otherwise unknown signal quality can be well quantified through the OSNR.

Noise, being the foremost significant source to signal degradation in most optical systems, is conventionally monitored through spectral analysis as explained in section 2.1. In this way, the OSNR evaluation is done by assuming that it is possible to interpolate the in-band background noise level with the noise out-of-

band, i.e. next to the channel in question. This is illustrated in Figure 5.7a). This normally gives a correct evaluation of the in-band noise level, and thus the correct OSNR value, but in cases of WDM networks, this method can be inadequate as illustrated in Figure 5.7b). Despite the high spectral resolution bandwidth of 0.01 nm it is not possible to resolve the spectrum well enough to estimate a correct OSNR. If the interpolation method is used, one would arrive at an OSNR value of 33 dB, whereas the correct value is closer to 41 dB. The problem will increase with decreasing channel spacing, optical noise filtering, demultiplexing and spectral broadening due to nonlinearities. Several factors can hinder accurate OSNR evaluations in WDM systems.

Even though single channel systems obviously do not suffer from this neighboring channel issue, optical filtering can cause a problem when estimating the OSNR later in the system. In single channels systems, cascaded optical filtering can cause a "noise shoulder" due to shaping of the noise around the channel. This makes it difficult to distinguish the true noise level from the shoulder created by the filter. Similarly can demultiplexing in WDM systems cause the noise levels on either sides of a channel to be suppressed again leading to a wrong OSNR evaluation.

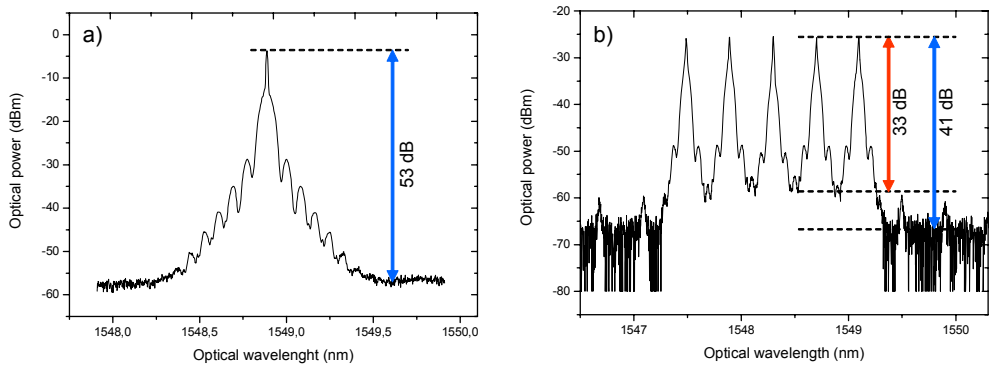

Figure 5.7: a) Illustrations of how OSNR traditionally is measured. The figure shows a 40 Gb/s NRZ coded channel transmitted through 4 km DCF fiber. The launch power was 0 dBm. b) In cases of several channels it can be difficult or impossible to measure OSNR.

5.2.1 Polarization extinction

Alternative methods for evaluation of a more correct OSNR have been developed. Especially one method using polarization extinction has been investigated intensively. This technique was first described by M. Rasztovits-Wiech et al. in [18] and exploits the fact that the ASE noise is unpolarized unlike the signal,

which usually has a well defined polarization, i.e. a high DOP[2]. The signal is passed through a polarization controller and a polarizer, which is followed by a spectrum analyzer or an optical filter and a power meter. Using the polarization controller, the state of polarization is changed to achieve maximum and minimum transmitted power. When the power is at a minimum the channel itself is rejected in the polarizer, and the remaining power corresponds to half of the total ASE power assuming 100% unpolarized ASE. Relating this to the maximum transmitted power will achieve an OSNR evaluation that is more accurate than the traditional interpolation method. Other methods similar in principle to this one have been developed [15], [19].

In [19], the degree of polarization (DOP) is measured and used to obtain the OSNR. As the DOP is the ratio between polarized light power and the total light power, it is shown that the OSNR can be derived from

$$\text{OSNR} = \frac{\text{DOP}}{1 - \text{DOP}}$$

Most of these methods suffer from being sensitive to PMD, polarization dependant loss (PDL) and also imperfect rejection of the orthogonal polarization state in the polarizer. As a consequence this limits the accuracy. For example only OSNR values up to approximately 25 dB can be measured with reasonable accuracy as described in [19].

For optical performance monitoring it can seem problematic that the monitor cannot be used for OSNR values better than 25 dB. This however, might not be an issue as described in [85], where the performance requirements to an OSNR monitor are investigated. There it is reported that OSNR changes above 26 dB is generally not of interest. This particular investigation was done for a 10 Gb/s RZ system. Although this limit is expected to grow at higher bit rates it indicates that it is not necessary to be able to monitor the OSNR up to the maximum value in the network.

5.2.2 OSNR monitoring in WDM systems using polarization interleaving

Inspired by the polarization extinction technique described above, an OSNR monitoring technique suitable for WDM networks has been developed and experimentally verified. Figure 5.8 illustrates the principle of how the OSNR monitoring is done; in this case in a 3 channel WDM system with 50 GHz channel spacing.

[2]PMD can reduce the degree of polarization of the carrier. This, however, is not relevant for the principles of the method and will be discussed later.

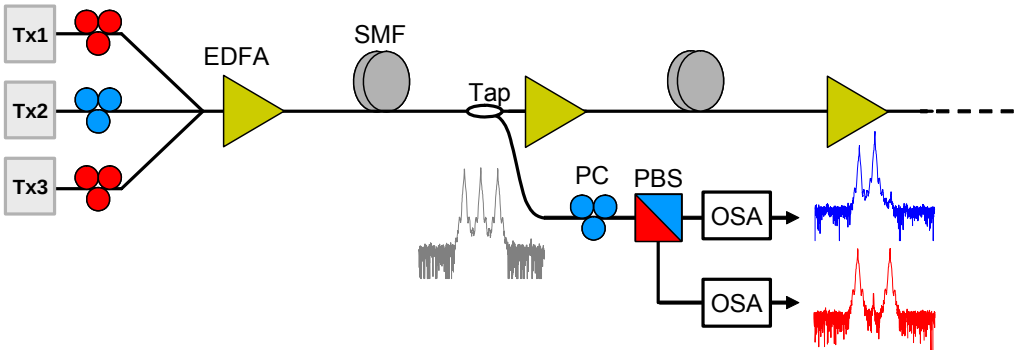

Figure 5.8: Principle of OSNR monitoring in a WDM network using channel polarization multiplexing.

Three channels are modulated with data and their polarization is oriented such that each neighboring channel is polarized orthogonally to the center channel. The technique is called polarization interleaving and can be used to enhance the spectral utilization as well as a method to reduce nonlinear signal degrading effects such as XPM [86], [87], and FWM [88]. The utilization of polarization interleaving in this matter is illustrated in Figure 5.8. At a point of interest, a part of the signal can be tapped off and the OSNR evaluated. The composite polarization interleaved WDM signal outlined in grey is sent to a polarization control (PC) followed by a polarization beam splitter (PBS). By aligning the polarization controller correctly, the signal is split into the two orthogonal polarization states by the PBS as illustrated in the figure. One part where the center channel (the probe channel) is strongly suppressed (red) and the orthogonal where the center channel is maximized and the neighboring channels are suppressed (blue). The two neighboring channels (channel 1 and 3) are not equally suppressed at high input powers, which can be seen from the blue spectrum. This is caused by birefringence in the fiber and it will be discussed further in Section 5.2.4.

In dense WDM systems, it is difficult or even impossible to resolve the spectrum well enough to observe the noise level next to the channel in question. If the channel spacing is for example 50 GHz, the channel side bands are actually covering up the noise level lying below so that it is impossible to find the ASE level needed to evaluate the OSNR, and therefore it is necessary to perform a more accurate OSNR evaluation. By using polarization interleaving it is possible to remove the neighboring channels by "polarization filtering" and the ASE level next to the probe channel can now be identified. Although similar to the polarization extinction method, the working principle as well as other features makes this method different. These features will be described in section 5.2.7.

5.2.3 Experimental setup

The experiment is carried out using three lasers as shown in Figure 5.9 and two MZ modulators. This is necessary in order to achieve the different polarizations, i.e. such that the center channel (Tx2) has a polarization orthogonal to that of the neighboring channels (Tx1 and Tx3). 10 Gb/s NRZ data signal is modulated onto the three carriers and combined using a PBS. It is important to make sure that the two polarization states of the channels are aligned correctly to the PBS in order to achieve equal channel power in the combined spectrum.

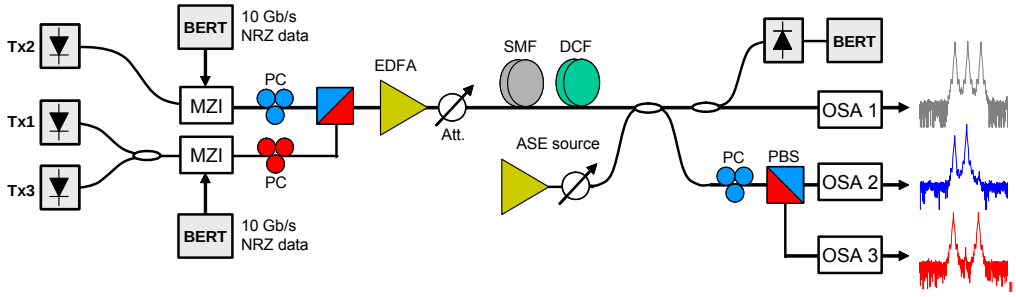

Figure 5.9: Experimental setup used to demonstrate OSNR monitoring using polarization interleaving in dense WDM systems.

After combining the channels in the PBS, the composite signal is sent through an EDFA and then transmitted to 80 km SMF and DCF fiber corresponding to 100% dispersion compensation. An optical attenuator makes it possible to vary the power and thus the spectral broadening generated through SPM and XPM in the SMF and DCF. After transmission, ASE noise can be added to the signal using a 3 dB coupler. It is generated using an EDFA with no input signal and varied using an optical attenuator.

From this signal is tapped a part for OSNR monitoring. The tapped off signal is directed to a polarization controller, which rotational plates is oriented such that each orthogonally polarized channel is separated in the PBS. It is vital to adjust the polarization incident to the PBS in order to avoid crosstalk between the channels. Crosstalk will cause inaccuracies when the OSNR is calculated. When adjusted properly, the two signals coming from the PBS will look as illustrated in Figure 5.10.

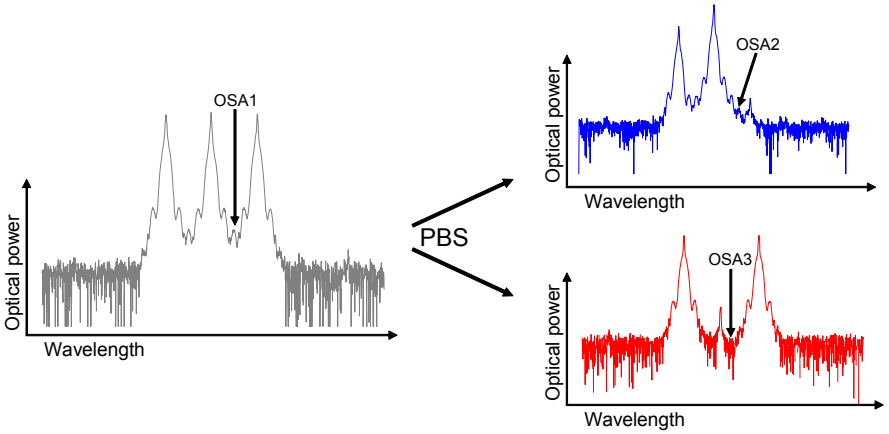

Figure 5.10: The optical power spectrum before and after the polarization beam splitter. The resolution bandwidth in these cases is 0.01 nm.

The center probe channels is maximized and minimized respectively. Note how the bottom red spectrum allows for an OSNR evaluation whereas this is not the case for the original grey spectrum on the left. The main signal continues from the tap-off towards a BER evaluation in the BERT as well as a conventional OSNR evaluation done using the left grey spectrum (OSA1) in Figure 5.10. The OSA 2 and OSA3 power levels also defined in the figure will be used below.

The following sections will describe OSNR monitoring experiments carried out using the setup in Figure 5.9. First, two different conceptual schemes are described.

Scheme 1 - Improved OSNR measurements in dense WDM systems

The channels are polarization multiplexing such that every channel is polarized orthogonal to the neighboring channels. This way the center channel can be "polarization filtered" away, and the OSNR can be determined as the in-band noise level is revealed. Thus the "true" OSNR is achieved rather than an OSNR affected by spectral overlap due to high spectral utilization. By relating the non-polarization-filtered OSNR and the polarization-filtered OSNR, one can in principle obtain information about the SPM and XPM generated crosstalk caused by spectral broadening. This enables a differentiation of the measured OSNR changes caused by nonlinear spectral broadening and noise respectively. However in practice the "OSNR degradation" arising from SPM and XPM is very small and will not influence the noise dominated OSNR significantly.

Scheme 2 - In-band noise evaluation

The in-band noise evaluation is done based on the difference in an OSNR measurement before and after "polarization filtering". If a single polarized channel is incident to the PBS and the polarization controller is correctly adjusted, one output from the PBS will only carry half the ASE noise and the other arm will carry the signal as well as half of the ASE noise. This is the case because the signal is polarized whereas the ASE noise is not. Using the information from these two outputs it is possible to evaluate the amount of in-band spectral noise much similar to the concept described in [18]. This principle does not only apply to single channel cases but can successfully be used in WDM systems as well. This scheme will not be investigated further here, as the principles are similar to that described in [18]. Instead the focus will be on the Scheme 1 approach described above.

5.2.4 Experimental results - ASE varied

In the first series of experiments, the ASE noise was varied by adjusting the optical attenuator, denoted as the "ASE source" in Figure 5.9. In practise the OSNR was degraded by turning down the attenuation and thereby admitting more ASE noise into the system. During these experiments the power to the SMF was kept at a constant 6 dBm. Figure 5.11 shows the result of a conventional OSNR evaluation in the case of 10 Gb/s NRZ coded data in a three channel WDM system with a frequency spacing of 50 GHz. The conventionally measured *inter-channel OSNR* is plotted versus the *true OSNR*, which is measured as the ratio of the channel power to the out-of-band noise level.

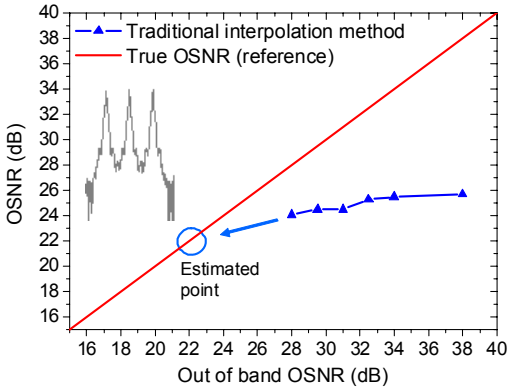

Figure 5.11: Conventional OSNR measurement results in a 3 channel system with 50 GHz spacing. Notice how the conventionally measured OSNR changes very little.

The out-of-band noise evaluation can be used only because the system consists

of only three channels and furthermore no optical filtering prior to the OSNR evaluation is performed in this single span transmission experiment. In practise optical filtering is necessary in multi-span optical transparent networks, and the optical filtering will in turn shape the spectrum and thereby alter the actual noise level. In these experiments, however, the out-of-band noise level will help to evaluate the OSNR monitoring technique.

The straight red line in Figure 5.11 illustrates the ideal OSNR, i.e. the result of an ideal OSNR measurement. This ideal line, however, is far from the inter-channel measured OSNR curve. It is clear from this that the conventional interpolation method provides insufficient information about the actual OSNR in the system.

If, instead, the tap-off sub-system is considered the result of the OSNR evaluation changes considerably. Figure 5.12 shows the result of OSNR calculations based on one of the outputs from the PBS.

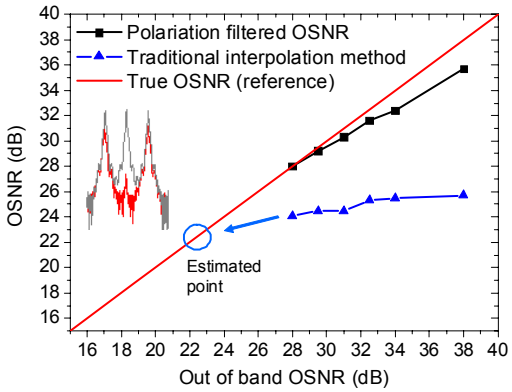

Figure 5.12: Figure showing an OSNR measurements on the same system using the polarization filtered signal. The polarization has been alligned orthogonal to the center channel. The inserted spectrum illustrates the original and polarization filtered signals.

In Figure 5.12 the center carrier is minimized and thus revealing the noise level that is used to calculate the OSNR. OSNR measurement results obtained from arranging the polarization filtering parallel to the signal (OSA2) provides a curve similar to that in Figure 5.12, however, using the OSA3 power produces the best result as this allows for best minimization of the neighbour channel. Refer to Figure 5.10 for details of how the OSA1, OSA2 and OSA3 power levels are defined.

The results in Figure 5.12 created via the OSA3 power should not be termed optical-signal-to-noise-ratio measurements as the ratio taken is somewhat differently. The ratio is found by subtracting the power of the probe channel from the OSA3 power. This *optical-signal-to-background-ratio* (OSBR) can be written as

$$\text{OSBR} = P_{Ch} \text{ - } OSA3 \text{ [dB]} \tag{5.1}$$

where P_{Ch} is the power in the probe channel and $OSA3$ is the power derived from the spectrum like illustrated in Figure 5.10.

The *OSBR* will be used forward on as the noise quantifying measure generated via OSA3.

Referring back to Figure 5.12a) it can be seen that the correlation with the true OSNR is not good at high OSNR values. At OSNR $>$ 34 the error is larger than 1 dB, and at OSNR $>$ 38 dB the error is larger than 2 dB. However, the need for accurately measuring very high OSNR values is generally not very strong as also mentioned in Section 5.2.1. Provided OSNR values $<$ 34 dB the OSBR thus successfully evaluates the level of noise in the system.

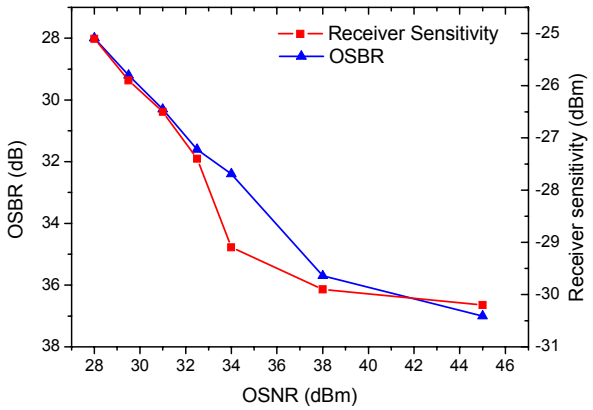

Figure 5.13: OSBR plotter together with the receiver sensitivity a 10 Gb/s NRZ system. The OSNR denoted on the x-axis is the true OSNR measured out-of-band.

Figure 5.13 shows a plot of the OSBR and the receiver sensitivity together, versus the true OSNR. The figure illustrates what influence the OSNR changes have on the OSBR and receiver sensitivity respectively, and also how each of the curves follow much the same development. A linear dependence between the OSNR and the signal sensitivity of a signal is not expected, as was also seen in Chapter 4, Section 4.1.2. The relatively good correlation between OSBR and receiver sensitivity seen in Figure 5.13 is not immediately predictable. The relationship between OSNR and receiver sensitivity can in small intervals be assumed linear, however, in the case of OSBR, the linear dependence appears to continue for high noise levels as well as low noose levels in the region plotted here. At some point though, when the noise level becomes large, the sensitivity will drop more rapidly than the corresponding OSBR drop. The good correlation between the OSBR and sensitivity at low noise levels can be explained via the

finite "noise floor" observed due to the side-bands from the neighboring channels. The cross-talk from channel 1 and 3 will therefore limit the OSBR when the OSNR rises above a certain level. The same is the case for the receiver sensitivity, which will not change significantly above OSNR values of 40 - 45 dB.

Interplaying polarization effects

Initially the two channels 1 and 3 are polarized parallel and launched into the transmission fiber with the exact same polarization and power. This was assured by monitoring the signal via a tap-off located between the modulator and the transmission fiber. Apart from the fact that the polarization of the channels will be rotated throughout transmission, one might assume that the two channels 1 and 3 will sustain an equal relative polarization state throughout the transmission fiber[3]. This, however, is not the case, which can also be seen from the optical spectrum inserted in Figure 5.12b). If the channels 1 and 3 had the same state of polarization both would be suppressed equally, so the polarization has in fact changed unequally for those two channels.

This is related to the birefringence in the fibers. When transmitting in a birefringent fiber the light will be split up into two degenerate modes, each travelling at different speeds. This is also known as the effect causing 1. order PMD within a single channel. When considering two separate channels launched into the fiber with the same state of polarization, the state will change unequally for the two channels underway. This is due to the difference in wavelength, as the polarization changes induced to each channel are wavelength dependant.

If $\Delta\Phi$ is the phase shift between the orthogonal states caused by the birefringence in the fiber, it can be expressed as

$$\Delta\Phi = \frac{2\pi}{\lambda} \left| \overline{n}_x - \overline{n}_y \right| L \tag{5.2}$$

where λ is the optical wavelength, L is the transmission length, and $\overline{n}_x$ and $\overline{n}_y$ are the modal refractive indices for the two orthogonal polarized states. As can be seen from Equation (5.2) the phase shift is dependant on the wavelength λ. Furthermore, as $\Delta\Phi$ is related to the change in polarization state of a channel, the two channels will end up with a different state of polarization hereby causing the phenomenon seen in Figure 5.10.

This phenomenon is also reported in [89], where an undersea cable was investigated and significant wavelength dependence was seen on the polarization states.

[3] If the channels experience the same polarization changes throughout the transmission, their relative state of polarization will be unchanged.

Cross-phase modulation also interplays with the polarization states. XPM induced de-polarization is described in [87] and [90], and is due to inter-channel cross-polarization modulation. It depends on the total launch power of all co-propagating channels but is independent of the channel spacing. Inter-channel cross-polarization modulation leads to de-polarization of the channels, which means that it will become increasingly difficult to properly minimize the power of a PBS demultiplexed channel when the power increases. This was also observed in the experiments, and to a larger degree for the more nonlinear pre-compensation case described later in Section C.1.2.

Finally, it has also been reported how PMD can cause perturbations in the state of polarization [91]. Considering the relative short fiber lengths used here and the obvious power dependence of the problem, PMD is not attributed any significant role in these results.

5.2.5 The effect of SPM and XPM on the OSNR measurement

It has earlier been documented (Section 5.1) how SPM will cause the optical spectrum to broaden when the signal is launched at high powers into an optical fiber. In the case of Section 5.1 the powers were relatively high, up to 21 dBm, and furthermore a special highly nonlinear fiber (HNLF) was used to amplify the effect of the spectral broadening and can therefore not be directly compared to this case.

Although these cases are not comparable, it is expected that SPM and XPM will cause some spectral broadening when the input powers are high, but the question arises whether or not this will cause a notable change in the results derived from this method. In extreme cases the spectral broadening effect of SPM and XPM can possibly render OSNR evaluations inaccurate in dense WDM systems, however, the signal would be strongly distorted due to the SPM and XPM influences at that point.

5.2.6 Distinguishing SPM/XPM and noise OSNR degradations

As mentioned briefly above, due to nonlinear effects (SPM and XPM), OSNR measurements can be inaccurate in dense WDM systems.

The spectral broadening caused by SPM and XPM will narrow the free spectral area between channels and if that broadening is significantly pronounced, the conventional OSNR evaluations, described in section 2.1 will be influenced. It can also be argued that it is important to identify the origin of the measured OSNR degradation as the signal will be influenced differently depending on the source of degradation. Although the same OSNR drop is observed, an OSNR degradation of 1 dB originating from a nonlinear spectral broadening is expected

to have a far more detrimental effect on the quality of the signal compared to a 1 dB OSNR drop originating from noise. Therefore it would be valuable to identify the origin of the OSNR degradation in order to be able to estimate the condition of the signal.

Experiments have been conducted in order to identify if it is possible to quantify the OSNR degradation in terms of ASE contributions and SPM/XPM spectral broadening contributions. These experiments are described in detail in Appendix C while only summarized results will be given here.

The results of the investigations described in Appendix C indicate the possibility of an additional use of the OSBR in regions of high input powers where nonlinearities are the limiting factor. Through a parameter termed the *cross-talk induced OSBR* ($\mathrm{OSBR_{XTALK}}$) the results showed it possible to identify the OSBR degradation caused by SPM and XPM. In general, the OSBR and $\mathrm{OSBR_{XTALK}}$ evaluations made it possible to explain several of the receiver sensitivity variations caused by nonlinear effects. Although the results showed that SPM/XPM spectral broadening could be quantified, the accuracy proved to be limited.

In practise, it would be advantageous to be able to distinguish between noise induced OSBR degradations and OSBR degradations induced by nonlinear effects. This can possibly be achieved by a combination of Scheme 1 and Scheme 2 [4]. While Scheme 2 would only evaluate the OSNR changes caused by noise, the OSBR and $\mathrm{OSBR_{XTALK}}$ (Scheme 1) could identify possible nonlinearity issues. Unfortunately there was no further time to perform these experiments.

5.2.7 Advantages and features

Polarization interleaving the channels is necessary for this method to function, but it also brings about other advantages. As already mentioned, polarization interleaving has been used before as a mean to decrease the creation of FWM products [88] and the detrimental effects of XPM [86], [87] that arise in dense WDM systems. Furthermore, the polarization interleaving assists in demultiplexing the channels, which leads to a better receiver sensitivity as seen in Figure 5.14a) where the sensitivity is plotted versus OSNR. The figure shows a comparison between a normal case and the polarization interleaved case where the signal is polarization demultiplexed before the receiver. This strongly diminishes the crosstalk, and gives a sensitivity improvement of approximately 7 dB. The sensitivity curve does not alter shape due to polarization demultiplexing, but is merely shifted vertically.

[4] Refer to page 70 for a definition of Scheme 1 and Scheme 2.

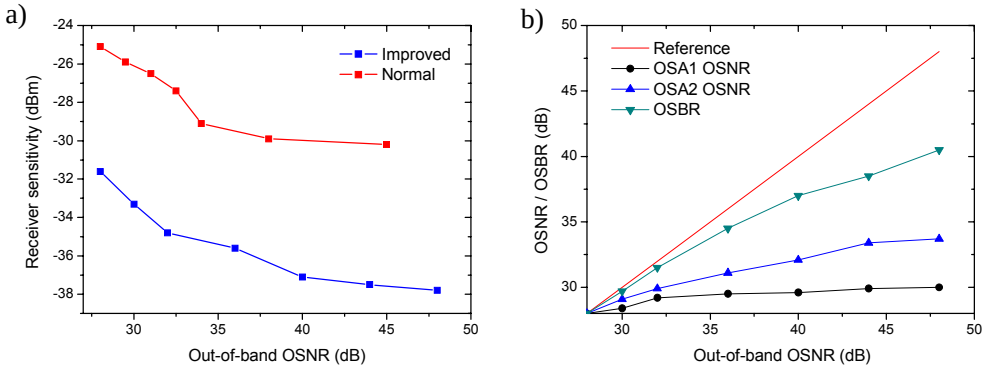

Figure 5.14: a) Comparison between a system with and without polarization interleaved neighbor channels. A clear improvement is observed for the polarization multiplexed case. b) The figure shows the OSA1, OSA2 and OSA3 calculated OSNR/OSBR values versus out-of-band OSNR.

In Figure 5.14b) the measured OSNR is shown for the various evaluation methods. Again the OSA3-derived OSBR provides the most accurate noise evaluation.

All in all, the features can be summarized to these bullet points:

- Monitoring the OSNR in dense WDM systems
- Improved channel receiver sensitivity due to polarization assisted demultiplexing.
- The possibility of a 3 dB reduction of ASE noise due to polarization filtering/demultiplexing.
- Increased resistance towards XPM and FWM leading to improved performance at high input powers.
- Access to for extra information about signal degradations induced by nonlinear effects.

Note however, that this comes at the price of increased complexity in both transmitter and receiver.

5.3 Simultaneous OSNR and dispersion monitoring

OSNR monitoring is very valuable in networks limited by ASE noise but an OSNR evaluation provides no information in regards to dispersion in the system. In networks where both dispersion and noise can be limiting factors additional monitoring is required. One way of doing this is to combine OSNR monitoring

with dispersion monitoring. A combined OSNR/dispersion monitor will be briefly discussed here.

By specifically evaluating both OSNR and dispersion, it is possible to determine exactly if dispersion or noise is creating the problem. This in turn helps to pinpoint the source of signal degradation and the proper steps can be taken to solve the issue.

5.3.1 Combining dispersion monitoring and OSNR monitoring using sideband filtering

The dispersion monitoring technique described in section 5.1 can with relative small changes be combined with the OSNR monitoring technique described in Section 5.2. Figure 5.15 illustrates one possibility to accomplish this double monitor functionality.

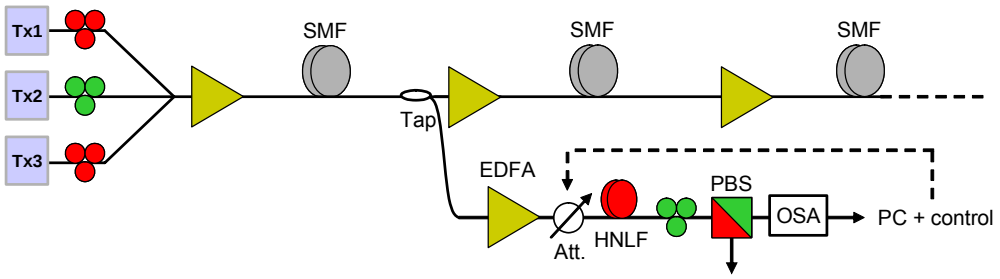

Figure 5.15: Simultaneous OSNR and dispersion monitoring can be done by combining the OSNR and dispersion monitoring techniques descriebed in sections 5.1 and 5.2. When the attenuator is on maximum and minimum attenuation it measures OSNR and dispersion respectively.

A part of the signal is tapped of at a point where the OSNR and dispersion information is required. By adjusting the optical attenuator, the system can be arranged in two configurations, one for monitoring OSNR and one for monitoring the dispersion. As will become evident now, it is not possible to monitor both at the same time in this particular configuration.

If the attenuator is adjusted to let through maximum optical power, the optical signal will excite nonlinearities exactly as explained in section 5.1. The signal will further pass the polarization control as well as the polarizer or as in this case a polarization beam splitter. Provided the polarization control is adjusted correctly, the PBS will merely pass the signal on to the OSA, where the spectral broadening can be analyzed and in turn the dispersion is evaluated.

In the OSNR monitoring mode, the attenuator is adjusted to a prior determined minimum power where no significant nonlinearities are excited. It is important to stay below the nonlinear limit as spectral broadening can lead to

errors in the OSNR evaluation. Keeping the power at 0 dBm, for example, would not excite nonlinearities to any significant extent.

It is thus rather simple to combine the methods of dispersion and OSNR monitoring just described.

5.4 Chapter summary

This chapter has focused on optical signal parameter monitoring where a specific signal parameter is investigated because it has a significant influence on the performance of the signal. A method for monitoring dispersion limited RZ or NRZ 40 Gb/s systems has been successfully demonstrated. By tapping off a part of the signal, amplifying it and passing it through a 1.5 km HNLF fiber, a monitoring signal is extracted by side-band filtering the SPM broadened spectrum. Furthermore, it is expected that the method is also applicable to PMD monitoring.

A method for improved OSNR monitoring in dense WDM systems was also presented. By imposing a polarization state making each channel orthogonal to its neighboring channels the level of in-band noise could be evaluated. It was demonstrated how OSBR can be used to monitor the OSNR, assuming OSNR values below a limit of approximately 38 dB. The OSBR method provides a considerably more accurate evaluation of in-band noise than the traditional technique[5] used for OSNR measurements. Furthermore, due to the orthogonal polarization of neighboring channels, the signal performance was further significantly improved.

Optical signal parameter monitoring can be a valuable tool in performance monitoring as it provides detailed signal information that is normally not available through optical signal quality monitoring techniques. This can be very helpful in determining the cause of bit-errors detected by for example the BIP-8 parity check performed in the SONET/SDH transport layer.

[5]Interpolating the out-of-band background noise level to the in-band noise level.

Chapter 6

Signal deterioration and optimization

As discussed in previous chapters, transparent networking can offer great advantages in terms of simplicity, bandwidth and potential savings in cost and power consumption. However, keeping the signals in the optical domain eliminates the possibility for convenient and advanced performance monitoring in the electrical domain, and prompts the need for optical performance monitoring schemes.

Several methods for monitoring optical signal parameters such as dispersion and OSNR have already been discussed in Chapter 5. In general, these methods only provide information about the specific parameter measured, and not the overall quality of the signal. Basically, the only direct measure of signal quality is the BER, but this is complicated, requires expensive equipment, and is only possible if the pattern is known.

The BER of an optical system can be degraded by many factors. An important parameter when setting up spans in optical systems is the launch power to the fiber. The power must be large enough to provide an acceptable OSNR at the output of the span but below the limit where excited fiber nonlinearities distort the signal. The specific limit depends on several different factors such as the type of fiber used, the bit rate, amplifier spacing and the applied dispersion map. Finding the optimal input power that provides the minimum BER is a difficult task to perform on an installed link and, as mentioned, requires expensive BER test equipment as well as comprehensive measurements.

This chapter will discuss the subject of signal quality imperfections caused by non-optimal launch power in the network. The focus will be on a proposed method for optimizing the launch power by adding a subcarrier tone to the baseband data. By establishing a correlation between the BER performance and the subcarrier tone power, it is possible to identify the launch power that provides

the optical signal quality by monitoring the subcarrier power. The scheme is investigated numerically and experimentally for different dispersion maps and network configurations.

6.1 Launch power optimization

As seen in Chapter 5 section 5.2, it is desirable to keep the launch power as high as possible to maximize the OSNR throughout transmission but still below the limit where fiber nonlinearities will degrade the signal quality.

Fiber nonlinearities limit the fiber launch power, but the specific limit depends on several different factors such as the type of fiber used, the bit rate, amplifier spacing, and the applied dispersion map. Even in today's point-to-point links it can be a difficult task to identify the optimal input power that provides the best signal quality. A nonlinearity monitor could provide the needed information to maximize the signal quality in terms of input power. This principle is illustrated in Figure 6.1, where a nonlinearity monitor tap-off provides information about the signal deterioration due to excessive launch power.

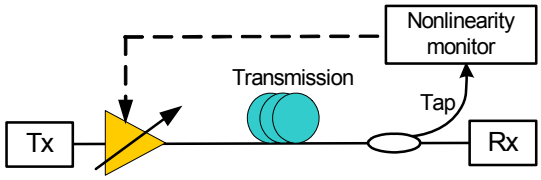

Figure 6.1: The principle of operation of the nonlinearity monitor. The subcarrier tone is added at the transmitter and subsequently extracted to provide information about the nonlinearities excited in the system.

From previous work, it is known that by adding a subcarrier tone to the baseband of the signal it is possible to monitor the accumulated chromatic dispersion [30]. However, it is found that if the dispersion is assumed constant in time, the subcarrier can also be used to monitor fiber nonlinearities, as the detected tone radio frequency (RF) power will fade according to the level of excited nonlinearities in the system. It is found that SBS and SPM are the two main contributors to signal degradation in the considered 10 Gb/s NRZ system. The effects of SPM and SBS have been investigated though experiments and simulations.

In the proposed method, a subcarrier tone has been added to the data signal. The subcarrier power will vary with the launched power to the fiber due to nonlinearities affecting the subcarrier. Both the signal quality and the monitored subcarrier power will be dependent on the used fiber types, dispersion map as

well as the transmission span layout. All these factors are related to the excited nonlinearities in the system so it is necessary to identify the interplaying nonlinearities and their importance to the system.

6.1.1 Interplaying nonlinear effects

When high optical power is launched into a fiber such as DCF or SMF, SPM will take place. Considering a subcarrier modulated system, SPM will also influence the phase of the subcarrier. In this context the single subcarrier is tone modulated and added to the data and resulting in a spectrum as illustrated in Figure 6.2. In [30] it was described how the lower and upper subcarrier side bands, denoted "L" and "U" in the figure respectively, would acquire different phases due to dispersion. Due to this dispersion initiated phase difference, the subcarrier power observed, after detection in the photodiode, would appear faded.

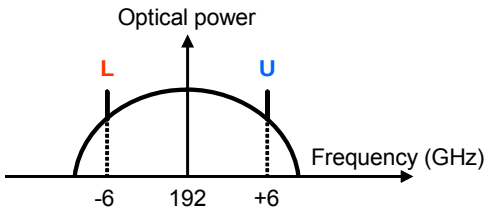

Figure 6.2: Optical spectrum illustrating a 10 Gb/s NRZ modulated data signal where a 6 GHz tone modulated subcarrier has been addded to the signal.

As explained in Chapter 2, SPM causes phase changes to the signal and will also cause fading of a subcarrier by introducing a phase mismatch between the upper and lower subcarrier side bands. As seen in Chapter 2, SPM also interacts with dispersion such that SPM and dispersion will interact to generate subcarrier fading. Although SPM-dispersion interactions can be well described for traditional data modulated systems such as for example RZ, it is nontrivial to analytically describe and predict the development of a subcarrier fading in subcarrier modulated systems. The 10 Gb/s NRZ system with a tone modulated subcarrier considered here will therefore be analyzed through simulations as well as numerous experimental investigations.

SBS is another nonlinear effect that needs to be taken into account. Section 2.9 in Chapter 2 explained the principles of SBS and also demonstrated how it could influence the performance in subcarrier based systems. Due to the backscattering nature of SBS, it is complicated to theoretically describe a model for a data transmission of SBS influenced data, and it was just recently in VPI Transmission Maker version 5.5 that SBS could be successfully included in the model. In version 5.5, VPI has introduced the so-called *UniversalFiber* module

where SBS effects can be included. More information about the SBS model used in VPI can be found in B.3.

6.2 Concept of signal optimization method

As mentioned above, subcarriers have previously been successfully used for monitoring dispersion by measuring the RF fading of a subcarrier tone [30]. The fading arises as a consequence of the phase difference that is imposed on each of the subcarrier side bands due to accumulation of dispersion in the fiber. When those experiments were performed, it was observed that the launch power also had an effect on the fading of a subcarrier. In terms of dispersion monitoring this obviously can be an issue as the result becomes ambiguous if the optical power in the system is not kept sufficiently constant.

The fact that the inserted subcarrier varies with the input power fueled the interest for further investigations and the phenomenon was investigated.

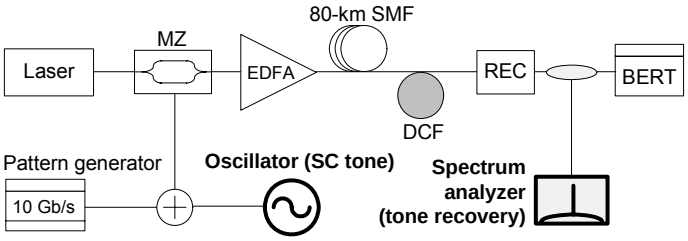

Figure 6.3: Principle setup used for the VPI simulations. This setup is in principle equal to the setup used later for the experimental demonstration.

The principal setup used in the simulations is shown in Figure 6.3. A subcarrier tone at 5.1 GHz is added electrically to the 10 Gb/s data signal using a power combiner. Both subcarrier and baseband signal are subsequently modulated onto the optical carrier with a MZ modulator, and transmitted through 80 km SMF followed by 16 km DCF corresponding to 100% dispersion compensation.

The subcarrier modulation index, m, is 10%. After transmission the composite signal is detected and the subcarrier power as well as the signal sensitivity can be recovered. Various subcarrier frequencies will be investigated underway and as will be seen, the 5.1 GHz subcarrier is an appropriate choice.

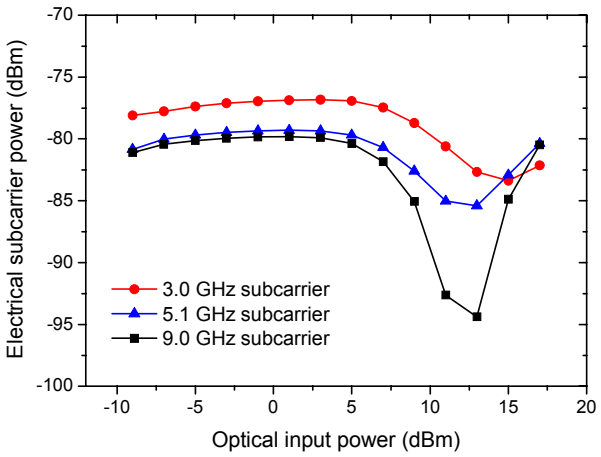

Figure 6.4: Simulated RF fading of a 3.0, 5.1 and 9.0 GHz subcarrier in a 10Gb/s NRZ system. Both the effect of SPM and SBS is enabled in the simulation.

In order to clarify the behavior of a subcarrier in a 10 Gb/s NRZ system, simulations were made with subcarriers of different frequencies. Figure 6.4 shows the results of simulations with a 3.0 GHz, 5.1 GHz and 9.0 GHz subcarrier in a 80 km post-compensated link. The figure shows the subcarrier power versus optical input power for the system illustrated in Figure 6.3. Note that the power to the pre-amplified receiver is kept constant at each subcarrier power measurement such that all subcarrier power changes are relative and thus comparable. The *Electrical subcarrier power* in the figure denotes the power of the subcarrier after O/E detection. This power was measured in a 50 MHz bandwidth using an electrical spectrum analyzer (ESA).

It is evident from Figure 6.4 that the change in optical input power influences the subcarrier power. The subcarrier frequency clearly influences the subcarrier power variations although the minima remains in the same region of 13-14 dBm input power for all three frequencies. The subcarrier frequency of 5.1 GHz was chosen to avoid the half-clock frequency at 5.0 GHz as it can cause a higher penalty to the data if the subcarrier is located at this frequency. This was reported in [21], Figure 5.18.

As mentioned earlier in section 6.1.1, it is expected that both SPM and SBS can influence not only the data signal, but also the subcarrier tone to some extent. In order to explore these two nonlinear effects further, the same 80 km post-compensated span is studied in four different cases as the VPI model allowed for independently switching on and off the effects of SBS and SPM. This provides a method for identifying which effect is the dominating one in terms of signal degradation as well as subcarrier fading.

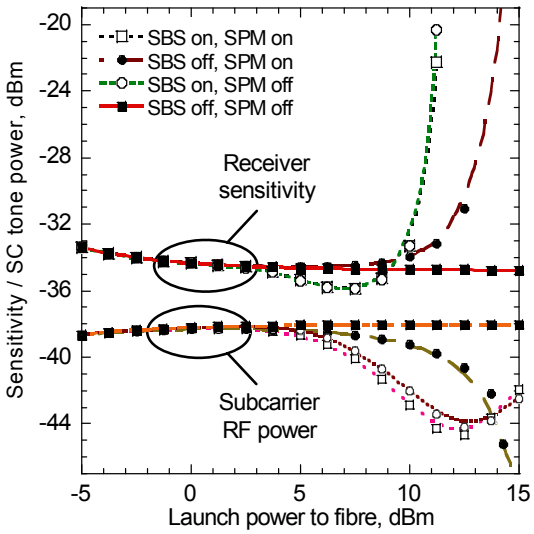

Figure 6.5: Simulation results done in one 80-km post-compensated span for a) No SPM, with SBS, b) No SBS, with SPM c) no SBS, no SPM, and d) with both SBS and SPM effects included in the model. The figure shows the individual nonlinear effects on the subcarrier RF power and the 10 Gb/s data signal.

Figure 6.5 shows the four combinations [SBS on, SPM on], [SBS off, SPM on], [SBS on, SPM off] and [SBS off, SPM off] [1]. The subcarrier frequency is 5.1 GHz and has a modulation depth of 5%. Considering the results from the simulations in Figure 6.5 it is clear that the fading of the subcarrier in this case is primarily due to SBS, and that the impact of SPM is only significant in the absence of SBS. This is not surprising as SBS is a narrowband scattering effect that influences the subcarrier tone due to its narrow bandwidth, in the order of a few kHz. The same is the case for the 10 Gb/s NRZ signal, where the power penalty is also dominated by SBS although the degrading effects of SPM and SBS set in almost simultaneously. Notice that if the degradation from SBS is somehow eliminated by for example carrier suppression [92] or broadening [93], the subcarrier power will still fade due to SPM.

Altogether, the correlation between receiver sensitivity and the detected subcarrier power is observed to be excellent, indicating that this correlation can be used for optimizing the launch power. The consequences of SPM and SBS in the subcarrier modulated system have been explained below:

[1] "SBS off" refers to switching the SBS effects off in the VPI model, so they are simply ignored. The SPM effects are switched off by putting the nonlinear index n_2 equal to zero.

- **SPM**

  The effect of SPM is to create a phase change throughout the optical spectrum of the combined signal. Through interactions with dispersion in the system, the result is a relative phase change in the two subcarrier sidebands, which in turn results in a RF power fading similar to what is exploited when using the subcarrier for dispersion monitoring [30]. Note that even though the dispersion is compensated 100%, a phase mismatch will still exist within the subcarrier sidebands as the effects of SPM are nonlinear and thus cannot be recovered.

- **SBS**

  SBS is a scattering effect and is therefore not causing any phase changes in the spectrum. This means that the subcarrier fading caused by SBS is, unlike SPM, not related to a phase mismatch between the two subcarrier sideband components but rather a direct scattering process of these two components.

The receiver sensitivity curves in Figure 6.5 are supported by previous work, concluding that SBS can give rise to notable power penalties in 10 Gb/s NRZ systems [94]. One more thing should be noted about the subcarrier curves in Figure 6.5. It can be seen that in the cases where SBS is "on", a rise in the subcarrier power is actually observed as the optical input power approaches 14-15 dBm. This might seem surprising as SBS would be expected to scatter the subcarrier and thus lead to a decrease in subcarrier power. In [55], however, it is explained how the modulation index, m, can increase due to SBS due to relative changes in the carrier as well as the subcarrier power.

The 5.1 GHz subcarrier used in the simulations seems to provide a good correlation with the data signal quality. A 5.1 GHz subcarrier with a 10% modulation depth was also used in the laboratory experiments carried out, again using a setup equal to that shown in Figure 6.3. The experimental results are shown together with the simulation results in Figure 6.6.

The figure illustrates the relation between the detected power of the subcarrier and the receiver sensitivity, and shows good agreement between experimental and simulated results. Further details on the parameters used in the simulation model can be found in the appendices B.

It was established above that the method is dependent on the nonlinear effects SPM and SBS both in terms of signal quality degradations and subcarrier power fading. Also SPM - dispersion interactions plays a role in the system, so it seems rational to study other variations of dispersion and nonlinear system configurations as well. The next section shortly introduces the most common

types of dispersion compensation configurations, which also have been used in the experiments presented in section 6.3.

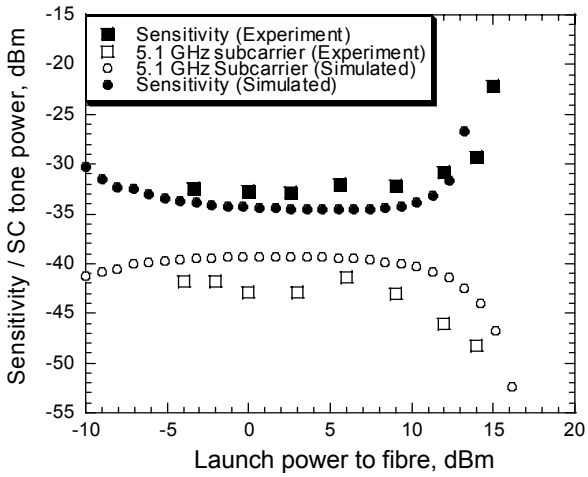

Figure 6.6: Subcarrier power and receiver sensitivity as a function of launch power for a post-compensated 80-km span. The simulation results are shown together with experimental results.

6.2.1 Dispersion compensated spans

Different types of dispersion configured spans exist that are suited for different purposes and costs. The ones considered here are identified below.

Post-compensated spans

The DCF fiber is placed after the transmission fiber, hence the term post-compensated. This is the standard approach as the SMF transmission fiber allows for a relatively high launch power considering the lower nonlinear coefficient in the SMF compared to DCF. Post-compensation is a frequently used approach, as standard systems are designed to excite a minimum of nonlinearities in the system while keeping the launch power as high as possible. Figure 6.7 illustrates the principle of post-compensation.

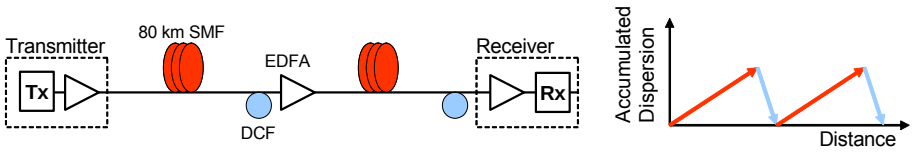

Figure 6.7: A two-span example utillizing post-compensation.

Pre-compensated spans

Consider a span where the DCF is placed before the transmission fiber such that

the dispersion compensation is applied before transmission. This approach is termed pre-compensation, and is applied less commonly. The advantage here is the possibility of SPM - dispersion supported transmission as explained in Section 2.6. Exploiting the pulse broadening in the DCF can assist in extending the transmission distance through a higher optimal launch power. This approach, however, is not straight forward and the optimal input power range is relatively narrow, such that a little too high input power will damage the signal rather than assist the transmission. Figure 6.8 illustrates pre-compensation.

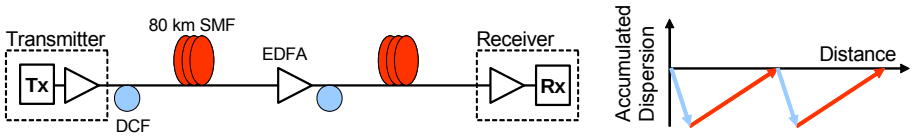

Figure 6.8: A two-span example utillizing pre-compensation.

Spans with residual dispersion

A span that is not compensated 100% is said to display residual dispersion. This means that the overall dispersion of the link is either positive or negative, i.e. under- or overcompensated. Residual dispersion can in some cases be an advantage for the type of links where it will work constructively with other effects such as excited nonlinearities in the system. Although it can be exploited in some special cases, residual dispersion can also cause problems to the system or network and are therefore usually avoided if possible. However, unknown dispersion properties in already installed systems as well as other factors discussed in Chapter 2 can render it very difficult to assure zero residual dispersion in a practical system.

Residual dispersion can be present in either post- or pre-compensated systems, but here only post-compensated systems will be investigated. Figure 6.8 illustrates a post-compensation system with a positive residual dispersion.

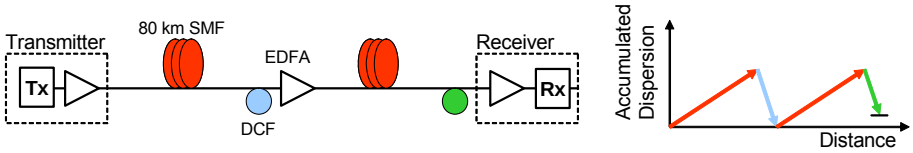

Figure 6.9: A two-span example utillizing post-compensation with a positive residual dispersion.

6.3 Launch power optimization in various span configurations

Experiments have been carried out for several dispersion maps and span configurations to further verify the signal sensitivity/subcarrier tone power correlation in different scenarios: 100% post-, 100% pre- and an under compensation of +100 ps/nm (post-compensated). These configurations have been used in one and two span experiments. In the case of two 80-km spans, each span is identical, i.e. both compensation and amplification in the second span is identical to the first span. Figure 6.10 illustrates the experimental setup used for launch power optimization in the case of a single pre-compensated span. The continuous 1550 nm wave is modulated in a single arm Mach-Zehnder (MZ) modulator by a combined 10 Gb/s NRZ data signal and a subcarrier tone. The data and subcarrier have been added using a power combiner. The combined signal is amplified before sent to the DCF, which is followed by 80 km SMF. The DCF has a length corresponding to 100% dispersion compensation of the 80 km SMF. After transmission, the signal is sent to a pre-amplified receiver that includes an EDFA, an optical ASE filter and the photo diode. After detection, the electrical signal is divided such that one part continues to BER estimation and another part continues to subcarrier power evaluation in the electrical spectrum analyzer.

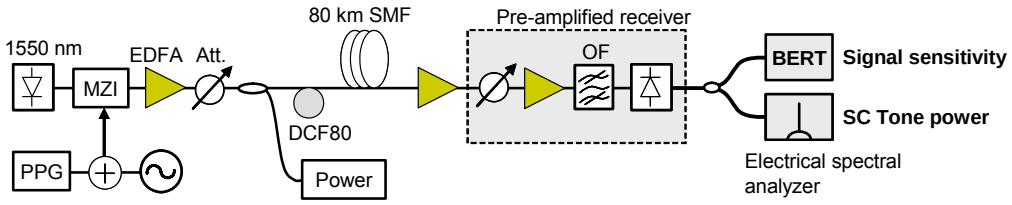

Figure 6.10: Illustration of the experimental setup used for launch power optimization in the case of a single pre-compensated span. The dispersion accumulated in the 80 km SMF span is 100% pre-compensated by the DCF80 module.

Measurements were made to compare a one and two span pre-compensated system and the results are shown in Figure 6.11. Note how the input power dynamic range[2] decreases when going from one to two spans and the subcarrier power tracks this behavior accurately. The eye diagrams to the right show the development for the pre-compensated single span case when the launch power increases. The pulse shape changes caused by the increase in power can clearly be seen in the eye diagrams.

[2] *The input dynamic range* describes the input power range within which the sensitvity remains below a certain level, for example, 1 dB.

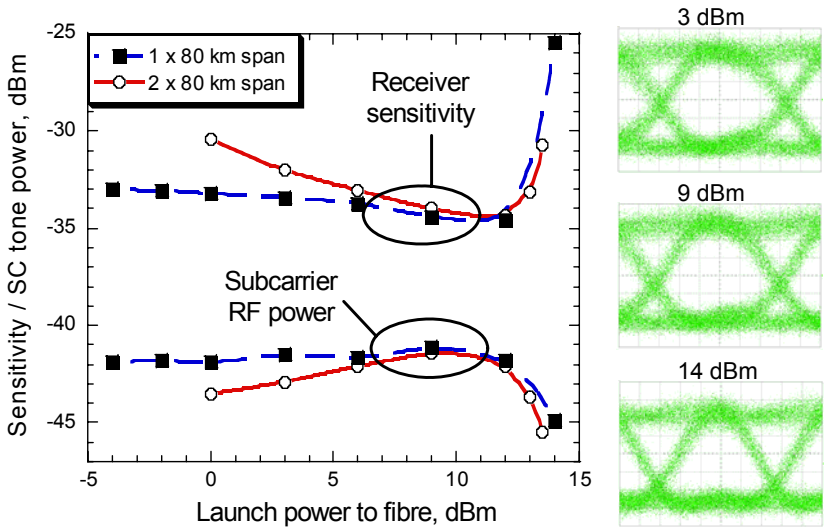

Figure 6.11: Measured sensitivity and subcarrier power for a 1 and 2 span 10 Gb/s pre-compensated system. The eye diagrams show the development for the pre-compensated case when the launch power increases.

As argued before, the correlated behavior of the signal sensitivity and the subcarrier power is attributed to the nonlinear effects of SPM and SBS as well as the interaction of SPM with dispersion. Therefore it might seem peculiar that the subcarrier tone power traces the changes at low input powers where no nonlinearities are interacting. This, however, is expected due to the drop in OSNR at lower input powers. When the input power drops, the signal will eventually suffer from excessive noise in the system. Similarly for the subcarrier, the subcarrier-to-noise ratio will drop, which effectively leads to a drop in the detected tone power. Clearly this is no disadvantage for the concept as it allows for an expanded usability in the low input power regions. This tendency is also observed from the simulations presented earlier in Figure 6.6.

Next, the various types of dispersion compensation configurations are studied. Figure 6.12 shows a comparison between the cases of 100% pre-, 100% post-, and post under-compensation as described in section 6.2.1. The experiments are performed using a two-span configuration in all three cases. The figure shows the differences in sensitivities depending on the compensation scheme, and again how the evolution of subcarrier power follows this behavior.

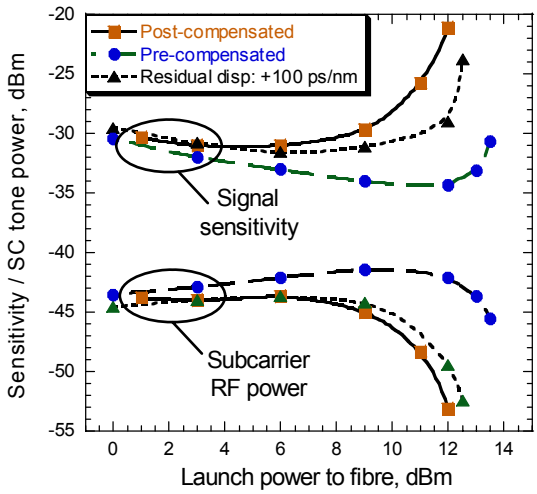

Figure 6.12: Measured sensitivity and subcarrier power for a single span configuration with pre-, post- and under-compensation. One span consists of 80 km SMF + DCF.

A method for optimizing the power launched into dispersion compensated fiber spans has now been demonstrated for various span and dispersion map configurations. The equipment used in these experiments is generally of high quality and is well-known in terms of performance characteristics. For example, the x-cut MZ modulator used exhibits very low chirp, but this is not always the case for modulators. Chirp in the modulator can alter the performance of an optical system significantly in terms how the signal will react to nonlinearities and dispersion.

The following section presents a number of experiments done using a z-cut modulator, which inflicts a significantly larger chirp to the signal compared to the previous one used.

6.3.1 Transmission of chirped pulses

Electro-optic modulators will usually induce chirp to the signal, but depending on the design and quality of the modulator, the magnitude of the chirp will vary. Modulators that are specifically designed to exhibit low chirp such as the x-cut JDS Uniphase (Model 21023816) will introduce very little chirp to the signal, whereas a modulator such as the older z-cut Sumitomo (Model PSNCOM1-001) will leave the signal significantly chirped prior to transmission. Very high chirp figures can also be found in signals that have been E/O modulated using direct modulation of the laser. This will create substantial chirp of the signal and this method is usually reserved for cost-effective low distance systems where chirp is of less concern [95].

The Figures 6.13a) and b) illustrates the effects of using a chirped modulator . The experiments in Figures 6.13a) is carried out using the z-cut Sumitomo modulator in a 1×80 km span with 1) 100% post- and 2) 100% pre-compensation. The subcarrier has a frequency of 6.0 GHz and the modulation depth is 10%. In both cases, the subcarrier is well correlated with the receiver sensitivity of the 10 Gb/s NRZ signal. Note especially for the pre-compensation case how the minimum sensitivity point at around 12 dBm input power is matched very well by the subcarrier power maximum.

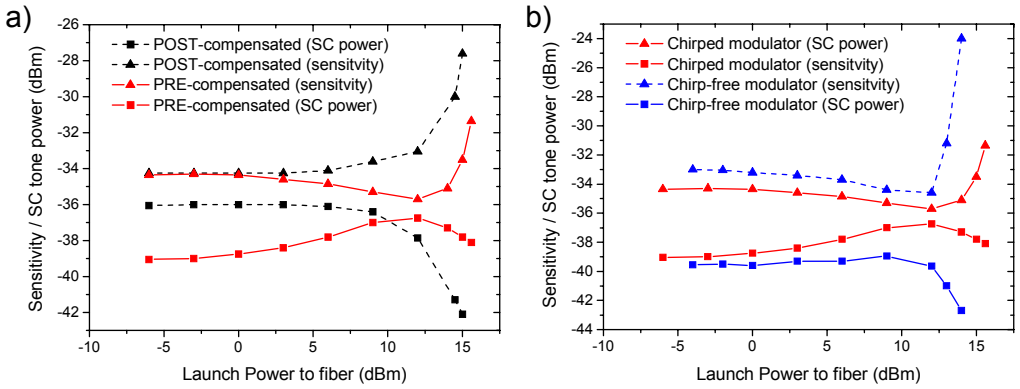

Figure 6.13: a) Experimental results showing the receiver senstivity and subcarrier power versus launch power when a chirping modulator is used. The results are for 1×80km pre- and post-compensation. b) The figure illustrates the difference between using a chirp-free and a modulator exhibiting chirp on to the signal. The comparison is done for a pre-chirped 1×80km span.

In order to illustrate the effects of a chirping modulator on the signal sensitivity and subcarrier fading, a comparison has been made with the chirp-free JDS Uniphase modulator in Figure 6.13b). The results are for a pre-compensated 80 km span, again using a 6.0 GHz subcarrier. The difference between the chirped and non-chirped case is clearly observed in the figure. Notice how it is possible to achieve a slightly better sensitivity using the chirped modulator as well as a higher launch power toleration. This is attributed to constructive interferences between the modulator created chirp, and the chirp created via SPM as well as dispersion interactions.

The last example of launch power optimization using a chirped modulator is for a post-compensated span with residual dispersion. Figure 6.14 shows the results for two cases of residual dispersion, one with -230 ps/nm and another with +100 ps/nm. As before, the subcarrier frequency is 6.0 GHz and the modulation index is 10%. Except for a small difference in sensitivity of approximately 1.5 dB the difference between the two cases is not very pronounced and the two subcarrier curves are also evolving in a similar manner.

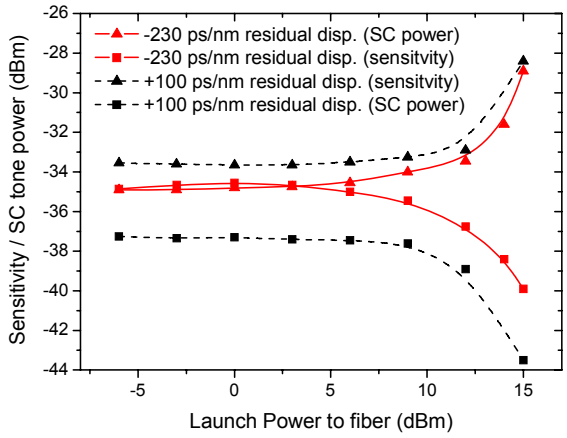

Figure 6.14: Measured receiver senstivity and subcarrier power versus launch power when a chirping modulator is used. The results shown are for a 1x80km post-compensated span with -230 ps/nm (red full line) and b) +100 ps/nm (black dashed line) residual dispersion.

The results in 6.13a) an 6.14 confirm that the correlations between the subcarrier and the receiver sensitivity is also achieved in the case of chirped modulators. The chirp of a pulse in a signal can be interpreted as a temporal frequency or phase change across the pulse. Chirp thus leads to altered phase properties in the optical spectrum of the combined signal and, as the data signal as well as the subcarrier are in fact dependent on the phase and dispersion properties in the system, this results in the different subcarrier - sensitivity relations seen in Figure 6.13b).

6.3.2 Subcarrier parameters

This section will deal with some of the concerns that might arise related to the characteristics of the added subcarrier. Adding a subcarrier in-band to the signal could very well give rise to a distortion of the signal. As reported in [30] and [21], the actual penalty will depend on the modulation index, the frequency and the data modulated onto the subcarrier. It was verified in [30] and [21] that the lower the frequency of the subcarrier is, the higher the penalty will be. Likewise, a higher modulation index, m, and broader subcarrier signal will also give rise to an increase in penalty. Fortunately, a simple subcarrier tone will usually be very narrow, in the order of kHz, and this was also the case in the experiments conducted here.

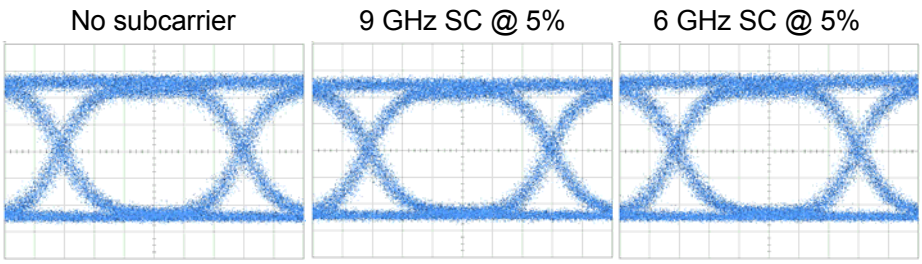

Figure 6.15: Eye-diagrams illustrating the negligible effect of adding an in-band subcarrier to the data signal.

A modulation index of 5-10% gives rise to very little distortion of the data signal, and a power penalty of less than 0.5 dB was observed for the 10 Gb/s NRZ system investigated using 6 GHz and 9 GHz subcarriers up to $m = 10\%$. Figure 6.15 compares the optical eye-diagrams for the two subcarrier frequencies. It is clear that the added subcarrier has very little impact on the system as it is virtually impossible to see any signal distortion.

Modulation index variations

Apart from the possible distortions induced to the data signal, changes in other parameters of the subcarrier could possibly influence the reliability of the launch power optimization technique. As the concept relies on SBS to some extent, the power of the subcarrier in the optical spectrum, which is controlled by the modulation index, is interesting to consider. It was explained in Chapter 2 how SBS relies on the power and spectral bandwidth of the signal in question.

Figure 6.16a) shows simulation results of a 5.1 GHz subcarrier tone variation versus input power for modulation indices $m = 2.5\%$ up to $m = 15\%$. The simulated system is a 10 Gb/s NRZ signal with a 5.1 GHz added subcarrier transmitted over one 80 km SMF span followed by 100% post-dispersion compensation using a DCF. In Figure 6.16b) the simulation results are plotted together with an experimental measurement of an equivalent system. Notice the relative good agreement between the two results.

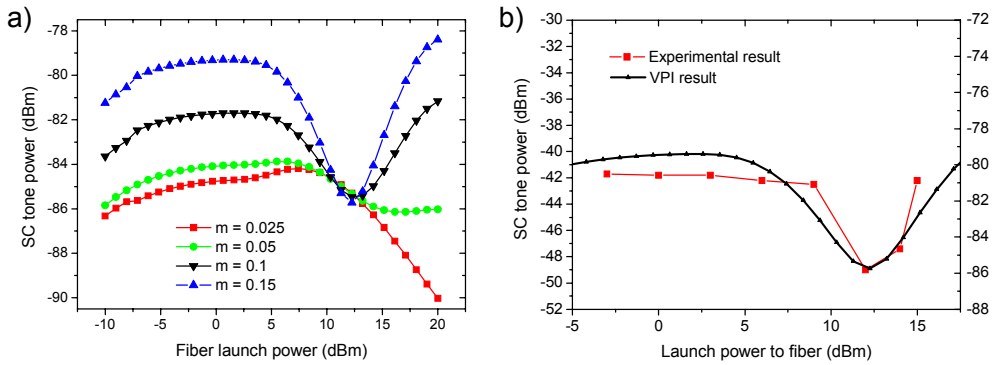

Figure 6.16: a) VPI simulation of SC tone power variations vs. launch power for various modulation indices for a 5.1 GHz subcarrier in a 80 km 100% post-compensated system. b) Comparison of simulation and experimental results for $m = 10\%$.

There are several interesting things to notice from Figure 6.16a). Firstly, there are two types of behaviors observed depending on the magnitude of m. For $m \geq 10\%$ the curves undergo a minimum at approximately 12.5 dBm input power, whereas for $m \leq 5\%$ this minimum is absent. In section 6.2 it was mentioned how SBS can cause a rise in the subcarrier power, as observed in Figure 6.16a) for $m \geq 10\%$ [55]. At this modulation index, the subcarrier power is high enough to experience changes due to SBS when the input power reaches 12 - 13 dBm. At $m \leq 5\%$ however, the spectral subcarrier power is not sufficient to excite SBS notably, and SPM thus takes over and causes the continuous fading of the subcarrier. All in all, the behavior is determined by whether SBS or SPM is the dominating effect, which again is determined by the subcarrier power, i.e. the modulation index.

It is not of that much practical interest, whether or not the curve has a minimum, as the data signal would be strongly distorted by nonlinear effects at this point - refer to Figure 6.5. In this post-compensated 80 km span case, the useful and interesting part of the curve is found up to about 12 dBm input power. Considering Figure 6.5 on page 86, the penalty would exceed 10 dB at 12 dBm input power. The question then arises, what modulation indices can be used? Although the curvatures of the different curves in Figure 6.16 display a similar trend in the region around 10 dBm, the high modulation indices $m = 10\%$ and $m = 15\%$ offers a notably better monitor signal magnitude and variation than the lower modulation indices. It is also important to note that it is not vital for the concept whether the modulation index is 8%, 10% or 11% as the behavior of the subcarrier is the same in this region. However, it is important to keep the tone power stable in order to avoid misinterpretations leading to wrong conclusions.

Subcarrier bandwidth

Another concern is related to the bandwidth of the subcarrier itself. As the spectral gain bandwidth of SBS is quite narrow, around 100 MHz for SMF, the tone would not experience scattering if it is too broad. 100 MHz is quite broad though, and in practice voltage controlled oscillators (VCO) exhibit a performance that surpasses this requirement. In the experiments done here, the 3 dB bandwidth of the tone was in the order of 200 kHz.

Figure 6.17 shows the simulation results from a comparison between a broadened and non-broadened subcarrier fading. The subcarrier has been broadened by adding phase noise to the tone. The results in Figure 6.17 confirm that a reasonable broadening of the subcarrier tone will not have any influence on the result.

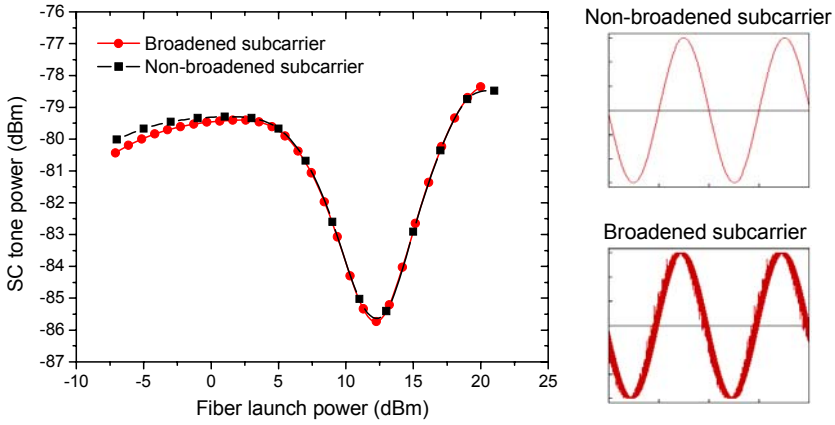

Figure 6.17: The significance of the spectral bandwidth of the subcarrier is investigated. The VPI simulation uses a 5.1 GHz subcarrier with $m = 10\%$. Refer to Appendix A for details on the simulation model.

Modulator bias

In today's communications systems, the MZ modulator is often used due to the appealing features such as low insertion loss, high extinction ratio and low chirp under proper operating conditions. When using the MZ modulator, the bias current is a crucial parameter that controls the operation point of the interferometer on the transfer curve. If the bias voltage is not adjusted correct, this can result in a distorted signal and the signal quality is limited. Normally it is desirable to adjust the bias point and the electrical signal amplitude such that the transfer curve is exploited optimally, and a good extinction ratio is achieved as illustrated

in Figure 6.18. Point A and B corresponds to an optimal adjustment of electrical signal amplitude and bias voltage. Note also in the figure that the transfer curve of the MZ modulator is not a linear transfer function, but instead a $\sin^2$ function.

When adding a subcarrier to the data signal, the situation becomes more complicated as the optimal operation conditions cannot automatically be assumed the same for the data and the subcarrier. The nonlinear transfer function is perfectly suited for the data to achieve a high extinction ratio, but the subcarrier tone is best transferred linearly as a nonlinear transfer function will distort the subcarrier. The modulation of the subcarrier onto the optical carrier is thus strongly dependant on the bias and voltage settings and higher subcarrier tone harmonics can be generated.

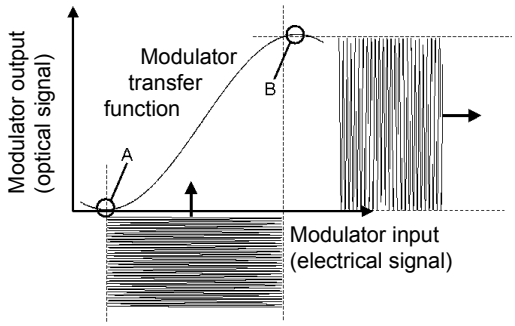

Figure 6.18: An principle illustration of a MZI transferfuntion. The points A and B represent the optimal points of operation.

Generally, the bias point used in the experiments is found by optimizing the optically modulated data signal as it is necessary to assure optimal signal transmission properties. In relation to the bias point discussion, a question could arise as to what influence a different bias would have on the reliability of the described technique. In order to clarify this further, a number of experiments were carried out to investigate this. Subcarrier tone power variations versus input power were experimentally measured for three different bias voltage settings in a 80 km post-compensated span using a 5.1 GHz subcarrier. The results are shown in 6.19a). It was found by optimization that the bias voltage of 200 mV is the optimal setting in terms of signal quality. The bias port switch voltage and RF signal peak-to-peak switch voltage for this modulator is 3.4 V and 5.5 V respectively. It is obvious from the figure that the bias voltage has a rather big impact on how the subcarrier power develops.

Figure 6.19b) shows how the subcarrier tone power varies with bias voltage for a fixed launch power of 9 dBm. A bias voltage change or fluctuation of 50-60 mV will give rise to a subcarrier power error of 1 dB at this particular launch

power.

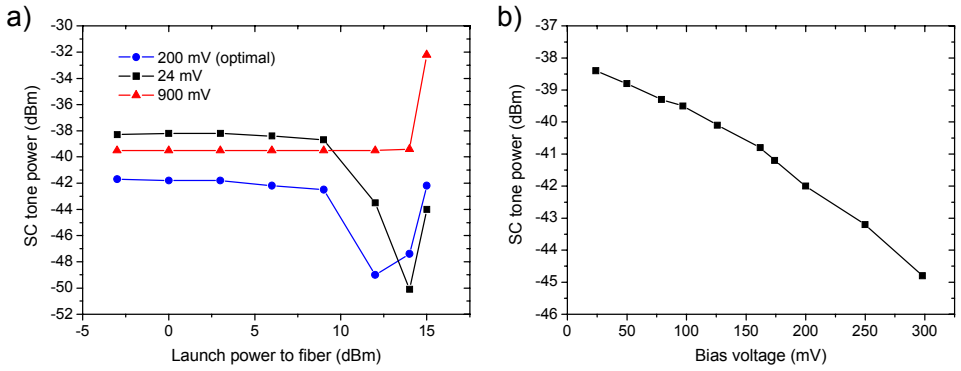

Figure 6.19: a) Experimental results of subcarrier tone power vs. launch power to a 80 km post compensated span for three different modulator bias voltages. The subcarrier frequency is 5.1 GHz. b) The subcarrier tone power dependance on modulator bias voltage is measured in the same system.

In conclusion, these investigations show that the modulation index and the modulator bias should be kept constant in order to avoid erroneous results. The bias voltage is normally monitored in modern communication systems, and stability would be expected.

6.4 Field-trial demonstration of performance monitoring and launch power optimization

This section reports on a 500-km field-trial, which demonstrates the launch power optimization method in a practical situation. By establishing the well known correlation between the BER performance and the subcarrier RF power, it is possible to minimize the BER, without prior knowledge of the data, by tuning the launch power to the link. The power of the subcarrier tone will indicate the optimum launch power, corresponding to the best signal quality. Basically this is the same principle as demonstrated above, however this time it will be demonstrated in a practical environment; a dark fiber network made up of four spans with varying distances.

6.4.1 The field-trial network

The dark fiber network used for the field-trial is a part of the Danish Research Network called DareNet. The network is owned and maintained by the Danish company Global Connect, and the part of the network used in these trials is shown in Figure 6.20. The fiber in the network complies with the G.652 ITU standard and has a dispersion parameter of 16-17 ps/nm/km. The total transmission

distance of approximately 500 km is broken up into four spans of 121 km, 131 km, 131 km and 121 km. The signal is launched from Lyngby, transmitted through Næstved, looped back in Odense, again through Næstved, and finally received in Lyngby; a total of four spans.

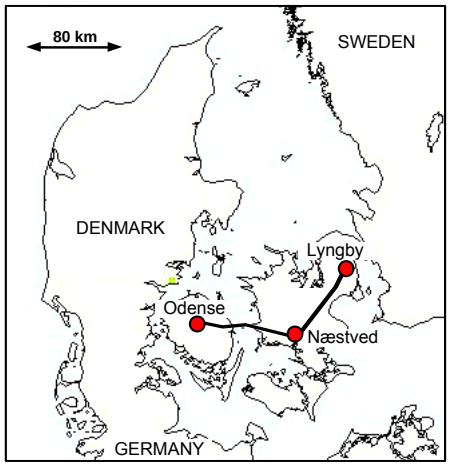

Figure 6.20: A map that illustrates the transmission path in the dark fiber network.

The single channel field trial experiment was conducted using a 5.1 GHz tone with a modulation depth of 10% relatively to the 10 Gb/s NRZ PRBS generated data. The trial setup is shown in Figure 6.21 in a simplified version. The three sites described in Figure 6.21, Lyngby, Næstved and Odense are also marked out in the map above as dots.

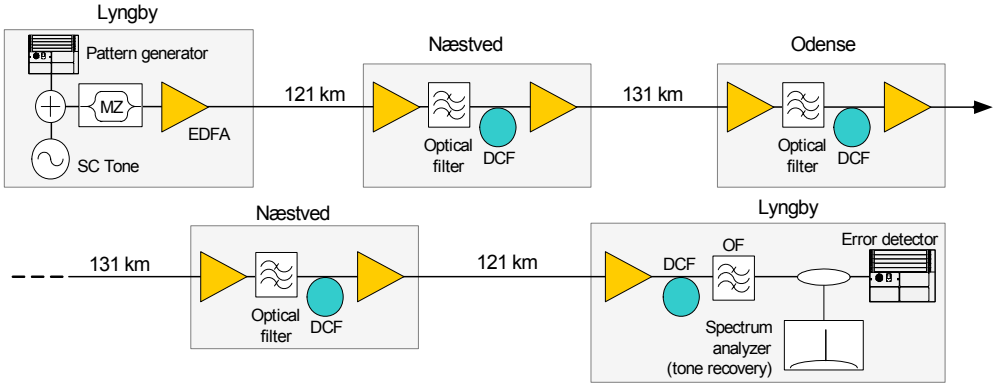

Figure 6.21: Figure illustrating the layout of the field-trial. The signal was sent from Lyngby via Næstved to Odense and looped back from Odense to Lyngby, again via Næstved. The total transmitted distance is 500-km through four spans. Also depicted is the insertion and extraction of the subcarrier tone, which in turn is used for monitoring and optimization of the power.

In each re-amplification site, the signal is dispersion compensated as well as optically filtered. Each DCF module compensates close to 100% for the previous stage and, as illustrated in the left of Figure 6.21, a double amplifier configuration is used. The first of the two amplifiers delivers a constant power of 0 dBm to the DCF that follows. An attenuator follows the second amplifier in order to vary the launch power to the following transmission span. Two scenarios were studied in the field-trial:
a) Equal launch power to all four spans, varied from 2 dBm to 14 dBm; refer to Figure 6.22a), and
b) The launch power to the first span is varied from 2 dBm to 14 dBm. The power to the remaining spans is left untouched. Refer to Figure 6.22b)

The reason for studying these two cases is that it might not be feasible or even possible to change the power to all spans in the transmission link. However, as will be evident from the results, this is the most desirable situation as a better signal quality can be achieved. In both the considered cases, the power to each span was changed and the variations of both the signal sensitivity and the subcarrier power were recorded.

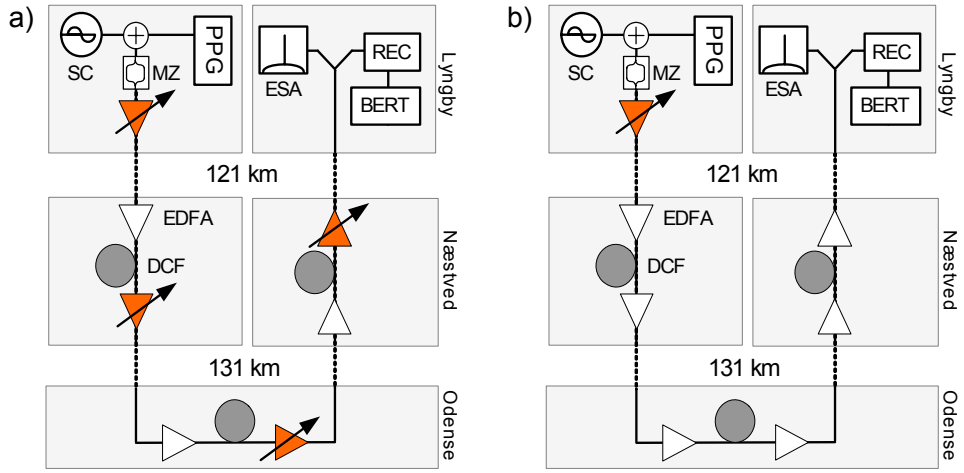

Figure 6.22: a) Equal launch power to all four spans, varied from 2 dBm to 14 dBm. b) Launch power to the first span is varied within the same range and the rest remained unchanged.

6.4.2 Field-trial results

Figure 6.23a) shows the results corresponding to scenario a), and it is clearly seen how the subcarrier power slowly rises towards higher input powers as the sensitivity improves. At 12 dBm input power, the change is radical and both sensitivity and the subcarrier power changes synchronously.

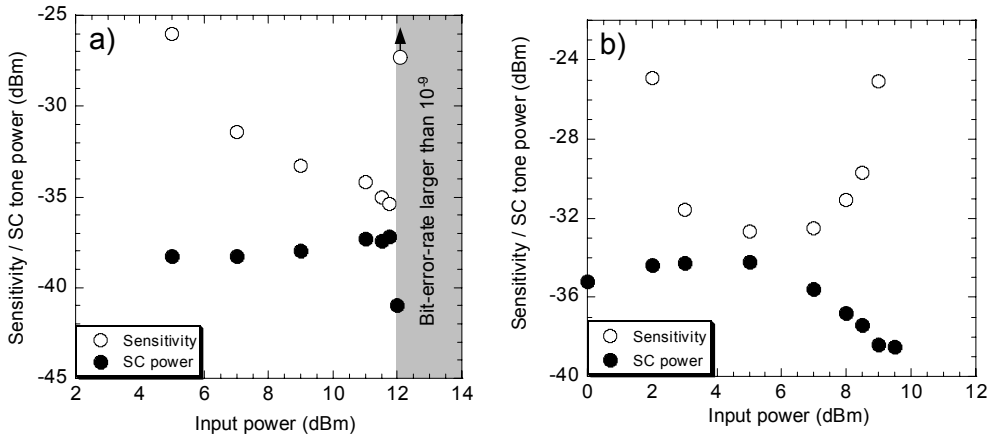

Figure 6.23: a) Sensitivity versus subcarrier RF power for case a) Equal launch power is launched to all four spans. Note the sharp drop in subcarrier power that is well synchronized to the sharp drop in signal quality. b) Sensitivity versus subcarrier RF power for case b) where the launch power to the first span was varied and the launch power to all the remaining spans was fixed at 7 dBm.

Figure 6.23b) shows the results of scenario b), where the same tendency is seen although not as radical as in case a). Case a), where the input power is the same to all spans in the link, clearly exhibits a much more rapid change in both sensitivity and subcarrier power as the input power exceeds 12 dBm. This is intuitively expected as nonlinearities will be excited throughout all the spans, whereas in case b) nonlinearities will primarily be excited in the first span.

These results demonstrate the successful use of the nonlinearity monitor in a practical and realistic scenario. With a miss-tuning of launch power of less than 2 dB, the effect on the power penalty can be several dB's. However, by keeping track of the subcarrier tone power evolution, this can be effectively avoided.

Several demonstrations of the launch power optimization have been presented in this section, and the behavior of the subcarrier and signal quality have been observed to be consistent. The method has proved itself reliable for various dispersion compensation maps, and span configurations, and the possible obstacles in terms of bias and modulation index have been identified and quantified.

6.5 Launch power optimization in WDM systems

The results presented up until now have been related to signal optimization in a single channel system. A natural question arises as to how the concept performs in a WDM system. It was seen experimentally and through simulations that both SPM and SBS has an effect on the subcarrier tone. The main difference when considering a WDM system would be related to the additional effects that

will affect the signal, and possibly also the subcarrier tone. Especially XPM and FWM should be considered when expanding to WDM systems. Regarding XPM, the effect on the data signal is comparable to the effect of SPM so the subcarrier would initially be expected to react likewise to XPM.

Experimental investigations were carried out, but without any successful results. The subcarrier did not act in the same manner as seen in the above results. Basically the fading of the subcarrier was very weak, and did therefore not correlate with the signal quality. Unfortunately, due to time constraints, there was no possibilities to further investigate the problem either experimentally nor through simulations.

Future simulations will study the launch power optimization method in detail to reveal the relevant mechanisms in a WDM system.

6.6 Chapter summary

The launch power in multi-span optical systems is a vital parameter that has a great effect on the signal quality. A low launch power can result in reduced signal quality due to low OSNR, whereas a high launch power can result in a signal impaired by nonlinearities. SPM and SBS were identified as the main contributors to signal degradation in the 10 Gb/s NRZ single channel system investigated. Furthermore, a method was proposed that enables signal quality optimization by optimizing the launch power to the spans. This was achieved adding a subcarrier tone to the data signal. The data signal and the subcarrier tone would in turn respond to the same effects such that a degradation in signal quality could be monitored through a drop in the subcarrier power. The method was successfully demonstrated for various dispersion maps, for single and multi-span systems, and finally the concept was demonstrated in a 500 km field-trial.

Chapter 7

The future optical transport network

This thesis has up until now considered various aspects of how performance monitoring could be done in a future all-optical network. Several suggestions have been given in the literature as to how the future optical networks would take form in terms of modulation formats, switching, protocols, capacity etc., and it is a complicated if not impossible matter to foretell this development. This chapter will not discuss the various possible developments in these many factors but rather consider the specific case of the transport layer technology, and proceed to discuss an example of a possible development.

It is by some believed that the current SDH/SONET transport technology will sustain, possibly in an adapted or modernized version called *Next Generation SDH/SONET* [7]. Next generation SDH/SONET features improved data quality of service (QoS), higher data rates, more flexibility, efficiency and scalability and is also a more data-effective technology. Especially the issue on data-effectiveness has been an often recurring criticism to the SDH/SONET technology, which was originally developed as a standard for telephony. In terms of being data-effective, Ethernet came about as a LAN standard in 1970, perfectly suited for handling data in small networks, and has recently been suggested as a possible candidate for the transmission layer technology in the metro-area-network (MAN) and wide-area-network (WAN) [96] [97]. Figure 7.1 illustrates some traditional SDH/SONET examples together with the suggested EoF approach.

This chapter will discuss some aspects of a future network using Ethernet in the transport layer rather than the legacy approach SDH/SONET. Furthermore, as a demonstration of use, a 10 Gb/s Ethernet-over-fiber (EoF) system has been implemented in a number of experiments such as long-haul transmission and GRID computing.

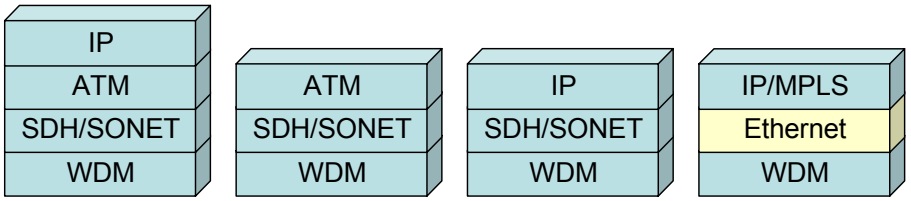

Figure 7.1: Examples of legacy SDH/SONET solutuions are shown together with a Ethenet-over-fiber approach.

More focus has been put on point-to-point Ethernet as an alternative to SDH/SONET for transmissions over WAN's and long-haul distances [98], [99]. Especially the introduction of the 10G Ethernet standard and its 1550 nm optics, makes it appealing to move Ethernet further in the metro-area-network MAN and towards the WAN. For Internet service providers (ISP's) and Ethernet customers, the Ethernet-over-SDH/SONET approach is often considered as being costly [100]. Moreover the emergence of CESoE (Circuit Emulation Service over Ethernet) can enable the use of real-time applications such as voice over a pure Ethernet infrastructure [96]. These are some of the factors making EoF attractive for service providers in future core networks.

Work has already been done in terms of moving Ethernet into the backbone and the WAN's [101], [102]. A 10 Gb/s Ethernet-over-SONET transmission from Geneva to Ottawa is reported in [101]. That article describes an Ethernet WAN PHY transmission where the Ethernet traffic is carried on an existing SONET infrastructure. This can have several advantages as well as disadvantages. For example, using SONET also implies the use of 3R regeneration, however it enables the well-known OAM (operations administration and maintenance) features of SDH/SONET such as protection, restoration, performance monitoring and provisioning quality of service guarantees.

The next section will discuss some of the obstacles that will be met using Ethernet as a transport protocol.

7.1 Ethernet as a layer 2 and transport protocol

With Ethernet already being the major protocol in the LAN and with the introduction of the 10Gb/s Ethernet standard (IEEE 802.3ae) [103], Ethernet has become an appealing and low-cost layer 1 option for the MAN and WAN [98], [99], [100].

The traditional use of SDH/SONET as a transport protocol in WAN's provides the often needed functionalities such as protection, administration and monitoring. Moving Ethernet to the transport layer brings these issues to attention as Ethernet does not have the native support in layer 1 for these functionalities.

However, there are suggestions of how to work around these potential problems, if necessary. The actual need for functionalities such as protection, management etc. is dictated by the specific and intended use of the network. For example, an Ethernet transporting only low priority and best effort traffic does not have the same requirements to protection switching as a network supporting real-time applications.

In this section, the use of pure Ethernet as a transport protocol for data traffic will be discussed. "Pure Ethernet" should in this context be understood as Ethernet-over-Fiber (EoF), i.e. no underlying layers like SDH or SONET. Please note, that it is not the scope of this thesis to address the different issues thoroughly and only an overall discussion will be given in this section. Where relevant, references will be given to ongoing work by various organizations and groups addressing these aspects.

7.1.1 Operations, administration & maintenance (OAM)

It is essential for service providers to have the ability to monitor their networks and insure they perform as guaranteed to the customer. Monitoring factors like basic connectivity and frame delay jitter and loss must be provided along with an alarm notification functionality. These are essential components for establishing services based on Ethernet [104]. Moreover, traffic profiling and bandwidth guarantees are necessary basics to obtain a satisfactory QoS in a layer 2 Ethernet network. Provided that Ethernet is employed as a transport protocol, profiling and bandwidth guarantees functionalities should be handled by the upper layer protocols such as multi protocol label switching (MPLS) for example. However, monitoring the basic connectivity factors, alarm notifications etc. is still a layer 1 functionality - a functionality that is not currently supported in the Ethernet protocol.

Several workgroups are looking at possible implementations and standards for support of OAM capabilities in Ethernet. The IEEE 802.3ah groups as well as ITU-SG13 are working on these issues, and furthermore the IEEE 802.1 working group has added a new project, which will also address Ethernet OAM functionalities [104].

Recently, Network Innovation Laboratories (NTT) has presented yet another possible solution to enable error rate monitoring, alarm indications and protection switching in layer 1 Ethernet networks [105]. The so-called GENIE (Gigabit Ethernet Network interface Extension to WAN), is very interesting because it is a layer 1 functionality that exploits the Ethernet inter-frame gaps between Ethernet frames. A part of this 12 byte inter-frame gap is simply used to insert information that in turn will enable sufficient monitoring of the network.

7.1.2 Quality of Service

QoS is here referred to as the quality of service that is assured to the user via delay, jitter and bandwidth requirements. Therefore, if Ethernet applied in the transport layer is considered, it is not relevant to talk about QoS as this is a layer 2 and layer 3 functionality. However, if we consider Ethernet in layer 2, a standardized way of ensuring QoS to the customers is likewise needed. They will include boundaries for parameters such as bandwidth, delay, jitter etc. If we consider Ethernet used as a switching layer (layer 2) protocol, it only allows for best-effort traffic in the simple Class of Service (CoS) prioritization, and provides therefore no guarantees for QoS parameters.

The framework of bringing support for QoS to the Ethernet MAN is underway from for example the Metro Ethernet Forum (MEF) [106]. They also work on a mechanism to support synchronous services over an asynchronous Ethernet infrastructure called Circuit Emulation Services over Ethernet (CESoE). CESoE can thus allow legacy TDM services to be transported over a low-cost Ethernet infrastructure [96].

7.1.3 Protection and Architecture

Another central element in the successful exploitation of Ethernet in the MAN and WAN is the ability to offer link protection and resilience. As the protection offered by the Ethernet infrastructure is directly related to the services supplied to the customer, protection mechanisms are essential to provide reliability. Protection in this manner requires fault detection and restoration ability, and a key parameter is the mean-time-to-restore.

The original Ethernet standard does not provide the above-mentioned functionalities in layer 1, but work has begun where potential solutions are looked into. MEF has recently published a document [97] that includes technical specifications for different layer 2 protection schemes. In addition, protection using resilient packet rings (RPR) could be considered. This however removes the MAC-layer of standard Ethernet and replaces this layer 2 functionality with one optimized for ring-based topologies [107]. Recently, an 8 node native Ethernet ring was successfully demonstrated for access networks [108] and in 2004 a resilient Ethernet ring for MAN's was demonstrated in [109].

Considering Ethernet used a transport protocol, Ethernet does not provide any immediate protection switching functionalities in layer 1. This can, however, be overcome using for example MPLS, where independent protection paths can be set up. That way, MPLS can provide a fast layer 2 protection switching that in principle can be as fast as the SDH/SONET protection switching done in the transport layer. Furthermore, MPLS path protection gives the possibility of

protecting only a selection of the traffic on a given path rather than all the traffic as required in SDH/SONET.

7.1.4 Section Summary

There are still a number of issues that needs to be resolved and standardized for Ethernet to really be suited for use in an all purpose MAN/WAN environment as pointed out in the previous sections. Several groups such as ITU, IEEE, etc. and additional work groups and forums like MEF, are working to resolve the problems of using Ethernet as a layer 1 and layer 2 technology in these environments.

Although issues like protection, detailed signal monitoring and CoS are important for applications such as for example real-time services, other applications do not require these features. ISP's providing basic Ethernet through best effort, and GRID computing are some to mention. Furthermore, the requirements to Ethernet functionalities also depend strongly on whether the protocol is used as a layer 1 or layer 2 technology. Bearing these aspects in mind, the prospects of Ethernet evolving into the MAN and WAN will thus be dependant on the applications and services this protocol is expected to support.

In terms of overcoming the lack of performance monitoring in EoF networks, Ethernet could be successfully combined with a number of basic monitoring and protection features and in turn constitute a cheap and simple network for the right applications. Reflecting back the to the previous chapters, this can be done by combining layer 1 Ethernet with an appropriate optical performance monitoring technology such as for example OSNR monitoring.

It is important to note that native Ethernet is not a protocol created to support advanced OAM features, and it can be complicated to incorporate all these functionalities, and further more, it can end up being too complex to operate. One of the main advantages of Ethernet compared to SDH/SONET is indeed the much simpler Ethernet equipment that are often considered to be "plug-and-play". Therefore, it seems sensible to identity the main areas of network applications where Ethernet could make up an advantage and also identify the needed functionalities in order to not end up re-inventing SDH/SONET.

7.2 Transport layer Ethernet and GRID computing

This section describes a project carried out in cooperation with several other partners in the joint EU project ESTA (Ethernet Switching at 10 Gb/s and Above). The now concluded project searched to discuss the possibilities and issues of using Ethernet in long haul and WAN network distances.

Here is described 10 Gb/s Ethernet field trial experiments carried out in the Danish Research Network illustrated in Figure 7.2. Cost is always a vital issue and, apart from demonstrating 10 Gb/s EoF, the focus in these trials has also been on minimizing equipment cost.

7.2.1 Field trial setup

The Danish Research Network has a number of dark fibers at their disposal in the Danish backbone infrastructure owned by Global Connect Denmark. The SMF fiber pairs used for this experiment runs from Lyngby to Odense as illustrated in Figure 7.2 and Figure 7.3. Underway there is access to the fiber pair in Næstved, which is also marked in the figure. Næstved is close to halfway between the two endpoints, which are separated by approximately 252-km.

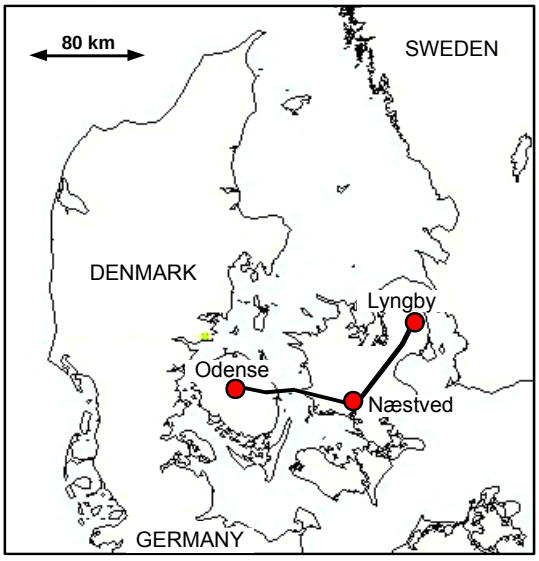

Figure 7.2: Illustration showing the 250 km path of the fiber pairs used in the 10 Gb/s Ethernet field trial.

Each of the two 10 Gb/s Ethernet switches used are manufactured by BATM and equipped with a 1550 nm XENPAK Optillion transceiver module having a specified reach of 40 km. Moreover, the switches have eight 1 Gb/s optical duplex ports that internally aggregates to a total data output of up to 8 Gb/s. This 8 Gb/s constraint on the throughput is related to the physical layout of the 8×1 Gb/s line cards that were available, and not the 10 Gb/s interface, which are in fact able to transmit at 10 Gb/s.

As the signal is not regenerated throughout the 250 km, the signal is optically amplified in Næstved, which is located 131 km from Odense and 121 km from

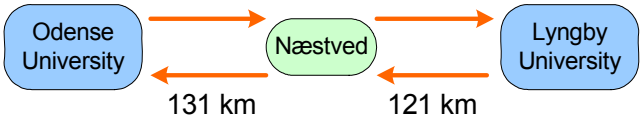

Figure 7.3: Distances between Odense and Lyngby. Both signals were optically amplified in Næstved.

Lyngby (Figure 7.3). The almost symmetrical location of Næstved was very convenient as both paths LY-OD and OD-LY could be amplified at the same site. The amplifiers used, were standard commercially available EDFA's.

At 10 Gb/s, pulse broadening will distort the signal due to chromatic dispersion so dispersion compensation is used. DCF spools were placed right after the transmitter and in the amplification site in Næstved as illustrated in Figure 7.4. Optical filters were used to filter out amplified ASE noise from the EDFA's.

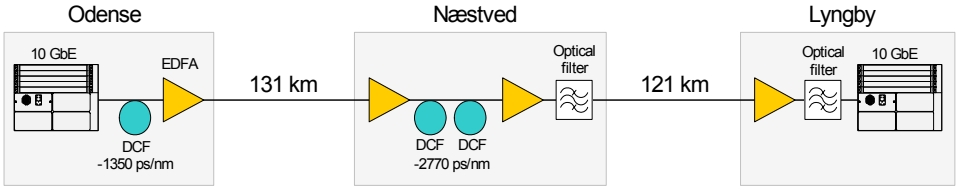

Figure 7.4: Placement of equipment used in the Odense-Lyngby direction.

Figure 7.4 illustrates the equipment used in the Odense-Lyngby direction. The locations of amplifiers, filters and DCF are the same for the Lyngby-Odense direction due to the symmetrical layout of the two paths. Note that the filter placed in Næstved was not strictly needed but merely applied to optimize the signal quality. Each of the three DCF spools has a length corresponding to a compensation used for a 80 km SMF span and thus resulting in a small under-compensation of approximately 100 – 200 ps/nm. The total loss in the two DCF spools in Næstved was about 15 dB, which therefore implied the use of double stage amplification as shown in the figure.

In order to generate Ethernet traffic, two industrial computers each equipped with eight 1 Gb/s Ethernet network interface cards (NIC's) were used. The 850 nm optical multimode interfaces on the NIC's comply with the eight optical 1 Gb/s interfaces on the Ethernet switch. These programmable NIC's are able to produce Ethernet frames in a rate of 1 Gb/s each. At the receiving switch the optical signal is amplified and filtered and an optical attenuator assures a constant power level of around -8 dBm to the XENPAK receiver in the switch.

This pre-amplified receiver configuration delivers a better sensitivity and power margin, as will be seen in the next section, but at the cost of an extra EDFA.

7.2.2 Ethernet transmission evaluation

The tests results from the trial can be divided up into two parts. The BER test part, which verifies the condition and quality of the 10 Gb/s optical signal after transmission, and a part related to the actual transmission of Ethernet frames.

Part 1. BER tests

It is obviously important to verify both that the 802.3ae Ethernet standard is fulfilled and further to ensure proper power margins in the system. The XENPAK transceiver modules are rated to 40 km transmission but in this case the transmission requirements are pushed to two spans of 121 km and 131 km respectively and thus well above the rated distance. Furthermore, due to the long spans, a booster amplifier is needed, which can be seen in Figure 7.4. This assures that the power level is kept high enough that the optical OSNR does not suffer substantially. The XENPAK transceiver modules used in the switches include the IEEE 802.3-2000 built-in-self-testing (BIST) capabilities used to make the BER measurements [103].

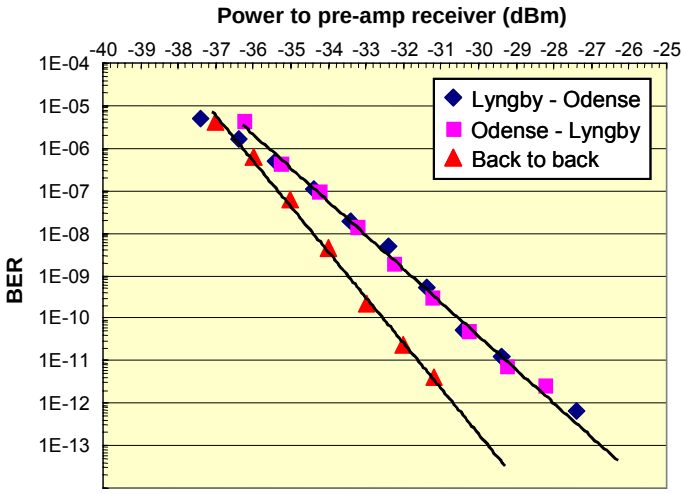

Figure 7.5: BER measurements from the two paths Lyngby-Odense and Odense-Lyngby. The transmission distance is 252-km.

Figure 7.5 shows the BER measurements for both directions Lyngby-Odense and Odense-Lyngby next to the back-to-back base line. These BER measurements are done with a setup configuration like the one shown in Figure 7.4, where a pre-amplified received setup is used. The sensitivity for both directions is better than -33.5 dBm and the power penalty compared to the back-to-back case is less than 1.5 dB. Both values are calculated using BER = $1{\cdot}10^{-9}$ as a

reference. Note that the optical power values on the horizontal axis denotes the power into the pre-amplified receiver and not the switch itself, which received a constant power of -8 dBm.

In order to assure that the BER performance satisfied the $1{\cdot}10^{-12}$ 802.ae Ethernet requirements, the BER was measured over a time period of more than 3 days. Within those 3 days there were zero errors, corresponding to a BER better than $1{\cdot}10^{-15}$. One of the objectives of these tests was also to expose any possibilities for reduction in equipment and thereby cost savings. This was done for the Lyngby-Odense link where the setup was reduced with one EDFA, one filter and one optical attenuator. The resulting setup can be seen in Figure 7.6.This setup still achieved a BER performance better than the required $1{\cdot}10^{-12}$ although far from the $1{\cdot}10^{-15}$ achieved for the setup shown in Figure 7.4. Basically this was done by replacing the pre-amplifier receiver configuration shown in Figure 7.4 with a direct detection configuration. Although this configuration is simpler and saves equipment, it is not as tolerant in terms of power fluctuations; the power margin is simply reduced compared to the pre-amplified receiver.

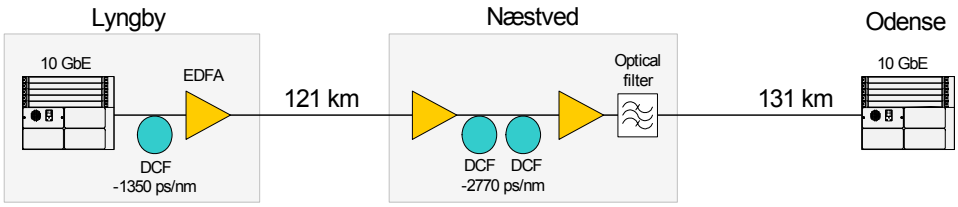

Figure 7.6: Figure showing the Lyngby-Odense setup after reduction of equipment. Compated to Figure 7.4, the setup has been reduced with one EDFA, a filter, and an optical attenuator.

Part 2. Transmission of Ethernet packets

The second part of the test is related to the actual transmission of Ethernet packets. Ethernet frames were generated from the eight programmable NIC's and then aggregated in the switch to a bit rate of 8 Gb/s. The frames were transmitted over the 252-km path and packet loss and throughput were measured. The NIC's have been custom programmed to produce 1518 bytes frames in a rate of 1 Gb/s. In another Ethernet frame transmission test, the frames sizes were randomized over the sizes specified by IEEE RFC 1944 used for testing Ethernet traffic and transmitted at a rate near 8 Gb/s. In both these tests performed, no packet losses were observed over the test period of approximately one hour.

7.2.3 10 GE GRID experiment

As a part of the Ethernet field trials, the Danish Research Network entered into an international GRID computing experiment. This experiment was running on

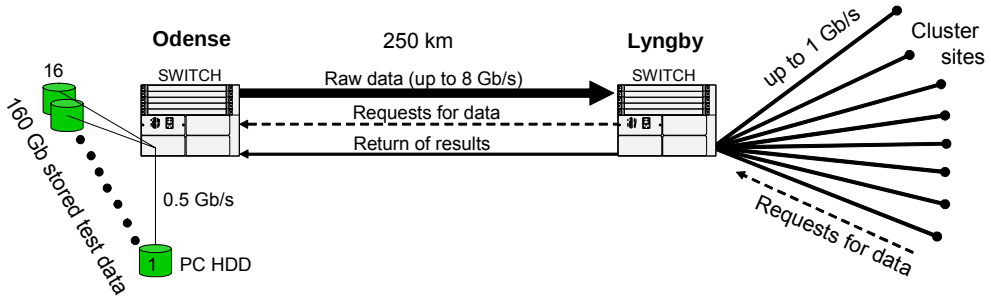

Figure 7.7: Illustration of the GRID computing experiment, which was run over the link shown in Figure 1 and 3.

the same setup as shown in Figure 7.4 except from the filter in Næstved which is omitted.

The objective of the experiment is foremost to acquire experience on the use of 10 Gb/s Ethernet for GRID computing and to verify that low cost Ethernet equipment can support the necessary transport network.

In Scandinavia there exist a number of CPU clusters, which with great benefits can be combined to work together on one designated project like the upcoming Large Hadron Collider (LHC) experiments scheduled to start at CERN in 2007 [110]. The huge amounts of data collected from these particle collisions are more than CERN itself can process and therefore some of the collected data will be streamed out to international collaborators including Canada as well as the Scandinavian countries Sweden, Norway and Denmark. When the LHC project will run at full speed, the data generated will be streamed from CERN in real-time, and approach rates of 10 Gb/s, so the calculation abilities of several CPU clusters needs to be combined in a computing GRID in order to overcome these great amounts of data. More information about the software used in the clusters, GRID software and technology can be found in references [111] and [112].

In order to simulate the future LHC project, the 10 Gb/s Ethernet link shown in Figure 7.2 and 7.4 was used. Odense is acting as the data provider or data-feeding source. 160 Gb of measurement data previously collected from CERN is hard drive stored on 16 PC's located in Odense. These 16 PC's are able to, upon request, from the individual clusters to provide a data feed of speeds up to 8 Gb/s. The configuration using 16 PC's is necessary to feed the data fast enough as one unit cannot deliver data at the required speeds. The setup is illustrated in Figure 7.7, where the clusters are shown on the right. These clusters constitute various Danish research centers and universities as well as the Swedish, Norwegian and Canadian collaboration partners.

Using the GRID structure, the individual clusters are able to request data in a tailored rate, which will then be transmitted over the 250 km path to the

clusters for computation. After the data has been processed in the CPU-clusters, the results are sent back to the data provider source in Odense for further analysis. Note that since only 160 Gb of data was available in this GRID demonstration, the data was continuously resent from the data provider every 6 to 7 minutes when running at maximum throughput.

The GRID experiment was running over three days, which allowed for data flow optimization and problem solving underway. The biggest problems were met in the outer skirts of the network – the last mile. Internal switch speed issues and capacity limitations into the local clusters became the largest bottleneck in the GRID experiment. Firewalls constituted another problem. It was initially the intention to use more clusters but firewalls made communication with these clusters impossible.

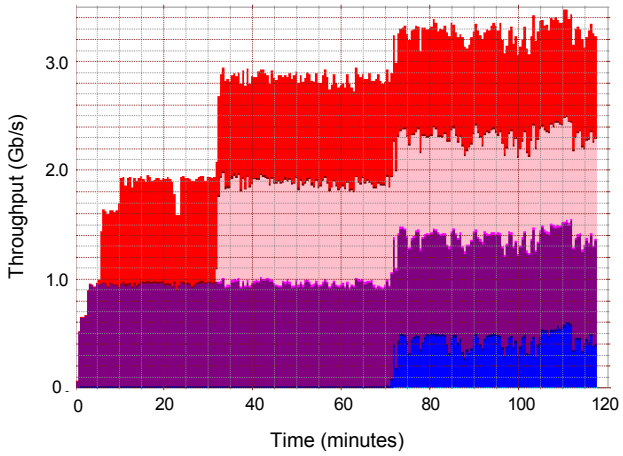

Figure 7.8: Illustration showing the throughput during a 2 hours time window. Notice the maximum throughput of about 3.2 Gb/s - 3.4 Gb/s.

The maximum throughput of approximately 3.4 Gb/s was achieved after all eight clusters were pulling data at their maximum rates. Although this is only a 40% utilization of the 8 Gb/s maximum link capacity, the GRID experiment is considered a success as the limitations are of external character and not as such related to the Ethernet GRID network. Figure 7.8 shows a load versus time plot for a 2 hour time frame during the GRID field trial. The different colors in the figure represents different CPU-clusters and, as can be seen, four of the clusters were the sites responsible for the overall traffic.

7.3 525 km demonstration of long-haul Ethernet

This section presents a 10 Gb/s Ethernet-over-Fiber long-haul field transmission without regeneration in an Ethernet link set up 525 km across Denmark. As well as the previous described field trial, this work was a part of the IST ESTA project. The 525 km transmission distance is, to the authors knowledge, the longest non-regenerated EoF transmitted distance. This section will present the field-trial details and results achieved.

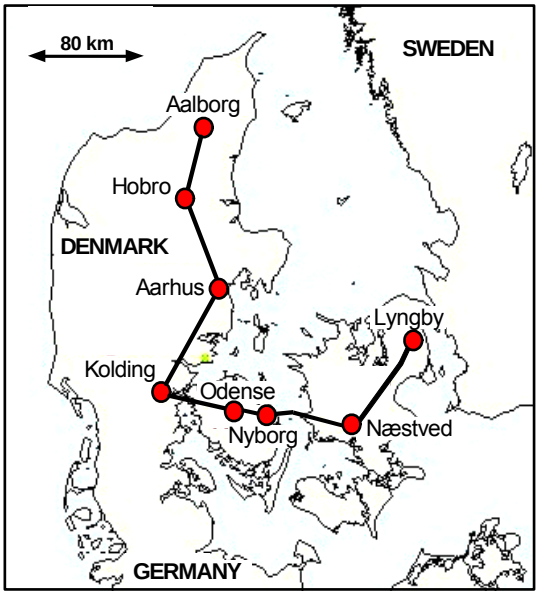

Figure 7.9: The 525 km path from Copenhagen to Aalborg used for the 10 Gb/s Ethernet transmission. Access points are marked as white dots on the path.

7.3.1 Field trial setup

Figure 7.9 shows the outline of the transmission link used in the field trial. The signal was launched from Lyngby, near Copenhagen, and transmitted 525 km to Aalborg with six sites underway providing optical amplification. These sites are shown as dots in the figure, the shortest and longest span being 38 km and 121 km respectively.

The detailed setup describing optical amplifiers, DCF modules and optical filters is shown in Figure 7.10. The placement of the DCF is dictated by two factors. Firstly, the total loss for the individual spans, as DCF fiber is a relative high loss fiber. Having a too high span loss will reduce the OSNR making it impossible to reach the full distance. Secondly, due to high launch powers, which trigger fiber nonlinearities, the accumulated dispersion must not become too

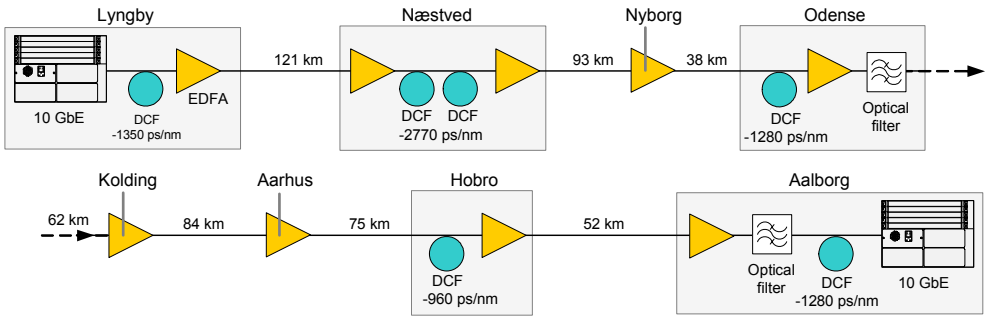

Figure 7.10: Detailed description of the equipment used in the 10 Gb/s Ethernet-on-fiber field transmission.

high at any point in the link. Nonlinearities will interact with dispersion to a higher degree when the accumulated dispersion is high so the aim is to keep the dispersion map centered around zero dispersion to the extend made possible by the OSNR and span losses [113].

Notice that the total amount of dispersion compensation corresponds to less than the transmitted 525 km. The reason for this so-called under-compensation is discussed below.

The nine double pumped EDFA's used in the trial have output powers in the range of 14-16 dBm. This output power was adjusted using optical attenuators before launching the signal to the fiber. Launch powers are in the range of 7 to 10 dBm, where approximately 10 dBm was launched to the first long span from Lyngby to Næstved (121 km). Lower launch powers were used for the much shorter Odense-Kolding span and Hobro-Aalborg span in order to avoid an accumulation of nonlinear effects.

Each of the two 10 Gb/s Ethernet switches used are manufactured by BATM and equipped with a 1550 nm XENPAK Optillion transceiver module having a rated reach of 40 km. This middle-distance transceiver can however transmit the full distance of 525 km with the aid of optical amplification and dispersion compensation.

At the receiving switch the optical signal is amplified and filtered and continues to an optical attenuator that assures a constant power level of around -8 dBm to the XENPAK receiver in the switch. This last amplifier is not strictly necessary and can be omitted. We chose to include it as it provides robustness in terms of better power margins in the link.

7.3.2 Field trial transmission results

The BIST function in the XENPAK transceiver modules were again used to make BER measurements. This feature was used to verify a bit-error-free 10 Gb/s

transmission period of 17 hours. Although the accuracy of the measurement was limited by time it indicates a BER of $1{\cdot}10^{-14}$ or better, which fulfills the IEEE 802.3ae Ethernet standard. A BER of $1{\cdot}10^{-14}$ would correspond to an error count of about 6 within the 17 hours.

In order to demonstrate Ethernet traffic transmission, a frame replay feature on the 10 Gb/s line card was used to generate Ethernet mix-sized frames at 10 Gb/s that were transmitted over the link, also without any packet losses.

In Aalborg it was possible to vary the dispersion compensation while investigating the effect on the received signal. An under-compensation of about 800 ps/nm was necessary to achieve the required BER performance. With 100% compensation the signal was significantly distorted leading to a significantly worse BER performance. The 10 dBm launched in the first 121 km span will initiate SPM and, as previously described, SPM distorts the pulses of the signal, which in turn leads to unwanted eye closure. This can however be rectified to some extent by means of dispersion compensation as described in [114] and [115]. This under-compensation which creates a soloton-like effect is therefore used to assure that the received signal can be recovered and detected. The dispersion - SPM interactions and their effect on pulse shape and signal quality were also discussed in Chapter 2 and 6.

7.4 Chapter summary

This chapter has put focus on Ethernet in layer 1, as a possible alternative to the legacy SDH/SONET as transmission technology. The relative increase of data traffic and its surpass of telephony in the networks held together with the equipment cost savings have brought this suggestion forward. Ethernet in the transport layer does, though, involve certain implications such the lack of OAM functionalities, no guarantee of service, etc. Work is being done to circumvent these issues, and monitoring in native Ethernet has been demonstrated previously as well as Ethernet rings.

The second part of the chapter presented some field trial experiments of Ethernet-over-fiber, that served to demonstrate an application as a high-capacity GRID computing network, as well as a 525 km long-haul transmission proving Ethernet applicable for WAN distances.

Even though a future implementation of Ethernet in layer 2 can seem appealing, one should not undermine the power and efficiency of the legacy transport technologies. SDH and SONET have been around for many years and has been proven reliable and effective in transporting voice and data. Equipped with features such as protection, restoration as well as an advanced management structure, these transport technologies are still ahead of any state of the art technology

in terms of providing stable, trustworthy and effective functionalities.

Chapter 8

Conclusion

It has been argued in Chapter 1 and Chapter 3 that optical networking will not continue in the form known today. Even though prophecies have been made stating that SDH and SONET are not the appropriate choice in a world dominated by data traffic rather than voice traffic, these are transport technologies that has proven themselves very robust and effective throughout the years and will most probably stick around for a few more to come. That said, the increase in capacity demand will eventually call for changes in the optical backbone. This will inevitably include an increase of optical components such as optical switches, optical regenerators, and possibly even optical logic. The thesis has argued how these changes will make optical performance monitoring advantageous and in several cases even a necessity. The required access to the data, that is required for legacy performance monitoring, is no longer available when termination of the signal becomes obsolete.

A number of signal degrading effects were identified in Chapter 2 and investigations have shown that several of these effects demand an increased attention as bit-rate and the optical transmitted distances increase. Especially nonlinear effects such as self phase modulation (SPM), cross phase modulation (XPM) and four wave mixing (FWM) as well as group velocity dispersion can have a tremendous influences on the signal quality. Discussions regarding performance monitoring parameters in Chapter 3 reasoned that, depending on especially bit-rates and optical transmission distances, different requirements could be set for the selection of performance monitoring parameters. It is believed though, that combining optical signal parameter monitoring, such as dispersion or optical-signal-to-noise-ratio (OSNR) monitoring, with a type of optical signal quality monitoring, for example bit-error-rate estimation, would offer significant advantages in terms of being able to both monitor bit-errors as well as determining the possible source of the bit-errors. Especially OSNR monitoring is considered

necessary as noise is one of the most significant sources for bit-errors.

The thesis proposed a number of optical performance monitoring techniques. In Chapter 4 a method for signal quality evaluation in noise dominated systems was presented. The method showed successful predictions of signal quality in a 40 Gb/s system using a 2.5 Gb/s reference channel. An all optical bit-parity calculator was also demonstrated, however bit-parity checking could not be achieved with the current setup.

Dispersion monitoring and OSNR monitoring was demonstrated experimentally in Chapter 5. Dispersion monitoring was performed in both 40 Gb/s NRZ and RZ systems using spectral broadening in a highly nonlinear fiber. A method for more accurate OSNR evaluations in dense WDM systems was achieved using polarization interleaving of the channels. Polarization interleaving the adjacent channels additionally brought in advantages such as decreased influence from crosstalk and nonlinearities.

The signal quality optimization and signal quality monitoring method proposed in Chapter 6 is considered one of the main results of this thesis. Signal quality optimization was achieved by tuning the launch power to the fiber. The consistency of the method was demonstrated through numerous experiments including various dispersion maps as well as a large-scale field trial over 500 km in the Danish Research Network.

The same network was used to demonstrate two Ethernet-over-Fiber (EoF) transmission experiments. Native Ethernet was successfully used as an alternative to SDH/SONET as transport technology. A comprehensive GRID computing experiment as well as a 525 km all-optical EoF transmission proved a rather simple and in-expensive Ethernet based back-bone network attractive for best effort data services. Several issues regarding operations, administration and management (OAM) are not yet fulfilled for EoF but considerable attention is given to the issues. For now, however, EoF can still be considered appealing for cost-effective data traffic services, and several of the OAM issues can be solved simply by over-sizing network capacities.

Appendix A

Receiver sensitivity

The electrical signal-to-noise ratio (SNR) determines the performance of a p-i-n receiver, can be written as

$$\text{SNR} = \frac{I_p^2}{\sigma^2} = \frac{(RP_{in})^2}{\sigma^2} \tag{A.1}$$

where I_p is the photo current generated by the incoming optical signal, σ^2 is the noise power, R the responsitivity of the p-i-n diode considered and P_{in} is the optical input power. The noise power can be made up of different terms such as thermal-noise and shot-noise and, depending on what limits the performance, certain reductions and simplifications can be made of the SNR expression. The noise term regarding the thermal noise for example is

$$\sigma_{th}^2 = N_{th}B_e$$

where N_{th} is the spectral density of the thermal noise which can be assumed to be frequency independent (white noise) for the applications considered here. B_e is the bandwidth of the electrical filter. For a receiver in an optical pre-amplified receiver configuration, the optical power to the receiver will usually be above the limit where thermal noise dominates. The power to the pre-amplifier can be fairly low, and this sets up a new regime where the performance can be limited by noise created via beating between the signal and the spontaneous ASE noise, the so-called signal-spontaneous beat noise, or the spontaneous-spontaneous beat noise. Signal-spontaneous is dependant on the signal power, P_{in}, itself, so the term P_{in} would be included in the expression for σ^2 in Equation A.1. Spontaneous-spontaneous beat noise on the other hand is not dependant on the optical signal power, and will have a noise much like the one for thermal noise:

$$\sigma_{sp-sp}^2 = N_{sp-sp}B_e$$

where N_{sp-sp} is the spectral density of the spontaneous-spontaneous beat noise. Again, this can be considered frequency independent.

If the signal-spontaneous beat noise is considered to be limiting the performance, formula A.1 gives

$$\mathrm{SNR}_{sig-sp} \propto \frac{P_{in}^2}{P_{in}B_e} = \frac{P_{in}}{B_e} \tag{A.2}$$

whereas in the spontaneous-spontaneous beat noise limit

$$\mathrm{SNR}_{sp-sp} \propto \frac{P_{in}^2}{N_{sp-sp}B_e} \propto \frac{P_{in}^2}{B_e} \tag{A.3}$$

What is important to notice here is the SNR dependence on P_{in}, which is squared in the case of signal-spontaneous beat noise domination but linear in the case of spontaneous-spontaneous beat noise domination.

Moving the focus to the electrical bandwidth, this has certain influences on the receiver sensitivity, which is related to SNR by the Equations A.2 and A.3.

Consider a change in the electrical bandwidth B_e. In order to keep the same SNR, the input power, P_{in}, will have to change. This change in receiver sensitivity, or power penalty, will scale linearly with the change in B_e if the receiver is signal-spontaneous beat noise limited, but with $\sqrt{B_e}$ if the system is spontaneous-spontaneous beat noise limited.

Therefore, the expected decrease in receiver sensitivity due to a change in the electrical filter bandwidth has to be determined from which noise is limiting the system. A spontaneous-spontaneous beat noise limited receiver will not display give rise to a 3 dB receiver sensitivity penalty if B_e is increased by 3 dB. A doubling of the electrical bandwidth will instead lead to a $\log(\sqrt{2}) = 1.5$ dB penalty.

A.1 Optical filtering in the pre-amplified receiver

The optical pre-amplifier uses an optical amplifier to increase the receiver sensitivity of the optical receiver. However, due to the inevitably noisy EDFA amplifiers, it is necessary to filter out ASE noise prior to the O/E receiver. The principle of the pre-amplified receiver is shown in Figure A.1.

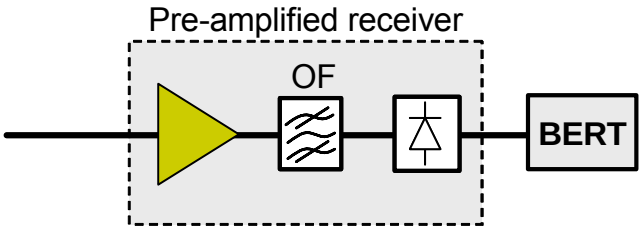

Figure A.1: The pre-amplified receiver.

The optical filtering that is done in a pre-amplified receiver has a big impact on the maximum achievable receiver sensitivity. For example has VPI simulations shown that a Gaussian band-pass filter with a 3-dB bandwidth of 50 GHz will lead to a -42.3 dBm receiver sensitivity whereas a 100 GHz band-pass filter will decrease the sensitivity to -35.1 dBm. The optical filter is directly related to the amount of noise let into the receiver, and therefore it controls to a big extent the best achievable receiver sensitivity.

In practise, choosing the optical filter bandwidth is a trade-off. A too narrow filter will result in a great power loss, and possibly also unwanted shaping of the signal spectrum, and choosing a broad filter will result in excessive noise being let into the receiver.

A.2 Filtering bandwidth versus bit-rate

The optical filter bandwidth in the pre-amplified receiver as well as the electrical low-pass filter in general have a significant influence on the performance on of the receiver. Ideally the filter has the purpose of removing the out of band noise which in turn will improve the signal SNR. Due to non-ideal filters this is however not possible, so a trade-off must be made as also described above in A.1.

Optical filters can be made quite narrow, but not without the price of a high loss and the risk of shaping the signal spectrum. Comparing a 2.5 Gb/s signal and a 40 Gb/s signal, the optical filter should be 16 times (12 dB) more narrow in the case of the 2.5 Gb/s signal but due to the issues listed above, there will usually not be a 12 dB difference in filter bandwidth for a 2.5 Gb/s and a 40 Gb/s system. Observed relatively, this increases the beat-noise contribution in the 2.5 Gb/s system, and a relative decrease in performance will be seen. The ideal receiver sensitivity difference of 12 dB can easily be reduced to 8 dB if the same optical receiver filters are used for both signals.

Appendix B

VPI Simulations

The parameters used in VPI simulations have been listed below. They are divided according to chapters.

B.1 Simulations in Chapter 4

In Chapter 4, a method for signal quality monitoring using polarization multiplexing was presented. VPI Transmission Maker version 6.5 was used for these simulations and the relevant simulation parameters are listed below together with the used value. Figure B.1 shows an example of a schematic in VPI used for these simulations.

Variable	**Value**	**Unit**
Timewindow	1024/2.5e9 s	s
SampleModeBandwidth	320e9	Hz
SampleModeCenterFrequency	193.1e12	Hz
SampleRateDefault	32*40e9	Hz
BitRateDefault	40e9	bit/s
RiseTime	1.0/4.0/BitRateDefault	s
MZM ExtinctionRatio	15	dB
EDFA NoiseFigure	5	dB
PRBS_Type	PRBS_N	
Optical 40 Gb/s receiver filter bandwidth	100e9	Hz
Optical 2.5 Gb/s receiver filter bandwidth	192e9	Hz

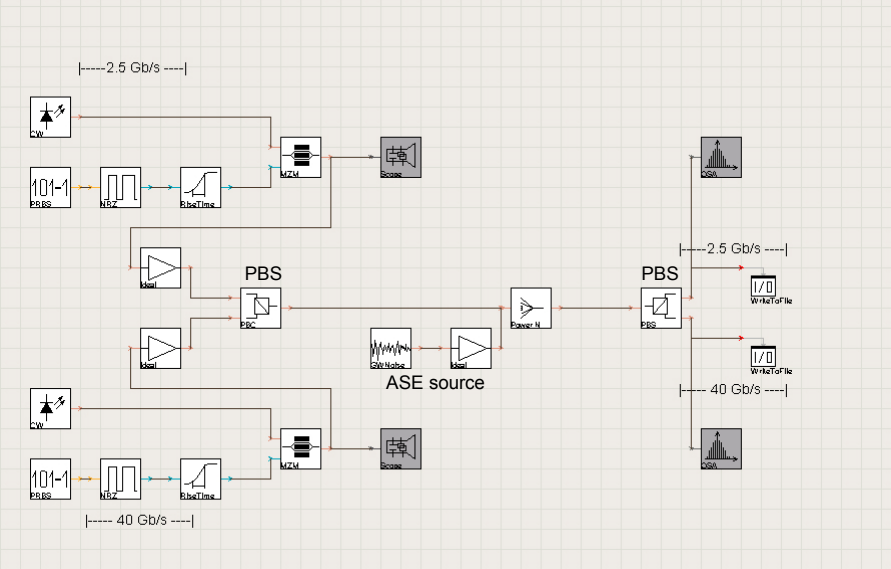

Figure B.1: Transmission configuration used in VPI simulations. The 2.5 Gb/s and 40 Gb/s NRZ signals are combined using the PBS. ASE is added using the ASE source after which the signals are split using the second PBS. The signals are saved in two seperate files.

B.2 Simulations in Chapter 5

Chapter 5, section 5.1 proposed a method for dispersion monitoring. The simulations done used VPI Transmission Maker version 5.1. The relevant simulation parameters are listed below together with the used value.

Variable	**Value**	**Unit**
Timewindow	1024/2.5e9 s	s
SampleModeBandwidth	128e10	Hz
SampleModeCenterFrequency	193.1e12	Hz
SampleRateDefault	32*40e9	Hz
BitRateDefault	40e9	bit/s
RiseTime	1.0/4.0/BitRateDefault	s
MZM ExtinctionRatio	15	dB
EDFA NoiseFigure	5	dB
PRBS_Type	PRBS_N	
SMF Attenuation	0.2e-3	dB/m
SMF Dispersion	16e-6	s/m^2
SMF DispersionSlope	0.08e3	s/m^3
SMF NonLinearIndex	2.6e-20	m^2/W
CoreArea	80.0e-12	m^2

B.3 Simulations in Chapter 6

The signal quality optimization technique using a subcarrier modulator was presented in Chapter 6. Two versions of VPI was used in this case. VPI version 5.5 and version 6.5 were used - both versions includes a SBS fiber model in the *UniversalFiber* module. The SBS description called *SBSGainParameter* was used for all SBS related simulations. For a detailed description of the numerical model used refer to the VPI 5.5 or 6.5 documentation for the *UniversalFiber* module.

Typical simulation parameters are listed below. The UniversalFiber values in parenthesis are related to (SMF) (DCF) values respectively.

Variable	**Value**	**Unit**
Timewindow	1024/2.5e9 s	s
SampleModeBandwidth	128e10	Hz
SampleModeCenterFrequency	193.1e12	Hz
SampleRateDefault	32*40e9	Hz
BitRateDefault	10e9	bit/s
RiseTime	1.0/4.0/BitRateDefault	s
MZM ExtinctionRatio	15	dB
EDFA NoiseFigure	5	dB
PRBS_Type	PRBS_N	
UniversalFiber_Attenuation	(0.2e-3) (0.5e-3)	dB/m
UniversalFiber_Dispersion	(17e-6) (-100e-6)	s/m^2
UniversalFiber_DispersionSlope	(57.8) (-340)	s/m^3
UniversalFiber_NonLinearIndex	(2.6e-20) (3.7e-20)	m^2/W
UniversalFiber_SBSBandwidth	100e6	Hz
UniversalFiber_SBSStokesShift	1.084e10	Hz
UniversalFiber_SBSGain	5.0e-11	m/W
UniversalFiber_SBSAdj.Factor	0.5	
UniversalFiber_RamanScattering	No	
UniversalFiber_CoreArea	(80.0e-12) (19.0e-12)	m^2
FuncSine_Amplitude	0.15	

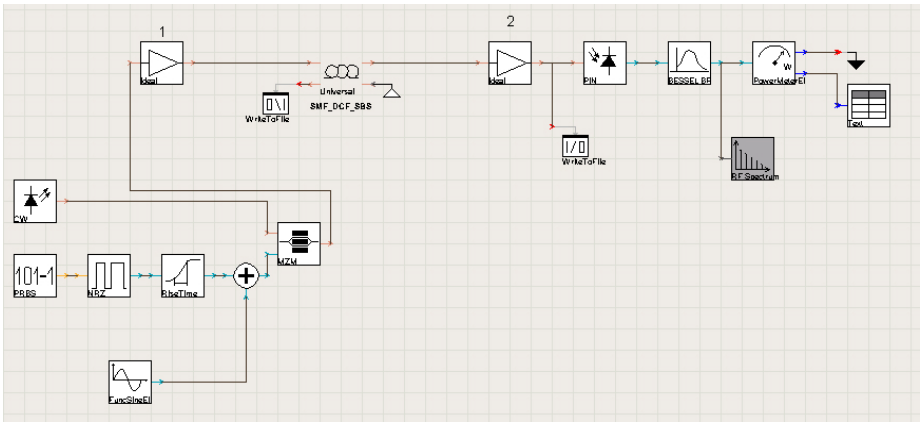

Figure B.2: VPI schematic used in Chapter 6 for power optimization demonstrations.

B.4 VPI receiver model

Figure B.3 shows the general receiver configuration used in VPI simulations to estimate BER. The signal is loaded from a file, amplified, optically filtered and sent to the photo diode having a responsitivity of 1.0 and a thermal noise figure of $10.0 \cdot 10^{-12}$ A/$\sqrt{\text{Hz}}$. The Bessel filter acts as a lowpass filter with a typical bandwidth of 75% of the signal bandwidth. The BER estimation is performed using the *BER_Stochastic_NoRef* module using the Gauss estimation method. Details on the Gauss estimation method can be found in the VPI modules manual.

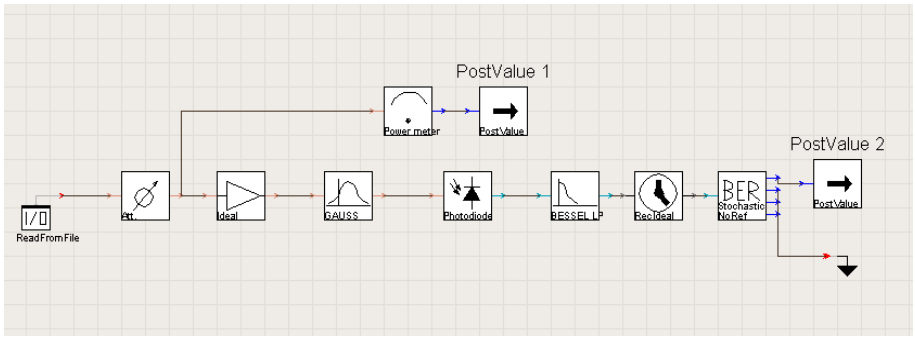

Figure B.3: Receiver schematic used for BER estimations.

Appendix C

SPM/XPM and OSNR measurements

This appendix describes some results related to section 5.2.2 in Chapter 5. These investigations seek to clarify the influence of SPM and XPM spectral broadening on OSNR evaluations. The setup used in the experiments is the same as used for the OSNR measurement method proposed in section 5.2.3. It is depicted in Figure C.1.

C.1 Experimental results - Optical input power varied

In these experiments the method is investigated further to clarify if nonlinearities contributes to changes in the OSNR/OSBR. This is done by varying the input power to the transmission fiber while keeping the amount of added ASE noise constant. Both the combination of SMF + DCF (post-compensation) as well as DCF + SMF (pre-compensation) was used. The first case described deals with SMF + DCF. All experiments are otherwise unchanged such that 10 Gb/s NRZ, and three channels with a spacing of 50 GHz are used.

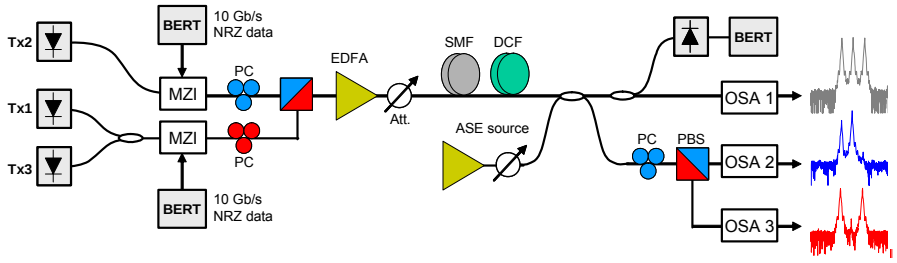

Figure C.1: Experimental setup used to demonstrate OSNR monitoring using polarization interleaving in dense WDM systems.

C.1.1 Post-compensation (SMF + DCF)

Figure C.2a) shows the OSNR measured via the conventional interpolation method (OSA1) as well as the sensitivity of the center channel referred to as the probe channel. As the amount of ASE added to the system is kept constant, the OSNR should increase linearly along with the increasing input power but this is not the case due to the side bands from neighboring channels.

In Figure C.2b), however, the OSNR is evaluated by taking the ratio of the out-of-band noise to the signal power for resolution bandwidths of 0.1 nm and 0.01 nm. As for the 0.01 nm curve, a better linear dependence is observed due to the fact that this bandwidth is less sensitive to FWM products. Both curves breaks off at high input powers, which is attributed to FWM and possibly also Brillouin scattering depleting the carrier. As OSNR in C.2b) is generated via the out-of-band noise level the OSNR evaluation is more accurate than the one represented in C.2a).

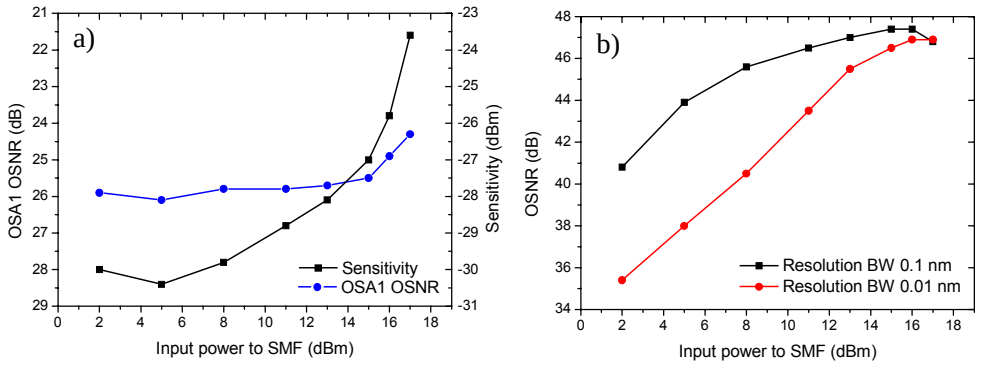

Figure C.2: a) OSNR measured via the conventional interpolation method (OSA1) versus optical input power to the fiber. b) The true OSNR, calculated using the out-of-band noise level, versus optical input power.

Again considering Figure C.2a) this method of OSNR evaluation is not suit-

able as the OSNR changes are barely visible and the curve provides little valuable information. This is due to the overlapping channel spectra as also seen in Figure 5.11 (refer to Chapter 5 page 71).

$$OSBR = P_{Ch} - OSA3\ [dB] \tag{C.1}$$

Similar to the case where the ASE was varied, an OSBR evaluation can be made via the data generated from OSA3. OSBR as a function of input power to the SMF can be seen in Figure C.3. Also shown in the figure is the receiver sensitivity as a function of input power. Refer to Equation C.1 for a definition of the OSBR.

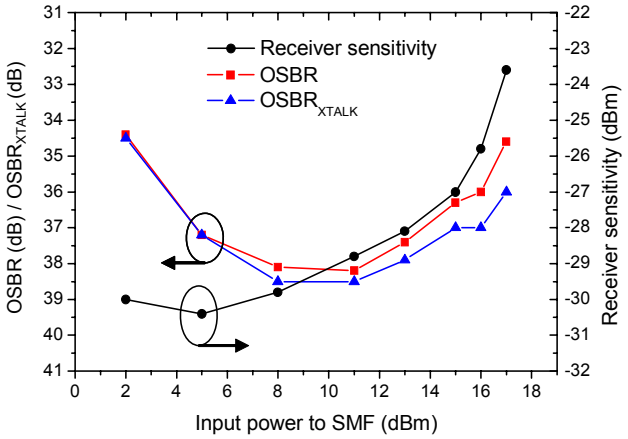

Figure C.3: The $OSNR_{XTALK}$ and OSBR curves are shown together with the receiver sensitivity versus input power to the SMF. The $OSBR_{XTALK}$ curve has been scaled vertically for illustration purposes. This has no practical meaning.

Various things can be seen from Figure C.3. First of all, the receiver sensitivity is evolving as expected. As the input power rises, various nonlinearities take effect, and the sensitivity rises. Equally the sensitivity is expected to rise when the input power drops enough for the ASE noise to limit the signal quality. In this experiment, the input power does not become low enough though to display this behavior well.

In this context, it is more interesting to study the OSBR curve as a rather good correlation with the receiver sensitivity is observed at input powers above 10 dBm. At low input powers the OSBR increases towards a maximum at around 10 dBm input power and does not follow the behavior of the receiver sensitivity. The increase in OSBR when going from low to higher input powers is expected as the probe channel power increases. Note the reverse OSBR-axis. The drop in OSBR at higher input powers can be explained through several nonlinear effects. First of all, the probe channel power will not continue to increase linearly with the input

power as FWM and SBS will consume power from the probe channel. Further more, the OSA3 power will increase relatively more at high input powers due to spectral broadening, which has been illustrated by plotting the $\mathrm{OSBR_{XTALK}}$ curve also. $\mathrm{OSBR_{XTALK}}$ corresponds to the OSBR measurements excluding the carrier depleting effects of FWM and SBS and thus reveal the effect of spectral broadening or spectral crosstalk at high input powers.

$$\mathrm{OSBR_{XTALK}} = \mathrm{OSBR} + P_{loss} = \mathrm{OSBR} + (P_{in} - P_{Ch}) = P_{Ch} - OSA3 + P_{in} - P_{Ch} = P_{Ch} - OSA3$$

where P_{loss} is the loss caused by nonlinear scattering (SBS) and FWM, and P_{in} is the input power of the probe channel to the fiber. The $\mathrm{OSBR_{XTALK}}$, but only the

The differences between the OSBR and the $\mathrm{OSBR_{XTALK}}$ curves[1] in Figure C.3 is due to FWM and SBS, and the drop in $\mathrm{OSBR_{XTALK}}$ at powers above 11 dBm are thus identified to be an SPM and XPM induced crosstalk drop. Figure C.3 therefore concludes that nonlinear effects influencing the signal quality also has an influence on the OSBR. This explains the rather good correlation with the receiver sensitivity seen in the figure. The cause of signal degradation above 6-7 dBm is attributed SPM and XPM.

In these experiments, a resolution bandwidth of 0.1 nm was used when collecting OSA3 data. Using another resolution bandwidth will create different results although similar in nature.

C.1.2 Pre-compensation (DCF + SMF)

The same experiments were performed using a pre-compensation map (DCF + SMF) instead. Placing the DCF before the SMF will result in a different situation as the high input power will now be incident to the DCF, which is a fiber type with a higher nonlinear index. The nonlinear coefficient of the DCF is approximately 7.0 $\mathrm{W^{-1}km^{-1}}$ whereas the value for SMF is around 1.3 $\mathrm{W^{-1}km^{-1}}$.

The results of the measurements are seen in Figure C.4. It can be seen how the receiver sensitivity curve have changed due to the fact that the DCF is now placed prior to the SMF in the span. The minimum located at approximately 18 dBm input power corresponds to optimal signal quality.

At a first glace one notices that the correlation seen between the OSBR and the sensitivity in Figure C.3 is not present here. However, some valuable and interesting information can be gathered from this figure. As before, the OSBR

[1] The $\mathrm{OSBR_{XTALK}}$ curve has been scaled vertically for illustration purposes and has no practical meaning.

curve includes the effects of both FWM and SBS channel power loss as well as spectral broadening effects due to SPM and XPM and the $OSBR_{XTALK}$ curve only includes the SPM and XPM effects leading to spectral crosstalk.

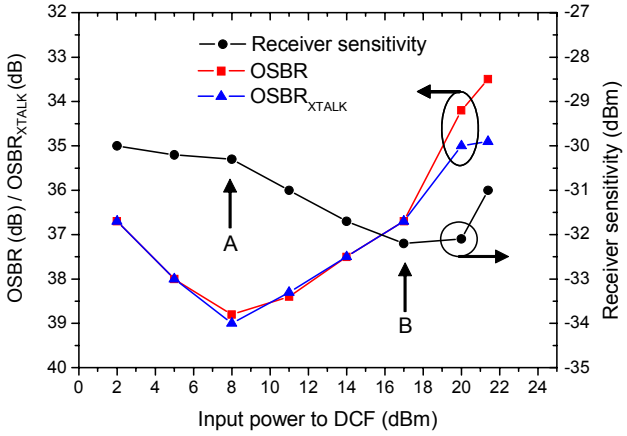

Figure C.4: The $OSNR_{XTALK}$ and OSBR curves are shown together with the receiver sensitivity versus input power to the DMF. The $OSBR_{XTALK}$ curve has been scaled vertically for illustration purposes. This has no practical meaning.

Two points have been marked in Figure C.4, "A" and "B". At point "A" the is a change in both receiver sensitivity and the OSBR curves. The sensitivity starts to improve at this point, which is attributed to SPM - dispersion interactions improving the signal quality. This effect is also discussed in Chapter 6. At this input power of 8 dBm, a break is also observed in the OSBR curves, which could further indicate that spectral broadening effects are initiated. The break however is also practically related to the noise floor issues and the resolution bandwidth in the OSA, so it cannot be attributed to spectral broadening alone. Referring back to Figure C.3, this break occurs at a higher input power. This indicates that the spectral broadening has some effect if the later break can be attributed the less nonlinear SMF fiber.

Around point "B", the optimum signal quality is reached and above 19-20 dBm the receiver sensitivity rises. At this point "B", the channel depleting effects such as SBS and FWM also sets in. These results confirm that SPM will interact constructively with the signal in the normal dispersion regime, and furthermore indicate that SBS and FWM carrier depletion are co-responsible for signal degrading above 19 dBm input power. Via spectral investigations, FWM is considered the main contributor to carrier depletion in this 10 Gb/s NRZ system. The role of SBS as a significant signal detrimental effect in a single channel 10 Gb/s NRZ system is discussed in Chapter 6.

The OSBR curves has explained some of the behaviors seen in the signal

sensitivity curve as the input power is varied. Optical-signal-to-noise-ratio measurements are less relevant at these high input powers, however, the OSBR finds new applications in explaining the nonlinear effects interacting with the 10 Gb/s data signal.

Appendix D

Ph.D. publications

1. M. N. Petersen, Z. Pan, S. Lee, S. A. Havstad, and A. E. Willner: “On-line chromatic dispersion monitoring and compensation using a single in-band subcarrier tone”, Photonic Technology Letters, 2002.

2. M. L. Nielsen, M. N. Petersen, M. Nord and Dagens, B: ”Compact all-optical parity calculator based on a single all-active Mach Zhender interferometer”. Optical Fiber Communications Conference OFC, pp. 274-275, 2003.

3. Nielsen, M.L.; Nord, M.; Petersen, M.N.; Dagens, B.; Labrousse, A.; Brenot, R.; Martin, B.; Squedin, S.; Renaud, M.: “40 Gbit/s standard-mode wavelength conversion in all-active MZI with very fast response”, Electronics Letters, Vol.39 Issue.4, pp. 385-386, 2003.

4. M. L. Nielsen, J. D. Buron, M. Nord and M. N. Petersen, "SOA-based Functional Devices for Future Optical Networks", in Tech. Digest SSDM 2003, paper F-9-1 (invited), Tokyo, Japan, 2003.

5. Martin Nordal Petersen and Mikkel Hasse Olesen: “10 Gb/s Non-Regenerated Ethernet Field Trial over 525-km Dark Fiber”, OECC/COIN Conference, 2004.

6. Martin N. Petersen and Mads L. Nielsen: “Experimental and Theoretical Demonstration of Launch Power Optimization using a Subcarrier Fibre Non-linearity Monitor”, Electronic Letters, Vol. 43 No. 10, 2004.

7. Martin N. Petersen, Mikkel H. Olesen and Michael S. Berger: “10 Gb/s Non-Regenerated Pure Ethernet Field Trials over Dark Fibers”, ONDM Conference in Tokyo, 2005.

8. Martin Nordal Petersen, Mads Lønstrup Nielsen and Jakob Buron: "Field-Trial Demonstration of Span Launch Power Optimization using a Subcarrier Non-Linearity Monitor", OFC Conference, 2005.

9. Martin N. Petersen and Mads L. Nielsen: “Signal Quality Monitoring of 40 Gb/s Dispersion Degraded RZ and NRZ Data”, OECC Conference in Seoul, 2005.

10. Martin Nordal Petersen Torger Tokle, "Accurate OSNR Monitoring and Nonlinear Analysis of Signals in Dense WDM Systems Utilizing Polarization Interleaving of Adjacent Channels", ECOC conference, 2006.

11. M.N. Petersen, K. Schulze and F. Ramos, "Dispersion monitoring in all-optical networks using wavelength conversion based on FWM", Electronic Letters, Vol. 43 No. 10, 2006.

12. Martin Nordal Petersen, "Performance Monitoring in the Next Generation of Optical Networks", Photonics in Switching conference (PS’2006), 2006.

References

[1] Govind P. Agrawal, *Fiber-Optic Communication Systems*, John Wiley and Sons, Inc., second edition edition, 1997.

[2] Lawrence G. Roberts, "Internet growth trends," .

[3] J. Devaney, "The great telecom crash: Where did it all go wrong?," *FibreSystems Europe*, pp. 40–42, September 2002.

[4] Paul Starr, "The great telecom implosion," *The Americal Prospect*, October 2002.

[5] Phone Plus Magazine, "Final ASCENT show spurs new optimism," *http://www.phoneplusmag.com/articles/411feat01.html*, vol. http://www.phoneplusmag.com/articles/411feat01.html, 2004.

[6] Mike Sexton and Andy Reid, *Broadband Networking: ATM, SDH and SONET*, Artech House Inc., 1997.

[7] Meghan Fuller, "Next generation sonet/sdh stays the course," *Lightwave*, vol. 21, no. 12, pp. 11+16, 2004.

[8] I. Froroth, K. Nygard-Skalman, and H. Eklund, "Next generation public access: Ethernet over fiber," *ISSLS 2002 - International Symposium on Services and Local Access*, pp. 148–57, 2002.

[9] O. Leclerc, B. Lavigne, E. Balmefrezol, P. Brindel, L. Pierre, D. Rouvillain, and F. Seguineau, "All-optical signal regeneration: from first principles to a 40 gbit/s system demonstration," *Comptes Rendus Physique*, vol. 4, no. 1, pp. 163–173, 2003.

[10] Gail Robinson and Margaret Quan, "Optical MEMS viewed as bandwidth solution," *EE Times*, 2001.

[11] J.T.W. Yeow and S.S. Abdallah, "Novel mems l-switching matrix optical cross-connect architecture: design and analysis-optimal and staircase-switching algorithms," *Lightwave Technology, Journal of*, vol. 23, no. 10, pp. 2877–2892, 2005.

[12] ITU, "G. 774.1 synchronous digital hierarchy (SDH) - bidirectional performance monitoring for the network element view," *ITU Recommendations*, 2002.

[13] P. Vorreau, D.C. Kilper, and J. Leuthold, "Optical noise and dispersion monitoring with soa-based optical 2r regenerator," *Photonics Technology Letters, IEEE*, vol. 17, no. 1, pp. 244–246, 2005.

[14] S.M.R. MotaghianNezam, Y.-W. Song, C. Yu, J.E. McGeehan, A.B. Sahin, and A.E. Willner, "First-order pmd monitoring for nrz data using rf clock regeneration techniques," *Lightwave Technology, Journal of*, vol. 22, no. 4, pp. 1086–1093, 2004.

[15] C.H Kim J.H Lee, D.K. Jung and Y.C. Chung, "OSNR monitoring technique using polarization-nulling method," *IEEE Phot. Tech. Lett.*, vol. Vol. 13, No. 1, pp. 88–90, 2001.

[16] E. Desurvire, M. Zirngibl, H.M. Presby, and D. DiGiovanni, "Characterization and modeling of amplified spontaneous emission in unsaturated erbium-doped fiber amplifiers," *IEEE Photonics Technology Letters*, vol. 3, no. 2, pp. 127 –129, 1991.

[17] G. Talli and M.J. Adams, "Amplified spontaneous emission in semiconductor optical amplifiers: modelling and experiments," *Optics Communications*, vol. 218, no. 1-3, pp. 161–166, 2003.

[18] W.R. Leeb M. Rasztovits-Wiech, M. Danner, "Optical signal-to-noise ratio measurement in WDM networks using polarization extinction," *ECOC 1998*, pp. 549–550, 1998.

[19] M. Karlson M. Petersson, H. Sunnerud and B.-E. Olsson, "Performance monitoring in optical networks using stokes parameter," *IEEE Phot. Tech. Lett.*, vol. Vol.16, No.2, pp. 686–688, 2004.

[20] Lars Gruner-Nielsen, Stig Nissen Knudsen, Bent Edvold, Torben Veng, Dorte Magnussen, C. Christian Larsen, and Hans Damsgaard, "Dispersion compensating fibers," *Optical Fiber Technology*, vol. 6, no. 2, pp. 164–180, 2000.

[21] M. N. Petersen, *Dispersion Monitoring*, Master Thesis carried out at the Technical University of Denmark, 2001.

[22] W.H. Hatton and M. Nishimura, "Temperature dependence of chromatic dispersion in single mode fibers," *Journal of Lightwave Technology*, vol. LT-4, no. 10, pp. 1552–5, 1986.

[23] M.E. Lines, "Physical origin of the temperature dependence of chromatic dispersion in fused silica," *Journal of Applied Physics*, vol. 73, no. 5, pp. 2075–2079, 1993.

[24] G. Ghosh, M. Endo, and T. Iwasaki, "Temperature-dependent sellmeier coefficients and chromatic dispersions for some optical fiber glasses," *Lightwave Technology, Journal of*, vol. 12, no. 8, pp. 1338 –1342, 1994.

[25] J.-X. Cai, K.-M. Feng, A.E. Willner, V. Grubsky, D.S. Starodubov, and J. Feinberg, "Simultaneous tunable dispersion compensation of many wdm channels using a sampled nonlinearly chirped fiber bragg grating," *IEEE Photonics Technology Letters*, vol. 11, no. 11, pp. 1455 –1457, 1999.

[26] L.M. Lunardi, D.J. Moss, S. Chandrasekhar, L.L. Buhl, M. Lamont, S. McLaughlin, G. Randall, P. Colbourne, S. Kiran, and C.A. Hulse, "Tunable dispersion compensation at 40-gb/s using a multicavity etalon all-pass filter with nrz, rz, and cs-rz modulation," *Lightwave Technology, Journal of*, vol. 20, no. 12, pp. 2136–2144, 2002.

[27] A. Sano, Y. Miyamoto, S. Kuwahara, and H. Toba, "Adaptive dispersion equalization by monitoring relative phase shift between spacing-fixed wdm signals," *Lightwave Technology, Journal of*, vol. 19, no. 3, pp. 336 –344, 2001.

[28] T.E. Dimmick, G. Rossi, and D.J. Blumenthal, "Optical dispersion monitoring technique using double sideband subcarriers," *IEEE Photonics Technology Letters*, vol. 12, no. 7, pp. 900 –902, 2000.

[29] S.A. Havstad, A.B. Sahin, O.H. Adamczyk, Y. Xie, and A.E. Willner, "Distance-independent rf fading compensation using a tunable nonlinearly-chirped fbg in a phase diversity configuration," *Optical Fiber Communication Conference, 2000*, vol. 2, pp. 323 –325 vol.2, 2000.

[30] M.N. Petersen, Z. Pan, S. Lee, S.A. Havstad, and A.E. Willner, "Online chromatic dispersion monitoring and compensation using a single inband subcarrier tone," *IEEE Photonics Technology Letters*, vol. 14, no. 4, pp. 570 –572, 2002.

[31] A. Sano, Y. Miyamoto, S. Kuwahara, and H. Toba, "Adaptive dispersion equalization by monitoring relative phase shift between spacing-fixed wdm signals," *Lightwave Technology, Journal of*, vol. 19, no. 3, pp. 336 –344, 2001.

[32] A. Sano, T. Kataoka, M. Tomizawa, K. Hagimoto, K. Sato, K. Wakita, and K. Kato, "Automatic dispersion equalization by monitoring extracted-clock power level in a 40-gbit/s, 200-km transmission line," *Optical Communication, 1996. ECOC '96. 22nd European Conference on*, vol. 2, pp. 207–210 vol.2, 1996.

[33] Z. Pan, Q. Yu, Y. Xie, S.A. Havstad, A.E. Willner, D.S. Starodubov, and J. Feinberg, "Chromatic dispersion monitoring and automated compensation for nrz and rz data using clock regeneration and fading without adding signaling," *Optical Fiber Communication Conference and Exhibit, 2001. OFC 2001*, vol. 3, pp. wh5–1, 2001.

[34] Carsten J. Videcrantz, "Chromatic dispersion: Not an issue for cost - effective 40gbit/s transmission," *EE Times*, March 2002.

[35] Thomas Tanggaard Larsen, *Polarization-Mode Dispersion*, Technical University of Denmark, COM Centre, 2002.

[36] Luo Rui, Ning Ti-gang, Li Tang-jun, Cai Li-bo, Qiu Feng, Jian Shui-sheng, and Xu Ang-jing, "Compensating the first-order pmd by using a novel tunable compensator," *Communications, Circuits and Systems, 2005. Proceedings. 2005 International Conference on*, vol. 1, pp. 561–564 Vol. 1, 2005.

[37] L.E. Nelson, H. Kogelnik, and K.J. Winzer, "Polarization mode dispersion and its impact on high bit-rate, fiber-optic communication systems," *Lasers and Electro-Optics, 2004. (CLEO). Conference on*, vol. vol.2, pp. 3 pp. vol.2, 2004.

[38] Bojun Yang, Minyu Yao, Hongming Zhang, Lin Chen, Tiecheng Yuan, Bin Wu, Na Zhang, Jianzhong Zhang, Yu Shen, Guangtao Zhou, Li Yu, Lixia Xi, and Xiaoguang Zhang, "Two-stage adaptive pmd compensation in 40 gb/s otdm optical communication system using pso algorithm," *Optical and Quantum Electronics*, vol. 36, no. 12, pp. 1089–1104, 2004.

[39] L.K. Oxenlowe, K.S. Berg, A.T. Clausen, J. Seoane, A.I. Siahlo, P. Jeppesen, M. Schmidt, M. Schilling, and Q. Le, "Specialty fibers for 160, 320 and 640 gb/s signal processing," *Lasers and Electro-Optics, 2004. (CLEO). Conference on*, vol. vol.2, pp. 2 pp. vol.2, 2004.

[40] M. Nissov, C.R. Davidson, K. Rottwitt, R. Menges, P.C. Corbett, D. Innis, and N.S. Bergano, "100 gb/s (10/spl times/10 gb/s) wdm transmission over 7200 km using distributed raman amplification," *Integrated Optics and Optical Fibre Communications, 11th International Conference on, and 23rd European Conference on Optical Communications (Conf. Publ. No.: 448)*, vol. 5, pp. 9 –12 vol.5, 1997.

[41] M. Onishi, T. Okuno, T. Kashiwada, S. Ishikawa, N. Akasaka, and M. Nishimura, "Highly nonlinear dispersion-shifted fibers and their application to broadband wavelength converter," *Optical Fiber Technology: Materials, Devices, and Systems*, vol. 4, no. 2, pp. 204–214, 1998.

[42] Govind P. Agrawal, *Nonlinear Fiber Optics*, Academic Press - Optics and Photonics, third edition, 2001.

[43] C. Peucheret, N. Hanik, R. Freund, L. Molle, and P. Jeppesen, "Optimization of pre- and post-dispersion compensation schemes for 10-gbits/s nrz links using standard and dispersion compensating fibers," *IEEE Photonics Technology Letters*, vol. 12, no. 8, pp. 992 –994, 2000.

[44] D.C. Kilper, A. Azarov, W. Weingartner, and P. Vorreau, "Q-factor monitoring for fault management applications," *Optical Fiber Communication Conference, 2004. OFC 2004*, vol. vol.2, pp. 3 pp. vol.2, 2004.

[45] I. Shake, H. Takara, and S. Kawanishi, "Simple q factor monitoring for ber estimation using opened eye diagrams captured by high-speed asynchronous electrooptical sampling," *IEEE Photonics Technology Letters*, vol. 15, no. 4, pp. 620–622, 2003.

[46] H. J. Thiele, R. I. Killey, and P. Bayvel, "Investigation of cross-phase modulation-induced transmission penalties using the pump-probe technique," *Optical Fiber Technology*, vol. 8, no. 1, pp. 71–81, 2002.

[47] C. Furst, J.-P. Elbers, C. Scheerer, and C. Glingener, "Limitations of dispersion-managed dwdm systems due to cross-phase modulation," *Lasers and Electro-Optics Society 2000 Annual Meeting. LEOS 2000. 13th Annual Meeting. IEEE*, vol. 1, pp. 23–24 vol.1, 2000.

[48] S. Schollmann, J. Leibrich, C. Wree, and W. Rosenkranz, "Impact of srs-induced crosstalk for different modulation formats in wdm systems," *Optical Fiber Communication Conference, 2004. OFC 2004*, vol. vol.2, pp. 3 pp. vol.2, 2004.

[49] S. Tariq and M.K. Dhodhi, "Limits of dwdm communication networks due to stimulated raman scattering and optical amplifier noise," *Microelectronics, 1999. ICM '99. The Eleventh International Conference on*, pp. 189–191, 1999.

[50] T. Tanaka and T. Naito, "Raman-amplifier-based submarine transmission systems," *Optical Fiber Technology*, vol. 8, no. 3, pp. 195–209, 2002.

[51] D.R. Hjelme, J. Eide, and B.J. Slagsvold, "Four-wave mixing efficiency in installed dispersion-shifted fibers: effects of zero-dispersion wavelength variations," *Optical Fiber Commuunication Conference and Exhibit, 1998. OFC '98., Technical Digest*, pp. 209 –210, 1998.

[52] M. Eiselt, "Limits on wdm systems due to four-wave mixing: a statistical approach," *Lightwave Technology, Journal of*, vol. 17, no. 11, pp. 2261 –2267, 1999.

[53] R. W Boyd, *Nonlinear Optics*, vol. Chapter 8, Academic Press, San Diego, 1992.

[54] Jinye Zhang and M.R. Phillips, "Cancellation of intensity noise caused by stimulated brillouin scattering in an optical fiber transmission system," *Optical Fiber Communication Conference, 2005. Technical Digest. OFC/NFOEC*, vol. Vol. 5, pp. 3 pp. Vol. 5, 2005.

[55] H. Yoshinaga, "Influence of stimulated brillouin scattering on nonlinear distortion in scm video transmission," *Electronics Letters*, vol. 29, no. 19, pp. 1707 –1708, 1993.

[56] F.W. Willems, W. Muys, and J.S. Leong, "Simultaneous suppression of stimulated brillouin scattering and interferometric noise in externally modulated lightwave am-scm systems," *IEEE Photonics Technology Letters*, vol. 6, no. 12, pp. 1476 –1478, 1994.

[57] L. Hu, A. Kaszubowska, and L.P. Barry, "Investigation of stimulated brillouin scattering effects in radio-over-fiber distribution systems," *Optics Communications*, vol. 255, no. 4-6, pp. 253–260, 2005.

[58] Takashi Mizuochi, "Recent progress in forward error correction for optical communication systems," *IEICE Transactions on Communications*, vol. E88-B, no. 5, pp. 1934–1946, 2005.

[59] I.S. Reed and G. Solomon, "Polynominal codes over certain finite fields," *SIAM J. Appl. Math*, vol. 8, pp. 300–304, June 1960.

[60] K. Sticht, H.F. Haunstein, M. Lorang, W. Sauer-Greff, and R. Urbansky, "Adaptation of electronic pmd equaliser based on ber estimation derived from fec decoder," *Optical Communication, 2001. ECOC '01. 27th European Conference on*, vol. 3, pp. 454–455, 2001.

[61] M. Rohde, C. Caspar, F. Raub, G. Bramann, H. Louchet, K. Habel, and E.-J. Bachus, "Control modulation technique for client independent optical performance monitoring and transport of channel overhead," *Optical Fiber Communication Conference and Exhibit, 2002. OFC 2002*, vol. 1, pp. 21–22 vol.1, 2002.

[62] J.H. Manton, "On optimal channel identification by use of training sequences and pilot tones," *Signal Processing and its Appications, Sixth International, Symposium on. 2001*, vol. 2, pp. 599–602, 2001.

[63] O. Audouin G. V. Moustakides, F. Cérou and L. Noirie, "Eye diagram reconstruction using asynchronous imperfect sampling, application to BER estimation for fiber-optic communication systems," *11th European Signal Processing Conference (EUSIPCO), Toulouse, III, EURASIP*, pp. 375–378, 2002.

[64] C. Schmidt, C. Schubert, J. Berger, M. Kroh, H.-J. Ehrke, E. Dietrich, C. Borner, R. Ludwig, H.G. Weber, F. Futami, S. Watanabe, and T. Yamamoto, "Optical q-factor monitoring at 160 gb/s using an optical sampling system in an 80 km transmission experiment," *Lasers and Electro-Optics, 2002. CLEO '02. Technical Digest. Summaries of Papers Presented at the*, pp. 579–580 vol.1, 2002.

[65] Pingjin Wen, Hongming Zhang, Mingyu Yao, Hua Wang, and Meng Yan, "Optical performance monitoring based on asynchronous sampling technology," *Optical Transmission, Switching, and Subsystems II and Proceedings of SPIE - The International Society for Optical Engineering*, vol. 5625, pp. 1001–1003, 2005.

[66] I. Shake, H. Takara, K. Uchiyama, and Y. Yamabayashi, "Quality monitoring of optical signals influenced by chromatic dispersion in a transmission fiber using averaged q-factor evaluation," *IEEE Photonics Technology Letters*, vol. 13, no. 4, pp. 385 –387, 2001.

[67] I. Shake, W. Takara, S. Kawanishi, and Y. Yamabayashi, "Optical signal quality monitoring method based on optical sampling," *Electronics Letters*, vol. 34, no. 22, pp. 2152 –2154, 1998.

[68] K. Mueller, N. Hanik, A. Gladisch, H.-M. Foisel, and C. Caspar, "Application of amplitude histograms for quality of service measurements of optical channels and fault identification," *Optical Communication, 1998. 24th European Conference on*, vol. 1, pp. 707 –708 vol.1, 1998.

[69] R. Wiesmann, O. Bleck, and H. Heppner, "Cost effective performance monitoring in wdm systems," *Optical Fiber Communication Conference, 2000*, vol. 2, pp. 171 –173 vol.2, 2000.

[70] M. Govindarajan et Al., "Method for performance monitoring of data tranaparent communications links," United States Patent number US 6,222,877 B1, April 24, 2001.

[71] A.J. Poustie and A.E. Kelly, "All-optical parity checker with bit-differential delay," *Optics Communications*, vol. 162, no. 1-3, pp. 37–43, 1999.

[72] M. Nielsen, M. Petersen, M. Nord, and B. Dagens, "Compact all-optical parity calculator based on a single all-active mach zehnder interferometer with all-soa amplified feedback," *Optical Fiber Communications Conference, 2003. OFC 2003*, pp. 274–275 vol.1, 2003.

[73] M. Pfennigbauer, M.M. Strasser, M. Pauer, and P.J. Winzer, "Dependence of optically preamplified receiver sensitivity on optical and electrical filter bandwidths-measurement and simulation," *IEEE Photonics Technology Letters*, vol. 14, no. 6, pp. 831–833, 2002.

[74] Y. Horikoshi, T. Kobayashi, and Y. Furukawa, "Lifetime of ingaasp-inp and algaas-gaas dh lasers estimated by the point defect generation model," *Japanese Journal of Applied Physics*, vol. 18, no. 12, pp. 2237–44, 1979.

[75] M. Caussanel, P. Signoret, J. Gasiot, O. Gilard, and M. Sotom, "Extrapolation of radiation-induced edfa gain degradation at space dose rate," *Electronics Letters*, vol. 41, no. 4, pp. 168–170, 2005.

[76] K.L. Hall, J.P. Donnelly, S.H. Groves, C.I. Fennelly, R.J. Bailey, and A. Napoleone, "40-gbit/s all-optical circulating shift register with an inverter," *Optics Letters*, vol. 22, no. 19, pp. 1479–81, 1997.

[77] T. Fjelde, D. Wolfson, A. Kloch, C. Janz, A. Coquelin, I. Guillemot, F. Gaborit, F. Poingt, B. Dagens, and M. Renaud, "10 gbit/s all-optical logic or in monolithically integrated interferometric wavelength converter," *Electronics Letters*, vol. 36, no. 9, pp. 813 –815, 2000.

[78] T. Fjelde, D. Wolfson, A. Kloch, B. Dagens, A. Coquelin, I. Guillemot, F. Gaborit, F. Poingt, and M. Renaud, "Demonstration of 20 gbit/s all-optical logic xor in integrated soa-based interferometric wavelength converter," *Electronics Letters*, vol. 36, no. 22, pp. 1863 –1864, 2000.

[79] D. Wolfson and K.E. Stubkjaer, "Bit error rate assessment of 20 gbit/s all-optical wavelength conversion for co- and counter-directional coupling scheme," *Electronics Letters*, vol. 34, no. 23, pp. 2259 –2261, 1998.

[80] M.L. Nielsen, M. Nord, M.N. Petersen, B. Dagens, A. Labrousse, R. Brenot, B. Martin, S. Squedin, and M. Renaud, "40 gbit/s standard-mode wavelength conversion in all-active mzi with very fast response," *Electronics Letters*, vol. 39, no. 4, pp. 385–386, 2003.

[81] M. L. Nielsen, *Experimental and Theoretical Inverstigation of Semiconductor Optical Amplifier (SOA) Based All-Optical Switches*, Ph.D. thesis, Technical University of Denmark. Research Centre COM, 2004, pp. 188-195.

[82] C. Dimopoulos and D. Simeonidou, "Optical-power transients in long-haul wdm trunk-and-branch networks," *Optoelectronics, IEE Proceedings-*, vol. 147, no. 5, pp. 329 –334, 2000.

[83] M. Karasek and J.C. van der Plaats, "Modelling of a pump-power-loss-controlled gain-locking system for edfa application in wdm transmission systems," *Optoelectronics, IEE Proceedings-*, vol. 145, no. 4, pp. 205 –210, 1998.

[84] P.S. Westbrook, B.J. Eggleton, G. Raybon, S. Hunsche, and Tsing Hua Her, "Measurement of residual chromatic dispersion of a 40-gb/s rz signal via spectral broadening," *IEEE Photonics Technology Letters*, vol. 14, no. 3, pp. 346–348, 2002.

[85] D.C. Kilper and W. Weingartner, "Monitoring optical network performance degradation due to amplifier noise," *IEEE Journ. of Lightwave Tehn.*, vol. Vol. 21, No. 5, pp. 1171–1178, 2003.

[86] T. Ono and Y. Yano, "Key technologies for terabit/second wdm systems with high spectral efficiency of over 1 bit/s/hz," *Quantum Electronics, IEEE Journal of*, vol. 34, no. 11, pp. 2080 –2088, 1998.

[87] D. vandenBorne, S.L. Jansen, S. Calabro, N.E. Hecker-Denschlag, G.D. Khoe, and H. deWaardt, "Reduction of nonlinear penalties through polarization interleaving in 10 gb/s polarization-multiplexed transmission," *Photonics Technology Letters, IEEE*, vol. 17, no. 6, pp. 1337–1339, 2005.

[88] K. Inoue, "Arrangement of orthogonal polarized signals for suppressing fiber four-wave mixing in optical multichannel transmission systems," *IEEE Photonics Technology Letters*, vol. 3, no. 6, pp. 560 –563, 1991.

[89] C. Poole Et. al, "Polarization dispersion and principal states in a 147-km undersea lightwave cable," *IEEE Journ. of Lightwave Tech.*, vol. 6 (7), pp. 1185–1190, 1988.

[90] G. Mohs, L. Didier Coelho, E. Gottwald, C. Scheerer, C. Furst, A. Faerbert, and C. Glingener, "Optimized inline dispersion compensation for self-phase modulation limited transmission," *Conference Proceedings. OECC/IOOC 2001 Conference. Incorporating ACOFT*, pp. 262–3, 2001.

[91] B.C. Collings and L. Boivin, "Nonlinear polarization evolution induced by cross-phase modulation and its impact on transmission systems," *IEEE Photonics Technology Letters*, vol. 12, no. 11, pp. 1582 –1584, 2000.

[92] F.S. Yang, M.E. Marhic, and L.G. Kazovsky, "Nonlinear crosstalk and sbs reduction by carrier suppression in an analog wdm optical communication system," *Optical Fiber Communication Conference, 1999, and the International Conference on Integrated Optics and Optical Fiber Communication. OFC/IOOC '99. Technical Digest*, pp. 280 –282 vol.2, 1999.

[93] L.E. Adams, G. Nykolak, T. Tanbun-Ek, A.J. Stentz, A.M. Sergent, P.F. Jr. Sciortino, and L. Eskildsen, "Sbs suppression using a multichannel tunable laser with data-encoding capability," *Fiber and Integrated Optics*, vol. 17, no. 4, pp. 311–315, 1998.

[94] A. Sano, Y. Miyamoto, T. Kataoka, H. Kawakami, and K. Hagimoto, "10 gbit/s, 300 km repeaterless transmission with sbs suppression by the use of the rz format," *Electronics Letters*, vol. 30, no. 20, pp. 1694 –1695, 1994.

[95] B. Dagens, A. Martinez, D. Make, O. Le Gouezigou, J.-G. Provost, V. Sallet, K. Merghem, J.-C. Harmand, A. Ramdane, and B. Thedrez, "Floor free 10-gb/s transmission with directly modulated gainnas-gaas 1.35-/spl mu/m laser for metropolitan applications," *Photonics Technology Letters, IEEE*, vol. 17, no. 5, pp. 971–973, 2005.

[96] Daniel Bar-Lev et Al., "Introduction to circuit emulation services over ethernet," Available through www.metroethernetforum.org, 2004.

[97] Metro Ethernet Forum, "Technical specification MEF 2, requirements and framework for ethernet services protection in MENs," Available through www.metroethernetforum.org, 2004.

[98] Jeff Caruso, "10g ethernet wans?," *Network World*, vol. 16, no. 33, pp. 1–2, 1999.

[99] Rod Wilson, "10 gige: A new service provider solution," *Telecommunications*, vol. 34, no. 5, pp. 63–64, 2000.

[100] Metro Ethernet Forum, "Comparison to legacy SONET/SDH MANs for metro data service providers," Available through www.metroethernetforum.org, 2003.

[101] Bill St. Arnaud, Erik Radius, Catalin Meirosu, Piotr Golonka, Wade Hong, René Hatem, and Bob Dobinson, "Transatlantic native 10 gigabit ethernet experiments: Connecting geneva to ottawa," *Lecture Notes in Computer Science*, vol. 3079, pp. 108–119, 2004.

[102] Wu-Chun Feng et Al., "Optimizing 10-gigabit ethernet for networks ofWorkstations, clusters, and grids: A case study," Available through www.sc-conference.org, 2003.

[103] "IEEE computer society IEEE standard 802.3ae," .

[104] Dirceu Cavendish, "Operation, administration, and maintenance of ethernet services in wide area networks," *IEEE Commmunication Magazine*, vol. 42, no. 3, pp. 72–79, 2004.

[105] Kenji Kawai, Kazuhiko Terada, Osamu Ishida, and Haruhiko Ichino, "Genie: Gigabit ethernet network interface extension to wan," *NTT R and D*, vol. 51, no. 5, pp. 59–73, 2002.

[106] "The metro ethernet forum," Available through www.metroethernetforum.org.

[107] "IEEE computer society," IEEE standard 802.17 and www.rpralliance.org.

[108] Taiji Sakamoto et Al., "Intergrated fully-native ethernet ring for optical acces networks," Proceedings of OptoElectronics and Communications Conference (OECC 2005), 2005, pp. 374–375.

[109] Ziwen Lian, Wen-De Zheng, S. Kumar Bose, and Yixin Wang, "Resilient ethernet ring for metropolitan area networks," *Communications Systems, 2004. ICCS 2004. The Ninth International Conference on*, pp. 316–320, 2004.

[110] "CERN homepage," Available through www.cern.ch.

[111] "The danish GRID computing centre," Available through www.dcgc.dk/10ge.

[112] H. H. Happe and B. Vinter, "A distributed shared memory experiment using a dedicated gigabit wide area network," *Proceedings of Parallel and Distributed Processing Techniques and Applications*, pp. 829–835, 2004.

[113] Y. Liu et al, ," National Fiber Optic Eng. Conference (NFOEC), 1998.

[114] R.J. Nuyts, Y.K. Park, and P. Gallion, "Performance improvement of 10 gb/s standard fiber transmission systems by using the spm effect in the dispersion compensating fiber," *IEEE Photonics Technology Letters*, vol. 8, no. 10, pp. 1406 –1408, 1996.

[115] Lutz Rapp, "Improved performance of wdm systems by partitioned dispersion compensation," *Journal of Optical Communications*, vol. 21, no. 6, pp. 213–219, 2000.

List of Acronyms

3R - reamplification, retiming and reshaping
AIS - alarm indication signal
APS - automatic protection switching
ASE - amplified spontaneous emission
ASM - analog symbol monitoring
ATM - asynchronous transfer mode
BER - bit error rate
BERT - bit error rate test set
BIP-n - bit interleaved parity number
BIST - built-in self test
CATV - cable TV
CESoE - circuit emulation services over Ethernet
CoS - classes of service
CRC - cyclic redundancy check
DCF - dispersion compensating fiber
DGD - differential group delay
DOP - degree of polarization
DQPSK - differential quadrature phase shift keying
EDFA - erbium doped fiber amplifier
EoF - Ethernet over fiber
ESA - electrical spectrum analyzer
FEC - forward error correction
FWM - four wave mixing
GRID - global resource information database
GVD - group velocity dispersion
HDTV - high definition TV
HNLF - highly nonlinear fiber
IPTV - Internet protocol TV
ISP - Internet service provider
LAN - local area network

LOS - loss of signal
MAC - machine address code
MAN - metro area network
MEF - Metro Ethernet Forum
MEMS - micro electro-mechanical systems
MPLS - multi protocol label switching
MZ - Mach-Zehnder
MZI - Mach-Zehnder interferometer
NIC - network interface card
NRZ - non return to zero
NZDSF - nonzero dispersion shifted fiber
OAM - operations, administration & maintenance
O-E-O - optical-electrical-optical
OSA - optical spectrum analyzer
OSBR - optical signal to background ratio
OSNR - optical signal to noise ratio
OTN - optical transport network
PBS - polarization beam splitter
PC - polarization control
PDH - plesiochronous digital hierarchy
PDL - polarization dependent loss
PM-AM - phase modulation to amplitude modulation
PMD - polarization mode dispersion
PPG - pulse pattern generator
PRBS - pseudo random bit sequence
QoS - quality of service
RAM - random access memory
RF - radio frequency
RMS - root mean square
RPR - resilient packet rings
RZ - return to zero
SBS - stimulated Brillouin scattering
SDH - synchronous digital hierarchy
SMF - single mode fiber
SNR - signal to noise ratio
SOA - semiconductor optical amplifier
SONET - synchronous optical network
SPM - self phase modulation
SRS - stimulated Raman scattering
TDM - time division multiplexing

TOAD - TeraHertz optical asymmetric demultiplexer
VCO - voltage controlled oscillator
WAN - wide area network
WDM - wavelength division multiplexing
XPM - cross phase modulation